ENCLOSURE 6

STRUCTURAL INTEGRITY ASSOCIATES, INC.
REPORT 0900634.401 REVISION 2 (NON-PROPRIETARY)

UPDATED LEAK-BEFORE-BREAK EVALUATION FOR SEVERAL RCS PIPING AT PRAIRIE ISLAND NUCLEAR GENERATING PLANT UNITS 1 AND 2

133 pages follow

Report No.: 0900634.401
Revision No.: 2
Project No.: 0900634
File No.: 0900634.401
December 2009
☒ Q ☐ Non-Q

# Updated Leak-Before-Break Evaluation for Several RCS Piping at Prairie Island Nuclear Generating Plant Units 1 and 2

*Prepared for:*

Xcel Energy
Contract No. 1006, Release 9

*Prepared by:*

Structural Integrity Associates, Inc.
San Jose, California

*Prepared by:* _____ Date: Dec 21, 2009
P. Jing

*Reviewed by:* _____ Date: Dec 21, 2009
H. Qian

*Approved by:* _____ Date: Dec 21, 2009
G. Angah Miessi

## REVISION CONTROL SHEET

Document Number: 0900634.401

Title: Updated Leak-Before-Break Evaluation for Several RCS Piping at Prairie Island Nuclear Generating Plant Units 1 and 2

Client: Xcel Energy Company

SI Project Number: 0900634

| Section | Pages | Revision | Date | Comments |
|---|---|---|---|---|
| 1-8<br>App. A | All<br>A1-A4 | 0 | Dec. 7, 2009 | |
| 1-8<br>App. A | All<br>A1-A4 | 1 | Dec. 14, 2009 | Addressed client comments. |
| 4<br>6<br>8 | 4-1,<br>4-21 -- 4-28<br>6-1, 6-6,<br>8-1, 8-2, 8-4 | 2 | Dec. 21,2009 | Deleted Westinghouse Proprietary Information<br>Changed references per client comments |

## SUMMARY

This report presents a leak-before-break (LBB) evaluation for piping systems attached to the reactor coolant system (RCS) at Prairie Island Nuclear Generating Plant, Units 1 and 2 (operated by Xcel Energy). The evaluation includes portions of the safety injection (SI) and residual heat removal (RHR) systems.

The LBB evaluation was performed in accordance with the 10 CFR 50, Appendix A GDC-4 and NUREG-1061, Vol. 3 as supplemented by NUREG-0800, Standard Review Plan 3.6.3. Additional criteria to address the application of LBB to small diameter piping taking guidance from NUREG/CR-6443 and NUREG/CR-4572 was developed in Section 5 of this report.

The evaluation is based on determining critical flaw sizes and leakage rates at all weld locations using weld-specific loads. The critical flaw size as used herein refers to the through-wall flaw length which becomes unstable under a given set of applied load. Critical flaw sizes were calculated using both the net section plastic collapse and the elastic-plastic fracture mechanics (EPFM) J-Integral/Tearing Modulus (J/T) approach with conservative generic material properties. The "leakage flaw size" was determined as the minimum of one half the critical flaw size with a factor of unity on normal operating plus SSE loads or the critical flaw size with a factor of $\sqrt{2}$ on normal operating plus SSE loads. Thus, the leakage flaw size as referred herein maintains a safety factor of 2 on the critical flaw size under normal plus SSE loads and a safety factor of 1 when the loads are factored by $\sqrt{2}$. Leakage rates were then calculated through the leakage flaw sizes per the requirements of NUREG-1061. The determination of critical flaw sizes and leak rates took into account the effects of restraint of pressure induced bending which has been shown to affect LBB analysis results especially for small diameter piping. A fatigue crack growth analysis was also performed to determine the growth of postulated semi-elliptical, inside surface flaws with an initial size based on ASME Code Section XI acceptance standards.

The following summary of the LBB evaluation is formatted along the lines of the "Recommendations for Application of the LBB Approach" in the NUREG-1061 Vol. 3 executive summary:

(a) The SI and RHR piping systems are constructed of very ductile stainless steel that is not susceptible to cleavage-type fracture. In addition, it has been shown that these systems are not susceptible to the effects of corrosion, high cycle fatigue or water hammer.

(b) Loadings have been determined from the piping analyses, and are based upon pressure, dead weight, thermal expansion and earthquake seismic motion. All highly-stressed locations in the piping were considered.

(c) Although plant specific certified material test report (CMTR) data is available, this information alone is not complete for the fracture mechanics evaluations. As such, lower-bound generic industry material properties for the piping and welds have been conservatively used in the evaluations.

(d) Crack growth analysis was conducted at the most critical locations on all the evaluated piping, considering the cyclic stresses predicted to occur over the life of the plant. For a hypothetical flaw with aspect ratio of 10:1 and an initial flaw depth of approximately 11% of pipe wall, it will take about 38 heatup and cooldown cycles to grow the hypothetical flaw to the ASME Section XI allowable flaw size (75% of pipe wall) at the most critical location. For the last ten years, Prairie Island has experienced 13 heatup/cooldown cycles. Given that this piping is inspected in accordance with ASME Section XI requirements in each 10-year interval, it is believed that crack growth can be managed by the current in-service inspection program.

(e) Based on evaluation of the critical cracks at all locations in the piping system, it was determined that the leakage at the limiting location was 3.4 gpm under Originally Licensed Thermal Power (OLTP) considering only RHR Normal Thermal. With a margin of 10 on leakage suggested in NUREG-1061 Vol. 3, the leakage detection

system at Prairie Island is capable of measuring leakage of 2.0 gpm. This leakage detection is assumed in the LBB evaluation.

(f) Since the systems considered in this evaluation consist of relatively small diameter piping (6-inch to 12-inch OD), the effect of the piping system flexibility and restraint was considered in the determination of the critical flaw sizes and leakage rates at the various weld locations. The most highly restrained piping systems were analytically modeled and various crack configurations were introduced at the weld locations to determine the reduction in applied moments due to piping system restraint. The leakage was then calculated. This evaluation showed that there was not a significant reduction in leakage as a result of piping system restraint.

(g) Crack growth of a leakage size crack in the length direction due to an SSE event is no more than 1% of the leakage flaw size. This is not significant compared to the margin between the leakage-size crack size and the critical crack size.

(h) For all locations, the critical size circumferential crack was determined for the combination of normal plus safe shutdown earthquake (SSE) loads. The leakage size crack was chosen such that its length was no greater than the critical crack size reduced by a factor of two. Axial cracks were not considered since critical axial cracks always exhibit much higher leakage and more margin than critical circumferentially-oriented cracks.

(i) For all locations, the critical crack size was determined for the combination of $\sqrt{2}$ times the normal plus SSE loads. The leakage size crack was selected to be no greater than this critical crack size. (The minimum of the crack sizes determined by this criterion, and that of the criterion of (h) above, was chosen for calculation of the leakage rate for each location).

(j-n) No special testing (other than information in the CMTRs) was conducted to determine material properties for fracture mechanics evaluation. Instead, generic lower bound

material toughness and tensile properties were used in the evaluations. The material properties so determined have been shown to be applicable near the upper range of normal plant operation and exhibit ductile behavior at these temperatures. This data is widely accepted by industry for conducting mechanics analysis.

(o) Limit load analysis as outlined in NUREG-0800, SRP 3.6.3, was utilized in this evaluation to supplement the EPFM J/T analyses in order to determine the critical flaw sizes. The most limiting results of these two analytical approaches were used in determining the critical flaw sizes for the various piping systems.

Thus, it is concluded that the 6-inch to 12-inch piping evaluated in this report qualifies for the application of leak-before-break analysis to demonstrate that it is very unlikely that the piping could experience a large pipe break prior to leakage detection under Power Uprate Conditions considering RHR Thermal Stratification. Under Uprate Conditions considering RHR Thermal Stratification, it was determined that the leakage meet the LBB acceptance criteria. Additional leakage evaluation using Primary Water Stress Corrosion Cracking (PWSCC) morphology shows that leakage drops to as low as 22% of what is evaluated using fatigue morphology.

Table of Contents


Section Page

1.0 INTRODUCTION ..... 1-1

1.1 Background ..... 1-1
1.2 Leak-Before-Break Methodology ..... 1-2
1.3 Leak Detection Capability at Prairie Island ..... 1-4

2.0 CRITERIA FOR APPLICATION OF LEAK-BEFORE-BREAK ..... 2-1

2.1 Criteria for Through-Wall Flaws ..... 2-1
2.2 Criteria for Part-Through-Wall Flaws ..... 2-2
2.3 Consideration of Piping Restraint Effects ..... 2-2
2.4 Consideration of Other Mechanisms ..... 2-2

3.0 CONSIDERATION OF WATER HAMMER, CORROSION AND FATIGUE ..... 3-1

3.1 Water Hammer ..... 3-1
3.2 Corrosion ..... 3-2
3.3 Fatigue ..... 3-2

4.0 PIPING MATERIALS AND STRESSES ..... 4-1

4.1 Piping System Description ..... 4-1
4.2 Material Properties and Geometry ..... 4-1
4.3 Piping Moments and Stresses for Originally Licensed Thermal Power (OLTP) considering only RHR Normal Thermal ..... 4-2
4.4 Piping Moments and Stresses for Uprate Conditions considering RHR Thermal Stratification ..... 4-4

5.0 LEAK-BEFORE-BREAK EVALUATION ..... 5-1

5.1 Evaluation of Critical Flaw Sizes ..... 5-1
*5.1.1 Critical Flaw Sizes Determined By J-Integral/Tearing Modulus Analysis ..... 5-1*
*5.1.2 Critical Flaw Sizes Determined by Limit Load Analysis ..... 5-5*
5.2 Leak Rate Determination ..... 5-7
5.3 Effect of Piping Restraint on LBB Evaluation ..... 5-12
5.4 LBB Evaluation Results and Discussions ..... 5-16
*5.4.1 Originally Licensed Thermal Power (OLTP) considering only RHR Normal Thermal ..... 5-16*
*5.4.2 Uprate Conditions considering RHR Thermal Stratification ..... 5-17*

6.0 EVALUATION OF FATIGUE CRACK GROWTH OF SURFACE FLAWS ..... 6-1

6.1 Plant Transients ..... 6-1
6.2 Stresses for Crack Growth Evaluation ..... 6-2
6.3 Model for Stress Intensity Factor ..... 6-3
6.4 Fatigue Crack Growth Analysis and Results ..... 6-4

7.0 SUMMARY AND CONCLUSIONS ..... 7-1

8.0 REFERENCES ..... 8-1

APPENDIX A .....

DETERMINATION OF RAMBERG-OSGOOD PARAMETERS AT 650°F ..... A-1

List of Tables

Table Page

Table 1-1. Summary of Response Time and Sensitivities for All Coolant Leakage Detection Methods at Prairie Island ..... 1-5
Table 4-1a. Lower Bound SMAW Material Properties Used in the LBB Evaluation [15, 16] ... 4-8
Table 4-2. Moments for the 6-inch Safety Injection Piping Attached to Reactor Pressure ..... 4-9
Table 4-3. Moments for the 12-inch Safety Injection Piping Attached to Cold Leg (Unit 1) ... 4-10
Table 4-4. Moments for the 8-inch Residual Heat Removal Piping Attached to Hot Leg (Unit 1)4-11
Table 4-5. Moments for the 6-inch RCS Draindown Line Attached to Hot Leg (Unit 1) ..... 4-13
Table 4-6. Moments for the 6-inch Safety Injection Piping Attached to Reactor Pressure Vessel and Cold Leg (Unit 2) ..... 4-14
Table 4-7. Moments for the 12-inch Safety Injection Piping Attached to Cold Leg (Unit 2) ... 4-15
Table 4-8. Moments for the 8-inch Residual Heat Removal Piping Attached to Hot Leg (Unit 2)4-16
Table 4-9. Moments for the 6-inch RCS Draindown Line Attached to Hot Leg (Unit2) ..... 4-18
Table 4-10 Bounding Leakage Rates for the Originally Licensed Thermal Power (OLTP) Considering Only RHR Normal Thermal ..... 4-19
Table 4-11 Loads for Uprate Conditions Considering RHR Thermal Stratification ..... 4-20
Table 5-1. Leakage Flaw Size Versus Stress Determined by J/T Analysis for 6-inch Safety Injection Lines Attached to RCS Cold Leg (Temperature = 550°F) ..... 5-19
Table 5-2. Leakage Flaw Size Versus Stress Determined by J/T Analysis for 12-inch Safety Injection Lines Attached to RCS Cold Leg (Temperature = 550°F) ..... 5-20
Table 5-3. Leakage Flaw Size Versus Stress Determined by J/T Analysis for 8-inch RHR Lines Attached to RCS Hot Leg (Temperature = 607.4°F) ..... 5-21
Table 5-4. Leakage Flaw Size Versus Stress Determined by J/T Analysis for 6-inch Draindown Lines and Nozzles Attached to RCS Hot Leg (Temperature = 607.4°F) ..... 5-22
Table 5-5. Leakage Flaw Size Versus Stress Determined by Limit Load for 6-inch Safety Injection Lines Attached to RCS Cold Leg (Temperature = 550°F) ..... 5-23
Table 5-6. Leakage Flaw Size Versus Stress Determined by Limit Load for 12-inch Safety Injection Lines Attached to RCS Cold Leg (Temperature = 550°F) ..... 5-24
Table 5-7. Leakage Flaw Size Versus Stress Determined by Limit Load for 8-inch RHR Lines Attached to RCS Hot Leg (Temperature = 607.4°F) ..... 5-25
Table 5-8. Leakage Flaw Size Versus Stress Determined by Limit Load for 6-inch Draindown Lines and Nozzles Attached to RCS Hot Leg (Temperature = 607.4°F) ..... 5-26
Table 5-9. Predicted Leakage Rates for 6-inch Safety Injection lines Attached to Reactor Pressure Vessel and RCS Cold Leg (Unit 1) ..... 5-27
Table 5-10. Predicted Leakage Rates for 12-inch Safety Injection ..... 5-29
Table 5-11. Predicted Leakage Rates for 8-inch RHR Lines Attached ..... 5-30
Table 5-12. Predicted Leakage Rates for 6-inch Draindown Lines Attached to RCS Hot Leg (Unit 1) ..... 5-32
Table 5-13. Predicted Leakage Rates for 6-inch Safety Injection Lines Attached to Reactor Pressure Vessel and RCS Cold Leg (Unit 2) ..... 5-33
Table 5-14. Predicted Leakage Rates for 12-inch Safety Injection Lines Attached to RCS Cold Leg (Unit 2) ..... 5-35
Table 5-15. Predicted Leakage Rates for 8-inch RHR Lines Attached to RCS Hot Leg (Unit 2)5-36

Table 5-16. Predicted Leakage Rates for 6-inch Draindown Lines ..... 5-38
Table 5-17. Predicted Leakage Rates for 6-inch Nozzles Attached to RCS Hot Leg (Units 1 and 2) ..... 5-38
Table 5-18. Moments Due to Kink Angle Restraint Effects for 6-inch Safety Injection Line Attached to RCS Cold Leg ..... 5-39
Table 5-19. Moments Due to Kink Angle Restraint Effects for 6-inch Draindown Line Attached to RCS Hot Leg ..... 5-40
Table 5-20. Moments Due to Kink angle Restraint Effects for 8-inch RHR Lines Attached to RCS Hot Leg ..... 5-41
Table 5-21. Leakage Flaw Size and Leakages for 6-inch Safety Injection Line Attached to RCS Cold Leg Considering Restraint Effect ..... 5-43
Table 5-22. Leakage Flaw Size and Leak Rates for 8-inch RHR Line Attached to RCS Hot Leg Considering Restraint Effects ..... 5-44
Table 5-23. Leakage Flaw Size and Leak Rates for 6-inch Draindown Line ..... 5-45
Table 5-24. Updated Leak Rates under Uprate Conditions Considering RHR Thermal Stratification using Fatigue Crack Morphology ..... 5-46
Table 5-25. Updated Leak Rates under Uprate Conditions Considering RHR Thermal Stratification using PWSCC Crack Morphology ..... 5-47
Table 6-1. Plant Design Transients Used for LBB Evaluations ..... 6-6
Table 6-2. Additional System Transients Used Specifically for LBB Evaluations ..... 6-7
Table 6-3. Combined Transients for Crack Growth, Hot Leg ..... 6-7
Table 6-4. Combined Transients for Crack Growth, Cold Leg ..... 6-8
Table 6-5. Bounding Moments ..... 6-8
Table 6-6. Maximum and Minimum Transient and Discontinuity Stress ..... 6-9
Table 6-7. Maximum and Minimum Transient Stress ..... 6-9
Table 6-8. Total Constant ($\sigma_0$) and Linear (($\sigma_1$) Through-Wall Stresses, 6" Sch 160 Cold Leg SI6-10
Table 6-9. Total Constant ($\sigma_0$) and Linear (($\sigma_1$) Through-Wall Stresses, 12" Sch 160 SI Accumulator ..... 6-10
Table 6-10. Total Constant ($\sigma_0$) and Linear ($\sigma_1$) Through-Wall Stresses, 8" Sch 140 RHR Suction ..... 6-11
Table 6-11. Total Constant ($\sigma_0$) and Linear ($\sigma_1$) Through-Wall Stresses, 6" Sch 160 Draindown6-11
Table 6-12. Initial Crack Depths for Various Locations ..... 6-12
Table 6-13. Results of Fatigue Crack Growth Analysis ..... 6-12

List of Figures

Figure | Page

Figure 1-1. Representation of Postulated Cracks in Pipes for Fracture Mechanics Leak-Before-Break Analysis ..... 1-6
Figure 1-2. Conceptual Illustration of ISI (UT)/Leak Detection Approach to Protection Against Pipe Rupture ..... 1-7
Figure 1-3. Leak-Before-Break Approach Based on Fracture Mechanics Analysis with In-service Inspection and Leak Detection ..... 1-8
Figure 4-1. Schematic of Piping Model and Selected Node Points for the 6-inch Safety Injection Piping Attached to Reactor Pressure Vessel and the Cold Leg (Unit 1 - Loops A and B) 4-22
Figure 4-2. Schematic of Piping Model and Selected Node Points for the 6-inch Safety Injection Piping Attached to Reactor Pressure Vessel and the Cold Leg (Unit 2 - Loops A and B) ..... 4-23
Figure 4-3. Schematic of Piping Model and Selected Node Points for the 12-inch Safety Injection Piping Attached to the Cold Leg (Unit 1 - Loops A and B) ..... 4-24
Figure 4-4. Schematic of Piping Model and Selected Node Points for the 12-inch Safety Injection Piping Attached to the Cold Leg (Unit 2 - Loops A and B) ..... 4-25
Figure 4-5. Schematic of Piping Model and Selected Node Points for the 8-inch Residual Heat Removal Piping Attached to Hot Leg (Units 1 - Loops A and B) ..... 4-26
Figure 4-6. Schematic of Piping Model and Selected Node Points for the 8-inch Residual Heat Removal Piping Attached to Hot Leg (Units 2 - Loops A and B) ..... 4-27
Figure 4-7. Schematic of Piping Model and Selected Node Points for the 6-inch RCS Draindown Line Attached to Hot Leg (Units 1 and 2) ..... 4-28
Figure 5-1. J-Integral/Tearing Modulus Concept for Determination of Instability During Ductile Tearing ..... 5-48
Figure 5-2. Leakage Flaw Size Versus Moment for 6-inch Schedule 160 Pipe Weld Determined by J/T and Limit Load Analyses ..... 5-49
Figure 5-3. Leakage Flaw Size Versus Moment for 6-inch Schedule 160 Nozzle/Draindown Weld Determined by J/T and Limit Load Analyses ..... 5-50
Figure 5-4. Leakage Flaw Size Versus Moment for 8-inch Schedule 140 Pipe Weld Determined by J/T and Limit Load Analyses ..... 5-51
Figure 5-5. Leakage Flaw Size Versus Moment for 12-inch Schedule 160 Pipe Weld Determined by J/T and Limit Load Analyses ..... 5-52
Figure 5-6. Depiction of Restraint Effect on Cracked Piping ..... 5-53
Figure 5-7. Schematic of Piping Layout Used to Determine the Effect of Restraint on LBB Evaluation (8-inch RHR Line - Prairie Island Unit 1, Loop A) ..... 5-54
Figure 5-8. Schematic of Piping Layout Used to Determine the Effect of Restraint on LBB Evaluation (6-inch Safety Injection Line – Kewaunee, Loop B) ..... 5-55
Figure 5-9. Schematic of Piping Layout Used to Determine the Effect of Restraint on LBB Evaluation (6-inch Draindown Line – Prairie Island Unit 2) ..... 5-56
Figure 5-10. Flow Path Deviation As Affected by Roughness and Crack Opening Displacement5-57
Figure 5-11. Roughness Depiction for Small and Large Crack Opening Displacements ..... 5-57

# 1.0 INTRODUCTION

## 1.1 Background

This report documents evaluations performed by Structural Integrity Associates (SI) to determine the leak-before-break (LBB) capabilities of the high energy non-isolable 6-inch to 12-inch piping attached to the reactor coolant system (RCS) at Prairie Island Units 1 and 2 under both Originally Licensed Thermal Power (OLTP) considering only Residual Heat Removal (RHR) Normal Thermal and Uprate Conditions considering RHR Thermal Stratification. These encompass portions of the safety injection (SI) system, including that from the SI accumulators, and the RHR piping. These evaluations were undertaken to address the potential for high energy line break at these locations. The portions of these lines evaluated extend from the nozzle at the reactor coolant loop to the first isolation valve.

The original LBB evaluation in Reference 1 was performed for both Prairie Island and Kewaunee. The current evaluation uses some of the design input data from Reference 1. The following lines are evaluated in this report for each unit at Prairie Island.

- 12-inch SI lines (Loop A and Loop B). These lines are connected to the SI accumulators. The Loop B line also serves as the RHR system return line.
- 8-inch RHR lines (Loop A and Loop B). These lines serve as the RHR system suction lines.
- 6-inch cold leg SI lines (Loops A and B). These lines provide flow from the high pressure SI pumps.
- 6-inch reactor vessel SI lines (Loops A and B). These lines are composed of 4-inch diameter lines for some distance from the reactor vessel nozzle and a shorter section of 6-inch diameter line near the isolation valves. Although these lines are included in the evaluation, the maximum break flow would be limited by the 4-inch piping.
- 6-inch RCS draindown line on the hot leg (Loop A on Unit 1 and Loop B on Unit 2). This line was added to the plant following initial construction and consists of a short section of 6-inch diameter piping prior to reducing to 2-inch diameter at the isolation valve.
- 6-inch capped nozzle on the hot leg (Loop B on Unit 1 and Loop A on Unit 2).

In addition, PI is planning for power uprate (Uprate) in 2010. Hence, the LBB evaluation is also performed under Uprate conditions. Available thermal stratification loads (STRAT) in the Units 1 and 2 residual heat removal (RHR) suction lines are considered under Uprate conditions.

## 1.2 Leak-Before-Break Methodology

NRC SECY-87-213 [2] covers a rule to modify General Design Criterion 4 (GDC-4) of Appendix A, 10 CFR Part 50. This amendment to GDC-4 allows exclusion from the design basis of all dynamic effects associated with high energy pipe rupture by application of LBB technology.

Definition of the LBB approach and criteria for its use are provided in NUREG-1061 [3], supplemented by NUREG-0800, SRP 3.6.3 [4]. Volume 3 of NUREG-1061 defines LBB as "...the application of fracture mechanics technology to demonstrate that high energy fluid piping is very unlikely to experience double-ended ruptures or their equivalent as longitudinal or diagonal splits." The particular crack types of interest include circumferential through-wall cracks (TWC) and part-through-wall cracks (PTWC), as well as axial or longitudinal through-wall cracks (TWC), as shown in Figure 1-1.

LBB is based on a combination of in-service inspection (ISI) and leak detection to detect cracks, coupled with fracture mechanics analysis to show that pipe rupture will not occur for cracks smaller than those detectable by these methods. A discussion of the criteria for application of LBB is presented in Section 2 of this report, which summarizes NUREG-1061, Vol. 3 requirements.

The approach to LBB which has gained acceptance for demonstrating protection against high energy line break (HELB) in safety-related nuclear piping systems is schematically illustrated in Figure 1-2. Essential elements of this technique include critical flaw size evaluation, crack propagation analysis, volumetric nondestructive examination (NDE) for flaw detection/sizing, leak detection, and service experience. In Figure 1-2, a limiting circumferential crack is modeled as having both a short through-wall component, or an axisymmetric part-through-wall crack component. Leak detection establishes an upper bound for the through-wall crack component while

volumetric ISI limits the size of undetected part-through-wall defects. These detection methods complement each other, since volumetric NDE techniques are well suited to the detection of long cracks while leakage monitoring is effective in detecting short through-wall cracks. The level of NDE required to support LBB involves volumetric inspection at intervals determined by fracture mechanics crack growth analysis, which would preclude the growth of detectable part-through-wall cracks to a critical size during an inspection interval. A fatigue evaluation is performed to ensure that an undetected flaw acceptable per ASME Section will not grow significantly during service. For through-wall defects, crack opening areas and resultant leak rates are compared with leak detection limits.

The net effect of complementary leak detection and ISI is illustrated by the shaded region of Figure 1-2 as the largest undetected defect that can exist in the piping at any given time. Critical flaw size evaluation, based on elastic-plastic fracture mechanics techniques, is used to determine the length and depth of defects that would be predicted to cause pipe rupture under specific design basis loading conditions, including abnormal conditions such as a seismic event and including appropriate safety margins for each loading condition. Crack propagation analysis is used to determine the time interval in which the largest undetected crack could grow to a size which would impact plant safety margins. A summary of the elements for a leak-before-break analysis is shown in Figure 1-3. Service experience, where available, is useful to confirm analytical predictions as well as to verify that such cracking tends to develop into "leak" as opposed to "break" geometries.

In accordance with NUREG-1061, Vol. 3 [3] and NUREG-0800, SRP 3.6.3 [4], the leak-before-break technique for the high energy piping systems evaluated in this report included the following considerations.

- Elastic-plastic fracture mechanics analysis of load carrying capacity of cracked pipes under worst case normal loading, with safe-shutdown earthquake (SSE) loads included. Such analysis includes elastic-plastic fracture data applicable to pipe weldments and weld heat affected zones where appropriate.

- Limit-load analysis in lieu of the elastic-plastic fracture mechanics analysis described above.

- Linear elastic fracture mechanics analysis of subcritical crack propagation to determine ISI (in-service inspection) intervals for long, part-through-wall cracks.

- A piping system evaluation to determine the effect of piping restraint on leakage for small diameter piping.

Piping stresses have a dual role in LBB evaluations. On one hand, higher maximum (design basis) stresses tend to yield lower critical flaw sizes, which result in smaller flaw sizes for assessing leakage. On the other hand, higher operating stresses tend to open cracks more for a given crack size and create a higher leakage rate. Because of this duality, the use of a single maximum stress location for a piping system may result in a non-conservative LBB evaluation. Thus, the LBB evaluation reported herein has been performed for each nodal location addressed in the plant piping system analysis.

### 1.3 Leak Detection Capability at Prairie Island

Application of LBB evaluation methodology is predicated on having a very reliable leak detection system at the plant, capable of measuring 1/10 of the leakage determined in the evaluation. The various leak detection systems employed at Prairie Island are detailed in Reference 5. Table1-1 taken from Reference 5 lists all the leak detection methods at Prairie Island, the minimum detectable leakage and the estimated response time for various leak rates. As can be seen from this table, twelve separate leak detection methods are utilized at Prairie Island with minimum detectable leakage of as low as 0.1 gpm.

In summary, Prairie Island has a very redundant leak detection system capable of detecting leakage as low as 0.1 gpm. However, to be consistent with previous Westinghouse LBB report, which used the capability for Prairie Island Reactor Coolant System pressure boundary leak detection system [Section 5.2.3 of Reference 40], the minimum detectable leakage is set to 0.2gpm. And since NUREG-1061, Vol. 3 requires that a margin of 10 be provided on leakage, the minimum allowable evaluated leakage rate is 2.0gpm.

Table 1-1. Summary of Response Time and Sensitivities for All Coolant Leakage Detection Methods at Prairie Island

| Method | Minimum Detectable Leakage (gpm) | Estimated Response Time of Method (min) | | | Control Room Alarm? |
|---|---|---|---|---|---|
| | | 0.5 gpm Leak | 1.0 gpm Leak | 5.0 gpm Leak | |
| Operator Inspection | 0.1 | 20160 | 20160 | 20160 | No |
| Volume Control Tank Makeup | 0.5 | 260 | 150 | 35 | Yes |
| Charging Rate Monitoring | 11 | 1 | 1 | 1 | Yes |
| Daily Coolant Inventory | 0.1 | 1440 | 1440 | 1440 | No |
| Sump Pump Operating Time | 0.21 | 1440 | 1440 | 1440 | No |
| Containment Temperature Monitoring | 0.5 | 180 | 120 | 72 | No |
| Containment Pressure Monitoring | 0.5 | 180 | 120 | 72 | No |
| Containment Relative Humidity Monitoring | 0.2 | 132 | 96 | 72 | No |
| Containment Radioactive Particulate Monitor R-11 | 0.1 | 60 | 30 | 6 | Yes |
| Containment Radioactive Gas Monitor R-12 | Note 1 | Note 1 | Note 1 | Note 1 | Yes |
| Containment Fan Coil Unit Condensate Measurement | 2.73 | Note 2 | Note 2 | 0 - 120 | Yes |
| Acoustic Emission Monitoring | Note 3 | 480 | 480 | 480 | No |

Notes:
1. Low levels of fission products in reactor coolant cause containment gas monitor to be ineffective.
2. Below minimum sensitivity of method.
3. Minimum detectable leakage has yet to be determined.

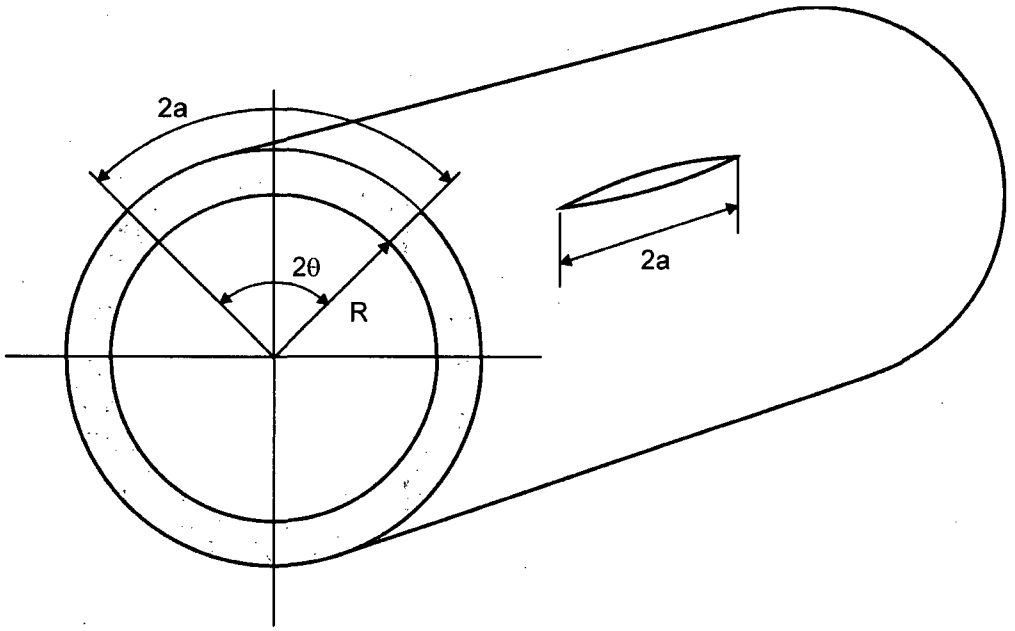


a. Circumferential and Longitudinal Through-Wall Cracks of Length 2a.

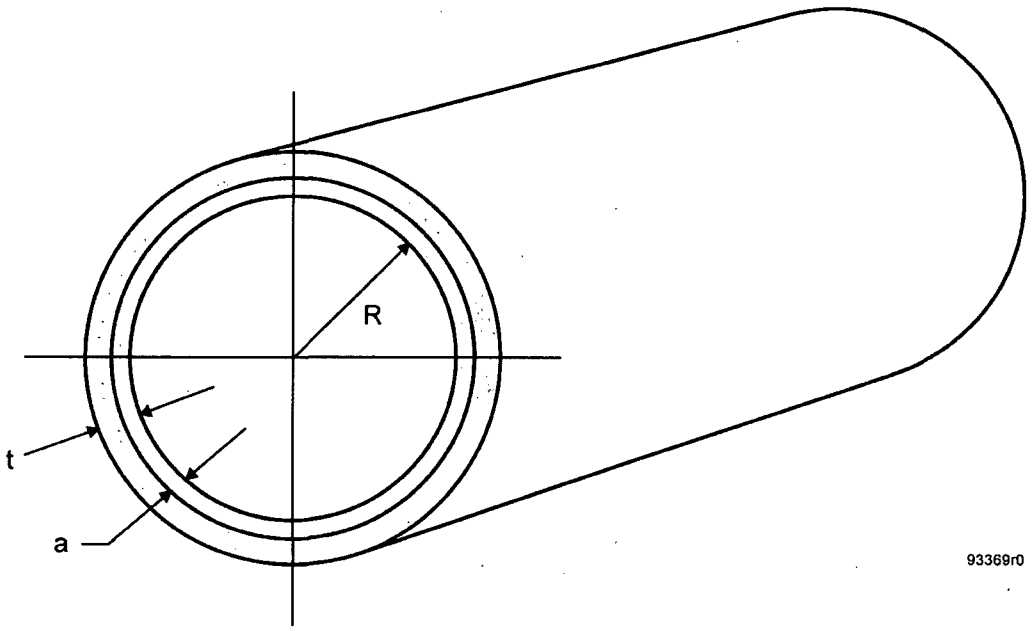


b. Circumferential 360 Part-Through-Wall Crack of Depth a.

Figure 1-1. Representation of Postulated Cracks in Pipes for Fracture Mechanics Leak-Before-Break Analysis

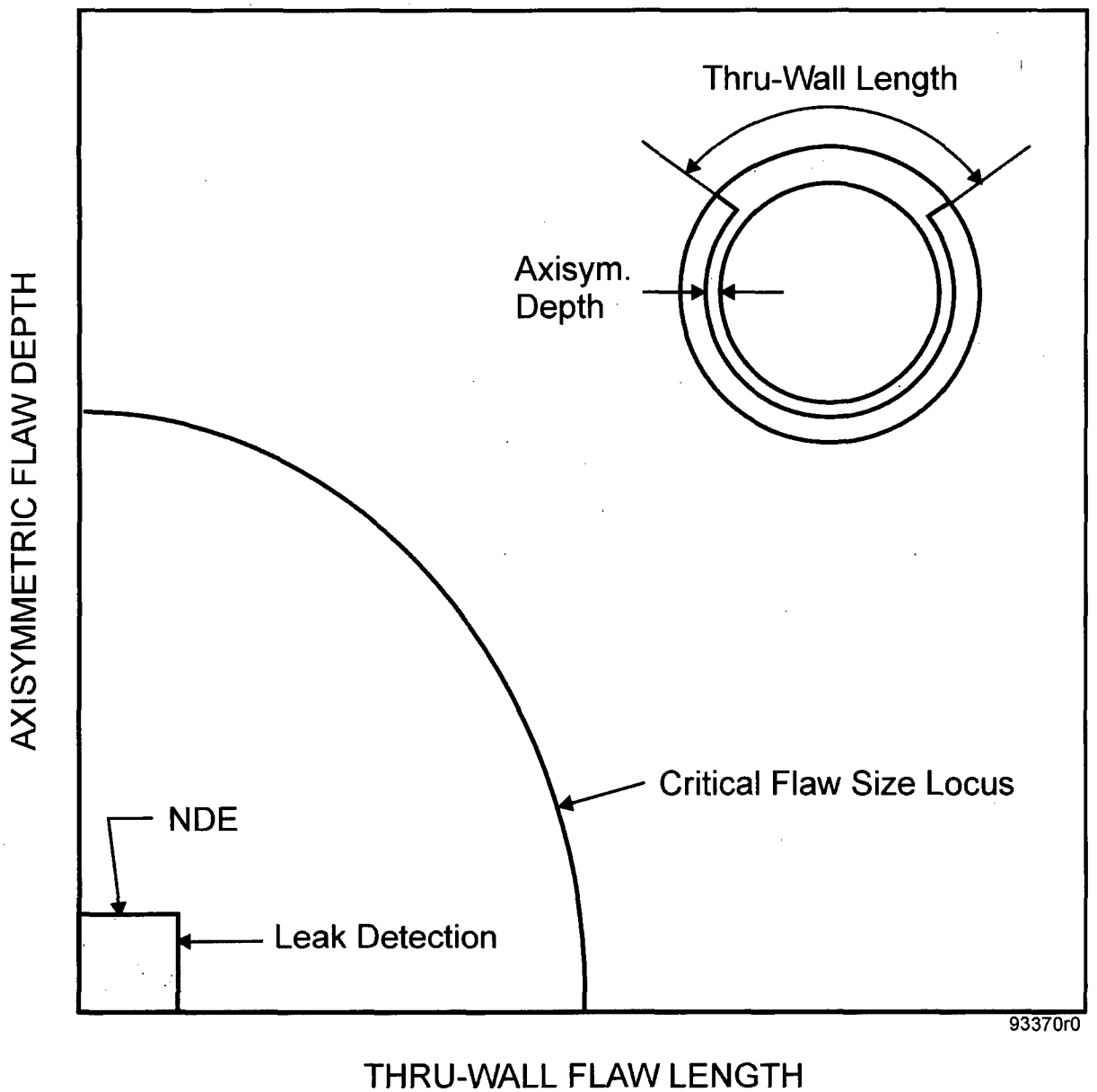


Figure 1-2. Conceptual Illustration of ISI (UT)/Leak Detection Approach to Protection Against Pipe Rupture

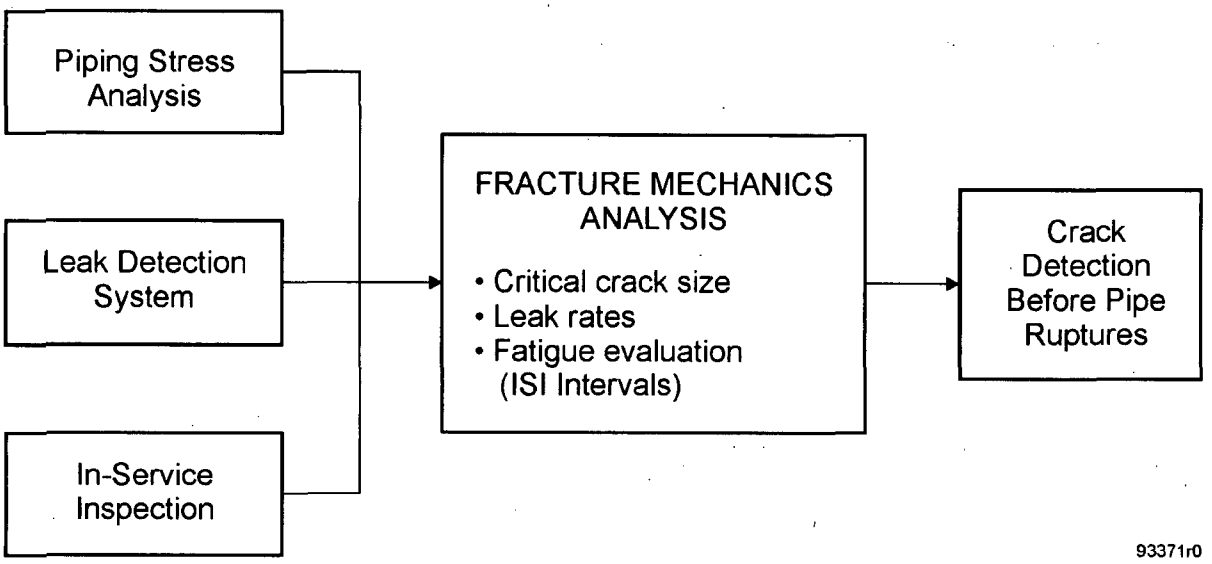


Figure 1-3. Leak-Before-Break Approach Based on Fracture Mechanics Analysis with In-service Inspection and Leak Detection

## 2.0 CRITERIA FOR APPLICATION OF LEAK-BEFORE-BREAK

NUREG-1061, Vol. 3 [3] identifies several criteria to be considered in determining applicability of the leak-before-break approach to piping systems. Section 5.2 of NUREG-1061, Vol. 3 provides extensive discussions of the criteria for performing leak-before-break analyses. These requirements are restated in NUREG-0800, SRP 3.6.3 [4]. The details of the discussions are not repeated here; the following summarizes the key elements:

### 2.1 Criteria for Through-Wall Flaws

Acceptance criteria for critical flaws may be stated as follows:

1. A critical flaw size shall be determined for normal operating conditions plus safe shutdown earthquake (SSE) loads. Leakage for normal operating conditions must be detectable for this flaw size reduced by a factor of two.

2. A critical flaw size shall be determined for normal operating conditions plus SSE loads multiplied by a factor of $\sqrt{2}$. Leakage for normal operating conditions must be detectable for this flaw size.

It has been found in previous evaluations conducted by Structural Integrity Associates (SI) that in general, the first criterion bounds the second. However, in this evaluation, both criteria were considered for completeness.

Either elastic-plastic fracture mechanics instability analysis or limit load analysis may be used in determining critical flaw sizes. NUREG-0800 SRP 3.6.3 [4] provides a modified limit load procedure that may be used for austenitic piping and weldments. Both approaches have been used in this evaluation as presented in Section 5.0 of the report.

## 2.2 Criteria for Part-Through-Wall Flaws

NUREG-1061, Vol. 3 [3] requires demonstration that a long part-through-wall flaw which is detectable by ultrasonic means will not grow due to fatigue to a depth which would produce instability over the life of the plant. This is demonstrated in Section 6.0 of this report, where the analysis of subcritical crack growth is discussed.

## 2.3 Consideration of Piping Restraint Effects

It was shown in Reference 27 that restraint of pressure induced bending in a piping system could affect the LBB analysis results. This has been shown to be especially important for small diameter piping (less than 10 inch NPS). An evaluation was therefore performed in Section 5.3 to address this issue for the small diameter piping at Prairie Island.

## 2.4 Consideration of Other Mechanisms

NUREG-1061, Vol. 3 [3] limits applicability of the leak-before-break approach to those locations where degradation or failure by mechanisms such as water hammer, erosion/corrosion, fatigue, and intergranular stress corrosion cracking (IGSCC) is not a significant possibility. These mechanisms were considered for the affected piping systems, as reported in Section 3 of this report.

## 3.0 CONSIDERATION OF WATER HAMMER, CORROSION AND FATIGUE

NUREG-1061, Vol. 3 [3] states that LBB should not be applied to high energy lines susceptible to failure from the effects of water hammer, corrosion or fatigue. These potential failure mechanisms are thus discussed below with regard to the affected RCS attached RHR and SI piping at Prairie Island 1 and 2, and it is concluded that the above failure mechanisms do not invalidate the use of LBB for this piping system.

### 3.1 Water Hammer

A comprehensive study performed in NUREG-0927 [7] indicated that the probability of water hammer occurrence in the residual heat removal systems of a PWR is very low. In NUREG-0927, only a single event of water hammer was reported for PWR residual heat removal systems with the cause being incorrect valve alignment. There was no indication as to which portion of the system was affected but it would not be that portion adjacent to the RCS-attached piping evaluated for LBB.

It was also reported in NUREG-0927 that the safety significance of water hammer events in the safety injection system is moderate. With four water hammer events reported in the SI systems, three of these events were associated with voided lines and the other event was associated with steam bubble collapse. Although there was no indication of the affected portions of the SI system, the portions susceptible to water hammer would not be that adjacent to the RCS-attached piping evaluated for LBB.

The portions of the piping evaluated for LBB are inboard of the first isolation valves for the SI and RHR piping. Thus, during normal operation, these lines experience reactor coolant pressure and temperature conditions such that there is no potential for steam/water mixtures that might lead to water hammer. The portions of these systems that are adjacent to the reactor coolant piping are not in use during normal operation. The RHR system is not used except during low-pressure low-temperature cooldown conditions. The SI system is used only during loss of coolant-accident (LOCA) condition. During normal plant operation, the portions of the system beyond the first isolation valve are expected to run at low temperature conditions. Thus, there should never be any

voiding or potential for steam bubble collapse, which could result in water hammer loads on the piping attached directly to the RCS considered in this evaluation. To date, there has been no experience related to water hammer events in either the RHR or SI systems at Prairie Island.

As such, this phenomenon will have no impact on the LBB analysis for the affected portions of the safety injection and residual heat removal systems at Prairie Island.

### 3.2 Corrosion

Two corrosion damage mechanisms which can lead to rapid piping failure are intergranular stress corrosion cracking (IGSCC) in austenitic stainless steel pipes and flow-assisted corrosion (FAC) in carbon steel pipes. IGSCC has principally been an issue in austenitic stainless steel piping in boiling water reactors [8] resulting from a combination of tensile stresses, susceptible material and oxygenated environment. IGSCC is not typically a problem for the primary loop of a PWR such as the SI and RHR systems under consideration since the environment has relatively low concentrations of oxygen.

FAC is not anticipated to be a problem for this system since it is fabricated from stainless steel piping which is not susceptible to FAC.

### 3.3 Fatigue

Metal fatigue in piping systems connected to the reactor coolant loops of Westinghouse-designed pressurized water reactor was identified in Bulletin 88-08 [9]. Evaluations performed by NSP and submitted to the Nuclear Regulatory Commission have concluded that this does not apply to Prairie Island. For the SI piping, there is no interconnection to the charging pumps that will lead to inleakage leading to cracking such was identified at Farley and Thihange. For the RHR piping, any outleakage at the isolation valve leak off lines is monitored and can be corrected such that cracking similar to that identified at the Japanese Genkai plant will not occur. Thus, there is no potential for unidentified high cycle fatigue. The potential for thermal fatigue cracking induced by swirl penetration in the 8" RHR piping is also considered. Using results from this project, the calculated cumulative usage factor considering swirl penetration is 0.00 for Unit 1 Loop A RHR

line and 0.23 for Unit 2 Loop B RHR line, based on 60 years of operation. This shows that thermal fatigue induced by swirl penetration is not significant; thus it is not considered as source for crack initiation.

Known fatigue loadings and the resultant possible crack growth have been considered by the analyses reported in Section 6.0 of this report. Based on the results presented in Section 6.0, it is concluded that fatigue will not be a significant issue for the SI and RHR piping at Prairie Island.

## 4.0 PIPING MATERIALS AND STRESSES

### 4.1 Piping System Description

The piping systems considered in this evaluation have been described in Section 1.1. Schematics of the mathematical models for these lines including selected nodal points are shown in Figures 4-1 through 4-4. The lines are fabricated from Schedule 160 stainless steel piping. The most conservative normal operating pressure and temperature from the reactor pressure vessel specification [10], the reactor vessel Stress Report [11] and design bases document for the plant [12] were used in the evaluation. From Reference 9, the RCS design operating pressure is 2235 psig while the design operating temperature for the cold leg is 544.5°F and that for the hot leg is 607.5°F. From Reference 11, the corresponding values are [redacted], and [redacted] and from Reference 12, they are 2235 psig, 535°F and 599.1°F, respectively. For the purpose of evaluating Originally Licensed Thermal Power (OLTP) considering only RHR Normal Thermal, normal operating pressure of 2235 psig was used. In addition, a temperature of 550°F was used for the cold leg and 607.4°F was assumed for the hot leg. The pressure and temperature used for Uprate Conditions considering RHR Thermal Stratification will be discussed in Section 4.2 " Piping Moments and Stresses for Uprate Conditions considering RHR Thermal Stratification".

### 4.2 Material Properties and Geometry

The material properties of interest for fracture mechanics and leakage calculations are the Modulus of Elasticity (E), the yield stress ($S_y$), the ultimate stress ($S_u$), the Ramberg-Osgood parameters for describing the stress strain curve ($\alpha$ and n), the fracture toughness ($J_{IC}$) and power law coefficient for describing the material J Resistance curve (C and N).

NUREG-1061, Vol. 3 requires that actual plant specific material properties including stress-strain curves and J-R material properties be used in the LBB evaluations. In lieu of this requirement, material properties associated with the least favorable material and welding processes from industry wide generic material sources have been used to provide a conservative assessment of critical flaw sizes and leakage rates.

The piping material is A-376, Type 316 stainless steel [13]. From Reference 14, the piping was fabricated using gas tungsten arc welding (GTAW) process for the root, and filled using the shielded metal arc welding (SMAW) process. The worst properties of GTAW and SMAW weldments have been used in the evaluation. Several studies have shown that of these three materials, the SMAW weldment, because of its low toughness and susceptibility to thermal aging, has the most conservative properties for estimation of critical flaw sizes. Hence, properties of SMAW have been conservatively used in this evaluation. The conservative stress-strain properties for the SMAW weldments at 550°F in Reference 15 which formed the basis for the flaw acceptance criteria in ASME Section XI were used for the evaluation. However, for the J-R curve properties, the values provided in Reference 15 for SMAW weldments were compared with the lower bound curve provided in NUREG-6428 [16] for thermally aged welds at 550°F. It was found that the lower bound curve in NUREG-6428 is more conservative and therefore was used in this evaluation. The 550°F temperature at which the material properties are determined for the cold leg is slightly different than the conservatively assumed operating temperature of 552°F. However, this difference is small and not expected to change the conclusions of the evaluation. The material properties at the hot leg temperature of 607.4°F were determined by adjusting the properties at 550°F by the ratio of the values in ASME Code Section III. The Ramberg-Osgood parameters were determined at 650°F as presented in Appendix A of this report and the values at 607.4°F were then interpolated from the values at 550°F and 650°F. The fracture toughness is not expected to change significantly from 550°F to 607.4°F and therefore the J-R curve from Reference 16 was also assumed at 607.4°F. The properties used for the SMAW weldments are shown in Table 4-1a.

Geometry details of the piping system obtained from References 17 and 18 are reproduced in Table 4-1b.

### 4.3 Piping Moments and Stresses for Originally Licensed Thermal Power (OLTP) considering only RHR Normal Thermal

The piping moments and stresses considered in the LBB evaluation are due to pressure (P), dead weight (DW), thermal expansion (TE) and safe shutdown earthquake inertia (SSE) consistent with the guidance provided in NUREG-1061, Vol. 3. Per the guidance provided in NUREG-

1061, other secondary stresses such as residual stresses and through-wall thermal stresses were not included in the evaluation.

Piping analysis was provided in References 17 and 18 and included moments for the nozzles, elbows and pipe-to-valve welds for all components. Summaries of the piping moments are shown in Tables 4-2 through 4-9, respectively. For calculation of critical flaw size, the moment and stress combination of pressure, dead weight, thermal expansion and SSE loads is used with a factor of unity and factor of $\sqrt{2}$. For leakage calculations, the moment and stress combination of pressure, deadweight and thermal expansion loads is used. These basic moment load combinations are shown in Tables 4-2 through 4-9 for the various nodal locations. Stresses were calculated directly from the piping analysis moments for the various lines considered in this evaluation [17, 18]. The resulting stresses used in the fracture mechanics analysis do not include the effects of stress indices.

The axial stress due to normal operating pressure is calculated from the expression:

$$\sigma_p = \frac{pD_i^2}{D_o^2 - D_i^2}$$

where p is the internal pressure, $D_o$ is the outside diameter of the pipe and $D_i$ is the inside diameter.

For Originally Licensed Thermal Power (OLTP) considering only RHR Normal Thermal, axial loads due to dead weight, thermal expansion, and seismic were not directly available from the piping stress analysis and therefore were not considered in the evaluation. A later study showed that at one location on 8-inch RHR lines, axial load due to dead weight, thermal expansion and seismic was 7.6% of the axial load due to pressure. As a result, the leakage decreased 7.2% when these non-pressure axial loads are included. Thus, the non-pressure axial load will be considered under Uprate Conditions considering RHR Thermal Stratification.

The axial stress due to dead weight, thermal expansion and seismic loads is calculated using the following equation:

$$\sigma_f = \frac{F \cdot 4}{\pi(D_o^2 - D_i^2)},$$

where, F = the sum of axial forces from dead weight, thermal expansion and seismic loads. The bending stress due to dead weight, thermal expansion and SSE is calculated from the bending moments using the expression:

$$\sigma_m = \frac{\sqrt{M_x^2 + M_y^2 + M_z^2}}{Z}$$

where:

| | | |
|---|---|---|
| $Z$ | = | the section modulus and, |
| $M_x$, $M_y$, $M_z$ | = | the three orthogonal moments. |

On occasions, furmanite clamps have been installed on the safety injection piping at Prairie Island to contain valve leakage. Evaluations were performed by Xcel Energy to assess the effect of the furmanite clamps on the stresses of the affected piping [19, 20]. The evaluations concluded that the change in stress is not significant (less than 5%). Hence, the piping loads without the furmanite clamps were used in the LBB evaluations. Consideration of the small stress changes due to furmanite clamps would not be expected to change the conclusions of the LBB evaluations.

## 4.4 Piping Moments and Stresses for Uprate Conditions considering RHR Thermal Stratification

References 34 and 35 list the updated loadings for the Uprate Conditions considering RHR Thermal Stratification (which includes effects of $T_{ave}$ reconciliation, measurement uncertainty recapture (MUR) and transition to 422V+ fuel). Reference 36 reports a 1% increase in the normal operating pressure. Also, the updated cold leg temperature is reported as 527.1°F or 527.4°F (conservatively considered 527.4°F for the purpose of the present evaluation as the

difference is negligible) and the hot leg temperature is reported as 592.6°F (References 34 and 35).

The following describes the input for the LBB analysis under Uprate Conditions considering RHR Thermal Stratification.

1. Material properties are conservatively taken from Table 4-1, which are reported at higher temperatures than the updated temperatures reported in References 34 and 35.

2. Code minimum flow stress of 51 ksi [4] is used for the critical flaw size calculation except for the 8-inch RHR line in Unit 2 for which the actual material property is used per SRP 3.6.3.

3. Normal operating pressure is taken as 2235 psig x 1.01 = 2257.4 psig = 2258 psig for critical flaw size calculations and 2235 psig, the nominal normal operating pressure, for leakage calculations.

4. For the thermal-hydraulic model used to calculate leakage using EPRI program, PICEP [24], cold leg temperature is taken as 527.4°F and hot leg temperature is taken as 592.6°F. The default inputs in PICEP are kept the same as those used in the existing LBB calculation that uses fatigue crack morphology.

5. Per SRP 3.6.3, Rev. 1 [4], loads for leakage are calculated as algebraic sums of P+DW+TH whereas, loads for critical flaw size are calculated using absolute sums of |P|+|DW|+|TH|+ |SSE| except for RHR lines for which the loads for leakage are calculated as algebraic sums of P+DW+TH+STRAT and the loads for critical flaw size are calculated as |P|+|DW|+|TH|+ |SSE|+|STRAT|.

6. Both the forces and moments are considered for the updated LBB analysis. For conservatism, the SRSS-ed forces are assumed to be compressive for the leakage calculation. Table 4-11 lists the updated forces and moments used for the LBB evaluation.

7. For Nodes 2000 and 2354 of 8-inch RHR line in Unit 1 and Nodes 100 and 270 of 8-inch RHR line in Unit 2, References 34 and 35, respectively, reports thermal loads for both normal operating and hot functional conditions. Therefore, both conditions are evaluated to yield maximum and minimum moments for critical flaw size and leakage, respectively. To comply with the fact that for leakage calculations a negative (compressive) force is conservatively considered, SRSS-ed forces from thermal load conditions are considered such that they are maximum for both critical flaw size and leakage.

8. Since not all the nodes reported in this report have updated loading data due to the Uprate Conditions considering RHR Thermal Stratification, the nodes reported in References 34 and 35 are analyzed for leakage. Table 4-10 is a summary of the nodes which have the limiting leakage on each piping line. It is based on the leakage results in Table 5-9 through Table 5-17. For a given line, if these nodes do not include the node(s) reported in Table 4-10 that gave critical leakage values, then the following heuristic scheme is adopted:

   a) For a given line in a given unit, the maximum and minimum percentage increase in SRSS-ed moment due to the Uprate conditions is identified for critical flaw size and leakage evaluations, respectively, for all the nodes of that particular line in that particular unit for which the Uprate data is available. Similar calculations are performed for the SRSS-ed forces except that for leakage, the maximum percentage increase is also considered. This is to comply with the fact that for leakage calculation a negative (compressive) force is conservatively considered.

   b) This percentage change is used to increase or decrease the existing SRSS-ed moment value for the Uprate conditions. Similar calculations are performed for the SRSS-ed forces.

   c) There exist some lines (i.e., 6-inch RCS draindown lines for both Units 1 and 2) for which there is no data (for any node) given for the Uprate conditions. In that

case, the worst possible changes (the most increase for critical flaw size evaluation and the most decrease for leakage calculation) in the SRSS-ed moment due to the Uprate conditions considering all nodes in all the lines for which the Uprate load data is available, is considered. For forces, the most increase is considered for both the critical flaw size and leakage calculations.

d) In general, the loop to which a node belongs is not considered to calculate the worst possible changes in the SRSS-ed moment due to the Uprate conditions except for the 8-inch RHR lines in Unit 2.

The nodes and corresponding loads for LBB evaluation under Uprate conditions are listed in Table 4-11.

Table 4-1a. Lower Bound SMAW Material Properties Used in the LBB Evaluation [15, 16]

| Parameter | Value | |
|---|---|---|
| Temp (°F) | 550 (Cold Leg) | 607.4 (Hot Leg) |
| E (ksi) | $25 \times 10^3$ | $24.72 \times 10^3$ |
| $S_y = \sigma_O$ (ksi) | 49.4 | 48.137 |
| $S_u$ (ksi) | 61.4 | 61.4 |
| $S_f = 0.5\ (S_y + S_u)$ (ksi) | 55.4 | 54.77 |
| Ramberg-Osgood Parameter $\alpha$ | 9.0 | 9.130 |
| Ramberg-Osgood Parameter n | 9.8 | 9.636 |
| $J_{IC}$ (in-k/in$^2$) | 0.288 | 0.288 |
| J-R Curve Parameter $C_1$ (in-k/in$^2$) | 3.816 | 3.816 |
| J-R Curve Parameter N | 0.643 | 0.643 |
| $J_{max}$ (in-k/in$^2$) | 2.345 | 2.345 |

Table 4-1b. Geometry used in the LBB Evaluation [17, 18]

| | **6″ (Schedule 160)** | **8″ (Schedule 140)** | **12″ (Schedule 160)** |
|---|---|---|---|
| **Outside Radius (in)** | 3.3125 | 4.3125 | 6.375 |
| **Wall Thickness (in)** | 0.718 | 0.812 | 1.312 |
| **Area (in$^2$)** | 13.32 | 19.93 | 47.15 |
| **Moment of Inertia (in$^4$)** | 58.97 | 153.72 | 781.13 |

Table 4-2. Moments for the 6-inch Safety Injection Piping Attached to Reactor Pressure Vessel and Cold Leg (Unit 1)

| Nodes | Thermal + DW | | | | Thermal + DW + DBE | | | |
|---|---|---|---|---|---|---|---|---|
| | Moment, ft-lbs | | | | Moment, ft-lbs | | | |
| | $M_x$ | $M_y$ | $M_z$ | SRSS(1) | $M_x$ | $M_y$ | $M_z$ | SRSS(1) |
| 1621(2) | -343 | 552 | -337 | 732 | -967 | 810 | -1073 | 1656 |
| 1622(2) | -145 | 552 | -386 | 689 | -611 | 810 | -934 | 1379 |
| 1630(2) | 1136 | 552 | -702 | 1445 | 1714 | 810 | -1386 | 2348 |
| 1640A(2) | 1246 | 552 | -730 | 1546 | 1898 | 810 | -1492 | 2546 |
| 1640B(2) | 1262 | 466 | -641 | 1490 | 1994 | 1008 | -1713 | 2815 |
| 1645(2) | 1151 | 438 | -579 | 1361 | 1835 | 1080 | -1677 | 2710 |
| 1646(2) | 1245 | 409 | -632 | 1455 | 1929 | 1153 | -1730 | 2836 |
| 1045(2) | -389 | 248 | 392 | 605 | -589 | 534 | 610 | 1002 |
| 1040(2) | -23 | 258 | 192 | 322 | -215 | 524 | 402 | 695 |
| 1025 | -220 | 9 | -6 | 220 | -278 | 77 | -158 | 329 |
| 1027 | -231 | 9 | -7 | 231 | -299 | 77 | -185 | 360 |
| 1030 | -252 | 9 | -12 | 252 | -338 | 77 | -238 | 420 |
| 1031 | -274 | 9 | -16 | 275 | -382 | 77 | -296 | 489 |
| 1039A | -274 | 9 | -16 | 275 | -382 | 77 | -296 | 489 |
| 1039B | -390 | 24 | -229 | 453 | -690 | 100 | -943 | 1173 |
| 1040 | -390 | 24 | -229 | 453 | -690 | 100 | -943 | 1173 |
| 1045 | -463 | 33 | -388 | 605 | -883 | 115 | -1364 | 1629 |
| 1236 | 153 | -226 | 59 | 279 | 269 | -654 | 91 | 713 |
| 1238 | 202 | -226 | 53 | 308 | 258 | -654 | 107 | 711 |
| 1250 | 243 | -226 | 48 | 335 | 287 | -654 | 160 | 732 |
| 1259 | 284 | -226 | 44 | 366 | 370 | -654 | 218 | 782 |
| 1260A | 284 | -226 | 44 | 366 | 370 | -654 | 218 | 782 |
| 1260B | 499 | -194 | 428 | 685 | 627 | -566 | 660 | 1072 |
| 1265 | 499 | -194 | 428 | 685 | 627 | -566 | 660 | 1072 |
| 1270 | 764 | -151 | 993 | 1262 | 888 | -453 | 1235 | 1587 |

Notes:

(1) $SRSS = \sqrt{M_x^2 + M_y^2 + M_z^2}$

(2) These nodes are on the safety injection lines attached to the reactor pressure vessel.

(3) The moments are for OLTP w/ RHR Normal Thermal only.

Table 4-3. Moments for the 12-inch Safety Injection Piping Attached to Cold Leg (Unit 1)

| Nodes | DW + TE | | | | DW + TE + SSE | | | |
|---|---|---|---|---|---|---|---|---|
| | Moment, ft-lbs | | | | Moment, ft-lbs | | | |
| | $M_x$ | $M_y$ | $M_z$ | SRSS(1) | $M_x$ | $M_y$ | $M_z$ | SRSS(1) |
| 175 | -25496 | 6185 | 9427 | 27878 | -27336 | 10635 | 11185 | 31392 |
| 180 | -25204 | 10126 | 9965 | 28932 | -26886 | 19990 | 11137 | 35306 |
| 185A | -25201 | 12260 | 9971 | 29746 | -26829 | 25428 | 10913 | 38542 |
| 185B | -22918 | 15216 | 7981 | 28644 | -26318 | 33000 | 11401 | 43722 |
| 190 | -22918 | 15216 | 7981 | 28644 | -26318 | 33000 | 11401 | 43722 |
| 855 | 48567 | -11503 | -21149 | 54207 | 58355 | -13121 | -31687 | 67687 |
| 860A | 48567 | -11503 | -21148 | 54206 | 58355 | -13121 | -31686 | 67687 |
| 860B | 51807 | -10307 | -21549 | 57049 | 62363 | -11601 | -30787 | 70509 |
| 865 | 51807 | -10307 | -21549 | 57049 | 62363 | -11601 | -30787 | 70509 |
| 870 | 35262 | -10307 | -8215 | 37645 | 43118 | -11601 | -15197 | 47167 |
| 875 | 18717 | -10307 | 5120 | 21972 | 23949 | -11601 | 10116 | 28469 |
| 880 | -349 | -10307 | 20487 | 22936 | -2969 | -11601 | 24147 | 26953 |
| 885 | -19416 | -10307 | 35853 | 42055 | -23144 | -11601 | 40307 | 47905 |
| 890A | -19418 | -10307 | 35854 | 42057 | -23146 | -11601 | 40308 | 47907 |
| 890B | -30338 | -16644 | 25218 | 42818 | -36136 | -17548 | 32120 | 51434 |
| 895 | -30338 | -16644 | 25218 | 42818 | -36136 | -17548 | 32120 | 51434 |
| 897 | -35019 | -21968 | 13129 | 43374 | -41711 | -23818 | 22651 | 53105 |
| 905A | -35017 | -21965 | 13134 | 43372 | -41709 | -23813 | 22654 | 53103 |
| 905B | -35249 | -28305 | -5002 | 45483 | -41893 | -31545 | -17344 | 55235 |
| 910 | -35249 | -28305 | -5002 | 45483 | -41893 | -31545 | -17344 | 55235 |

(1) $SRSS = \sqrt{M_x^2 + M_y^2 + M_z^2}$

(2) The moments are for OLTP w/ RHR Normal Thermal only.

Table 4-4. Moments for the 8-inch Residual Heat Removal Piping Attached to Hot Leg (Unit 1)

| Nodes | DW + TE | | | | DW + TE + SSE | | | |
|---|---|---|---|---|---|---|---|---|
| | Moment, ft-lbs | | | | Moment, ft-lbs | | | |
| | $M_x$ | $M_y$ | $M_z$ | SRSS(1) | $M_x$ | $M_y$ | $M_z$ | SRSS(1) |
| 2000 | 2825 | -4723 | 14998 | 15976 | 4159 | -8507 | 15790 | 18412 |
| 2005 | 3689 | -3859 | 11658 | 12822 | 4455 | -6881 | 12044 | 14569 |
| 2010A | 3689 | -3859 | 11658 | 12822 | 4455 | -6881 | 12044 | 14569 |
| 2010B | 4094 | -3691 | 11398 | 12661 | 4774 | -6567 | 11562 | 14128 |
| 2015 | 4094 | -3691 | 11398 | 12661 | 4774 | -6567 | 11562 | 14128 |
| 2020A | 4094 | -3691 | 11398 | 12661 | 4774 | -6567 | 11562 | 14128 |
| 2020B | 3006 | -3675 | 9359 | 10494 | 3728 | -6105 | 9631 | 11997 |
| 2025 | 3006 | -3675 | 9359 | 10494 | 3728 | -6105 | 9631 | 11997 |
| 2030 | -2945 | -3625 | -1597 | 4936 | -3311 | -5163 | -2679 | 6693 |
| 2035 | -9389 | -3576 | -13459 | 16795 | -10227 | -5490 | -15835 | 19634 |
| 2040A | -9389 | -3576 | -13459 | 16795 | -10227 | -5490 | -15835 | 19634 |
| 2040B | -10819 | -3560 | -16125 | 19742 | -11669 | -5604 | -18253 | 22377 |
| 2045 | -10819 | -3560 | -16125 | 19742 | -11669 | -5604 | -18253 | 22377 |
| 2050 | -9109 | -3560 | -13070 | 16324 | -9963 | -5622 | -13542 | 17727 |
| 2055 | -4834 | -3560 | -5432 | 8096 | -6714 | -5604 | -10032 | 13309 |
| 2060 | -487 | -3560 | 2332 | 4284 | -2839 | -5604 | 10480 | 12219 |
| 2070A | -487 | -3560 | 2332 | 4284 | -2839 | -5604 | 10480 | 12219 |
| 2070B | -4522 | -1086 | 83 | 4651 | -7000 | -2554 | 9525 | 12093 |
| 2075 | -4522 | -1086 | 83 | 4651 | -7000 | -2554 | 9525 | 12093 |
| 2324 | 6686 | -2680 | -6842 | 9935 | 11788 | -3530 | -15364 | 19684 |
| 2326 | 7131 | -4112 | -6023 | 10200 | 12947 | -5592 | -13205 | 19320 |

(1) $SRSS = \sqrt{M_x^2 + M_y^2 + M_z^2}$

(2) The moments are for OLTP w/ RHR Normal Thermal only.

Table 4-4. Moments for the 8-inch Residual Heat Removal Piping Attached to Hot Leg (Unit 1) (Continued)

| Nodes | DW + TE | | | | DW + TE + SSE | | | |
|---|---|---|---|---|---|---|---|---|
| | Moment, ft-lbs | | | | Moment, ft-lbs | | | |
| | $M_x$ | $M_y$ | $M_z$ | SRSS(1) | $M_x$ | $M_y$ | $M_z$ | SRSS(1) |
| 2328A | 7131 | -4112 | -6023 | 10200 | 12947 | -5592 | -13205 | 19320 |
| 2328B | 6339 | -5552 | -4464 | 9536 | 11773 | -9268 | -7676 | 16835 |
| 2330 | 4841 | -5552 | -3700 | 8243 | 9023 | -9268 | -4256 | 13617 |
| 2332 | 506 | -5552 | -2689 | 6190 | 3582 | -9268 | -3957 | 10695 |
| 2334 | -1470 | -5552 | -2227 | 6160 | -3836 | -9268 | -3851 | 10744 |
| 2336 | -5585 | -5552 | -1267 | 7976 | -6523 | -9268 | -3689 | 11919 |
| 2338 | -6902 | -5552 | -959 | 8910 | -7350 | -9268 | -3471 | 12327 |
| 2340A | -6902 | -5552 | -959 | 8910 | -7350 | -9268 | -3471 | 12327 |
| 2340B | -7331 | -4900 | -380 | 8826 | -8029 | -8378 | -1524 | 11704 |
| 2342 | -7331 | -4900 | -380 | 8826 | -8029 | -8378 | -1524 | 11704 |
| 2344 | -7040 | -3780 | 155 | 7992 | -9026 | -6884 | 1497 | 11450 |
| 2346A | -7040 | -3780 | 155 | 7992 | -9026 | -6884 | 1497 | 11450 |
| 2346B | -7591 | -3128 | 507 | 8226 | -10607 | -6048 | 3261 | 12638 |
| 2348 | -7591 | -3128 | 507 | 8226 | -10607 | -6048 | 3261 | 12638 |
| 2350A | -7591 | -3128 | 506 | 8226 | -10607 | -6048 | 3260 | 12638 |
| 2350B | -8059 | -2933 | 642 | 8600 | -11261 | -5801 | 3860 | 13242 |
| 2352 | -8059 | -2933 | 642 | 8600 | -11261 | -5801 | 3860 | 13242 |
| 2354 | -8482 | -2511 | 755 | 8878 | -11856 | -5271 | 5005 | 13907 |

(1) $SRSS = \sqrt{M_x^2 + M_y^2 + M_z^2}$

(2) The moments are for OLTP w/ RHR Normal Thermal only.

Table 4-5. Moments for the 6-inch RCS Draindown Line Attached to Hot Leg (Unit 1)

| Nodes | DW + TE | | | | DW + TE + SSE | | | |
|---|---|---|---|---|---|---|---|---|
| | Moment, ft-lbs | | | | Moment, ft-lbs | | | |
| | $M_x$ | $M_y$ | $M_z$ | SRSS(1) | $M_x$ | $M_y$ | $M_z$ | SRSS(1) |
| 730 | -883 | 79 | 594 | 1067 | -1117 | 631 | 1144 | 1719 |
| 720 | 883 | -37 | -269 | 924 | 1117 | -579 | -803 | 1493 |

(1) $SRSS = \sqrt{M_x^2 + M_y^2 + M_z^2}$

(2) The moments are for OLTP w/ RHR Normal Thermal only.

Table 4-6. Moments for the 6-inch Safety Injection Piping Attached to Reactor Pressure Vessel and Cold Leg (Unit 2)

| Nodes | Thermal + DW | | | | Thermal + DW + DBE | | | |
|---|---|---|---|---|---|---|---|---|
| | Moment, ft-lbs | | | | Moment, ft-lbs | | | |
| | $M_x$ | $M_y$ | $M_z$ | SRSS(1) | $M_x$ | $M_y$ | $M_z$ | SRSS(1) |
| 695(2) | 425 | 920 | -703 | 1233 | 791 | 1144 | -1593 | 2115 |
| 690(2) | 822 | 2907 | -1073 | 3206 | 1954 | 3513 | -2679 | 4831 |
| 685B(2) | 822 | 2907 | -1073 | 3206 | 1954 | 3513 | -2679 | 4831 |
| 685A(2) | 936 | 3012 | -1114 | 3345 | 2212 | 3638 | -2774 | 5082 |
| 680(2) | 936 | 3012 | -1114 | 3345 | 2212 | 3638 | -2774 | 5082 |
| 675(2) | 1146 | 2861 | -1088 | 3268 | 2666 | 3485 | -2740 | 5173 |
| 552(2) | 2410 | -555 | -30 | 2473 | 2932 | -1149 | -114 | 3151 |
| 551(2) | 2082 | -555 | -10 | 2155 | 2554 | -1149 | -182 | 2806 |
| 550B(2) | 2082 | -555 | -10 | 2155 | 2554 | -1149 | -182 | 2806 |
| 550A(2) | 2276 | -837 | -490 | 2474 | 2622 | -1329 | -938 | 3086 |
| 548(2) | 2276 | -837 | -490 | 2474 | 2622 | -1329 | -938 | 3086 |
| 558 | 438 | 27 | 126 | 457 | 626 | 31 | 240 | 671 |
| 560 | 501 | 27 | 155 | 525 | 687 | 31 | 267 | 738 |
| 562 | 626 | 27 | 213 | 662 | 806 | 31 | 323 | 869 |
| 564 | 753 | 27 | 271 | 801 | 933 | 31 | 393 | 1013 |
| 566A | 753 | 27 | 271 | 801 | 933 | 31 | 393 | 1013 |
| 566B | 781 | 139 | 456 | 915 | 869 | 147 | 764 | 1166 |
| 568 | 781 | 139 | 456 | 915 | 869 | 147 | 764 | 1166 |
| 570 | 721 | 215 | 566 | 941 | 747 | 227 | 990 | 1261 |
| 826 | -850 | 47 | -251 | 888 | -1002 | 69 | -359 | 1067 |
| 828 | -954 | 47 | -279 | 995 | -1130 | 69 | -401 | 1201 |
| 830A | -954 | 47 | -279 | 995 | -1130 | 69 | -401 | 1201 |
| 830B | -967 | 133 | -437 | 1069 | -1149 | 169 | -581 | 1299 |
| 832 | -967 | 133 | -437 | 1069 | -1149 | 169 | -581 | 1299 |
| 834 | -909 | 191 | -545 | 1077 | -1085 | 237 | -703 | 1314 |

Notes:

(1) $SRSS = \sqrt{M_x^2 + M_y^2 + M_z^2}$

(2) These nodes are on the safety injection lines attached to the reactor pressure vessel.

(3) The moments are for OLTP w/ RHR Normal Thermal only.

Table 4-7. Moments for the 12-inch Safety Injection Piping Attached to Cold Leg (Unit 2)

| Nodes | DW + TE | | | | DW + TE + SSE | | | |
|---|---|---|---|---|---|---|---|---|
| | Moment, ft-lbs | | | | Moment, ft-lbs | | | |
| | $M_x$ | $M_y$ | $M_z$ | SRSS(1) | $M_x$ | $M_y$ | $M_z$ | SRSS(1) |
| 225 | -51046 | -4212 | -16259 | 53738 | -59760 | -7946 | -24339 | 65014 |
| 230A | -51046 | -4212 | -16259 | 53738 | -59760 | -7946 | -24339 | 65014 |
| 230B | -43014 | -9042 | -20341 | 48433 | -51324 | -14140 | -29261 | 60748 |
| 235 | -43014 | -9042 | -20341 | 48433 | -51324 | -14140 | -29261 | 60748 |
| 240 | -35470 | -9042 | -19425 | 41439 | -42984 | -14140 | -27905 | 53163 |
| 436 | 23987 | -9308 | -9247 | 27341 | 29369 | -13550 | -20149 | 38107 |
| 440A | 23987 | -9309 | -9247 | 27341 | 29369 | -13551 | -20149 | 38107 |
| 440B | 21619 | -10987 | -8404 | 25666 | 26501 | -16233 | -19258 | 36561 |
| 441 | 21619 | -10987 | -8404 | 25666 | 26501 | -16233 | -19258 | 36561 |
| 445 | 17692 | -10987 | -6525 | 21824 | 22510 | -16233 | -16495 | 32285 |

(1) $SRSS = \sqrt{M_x^2 + M_y^2 + M_z^2}$

(2) The moments are for OLTP w/ RHR Normal Thermal only.

Table 4-8. Moments for the 8-inch Residual Heat Removal Piping Attached to Hot Leg (Unit 2)

| Nodes | DW + TE | | | | DW + TE + SSE | | | |
|---|---|---|---|---|---|---|---|---|
| | Moment, ft-lbs | | | | Moment, ft-lbs | | | |
| | $M_x$ | $M_y$ | $M_z$ | SRSS(1) | $M_x$ | $M_y$ | $M_z$ | SRSS(1) |
| 100 | 173 | -1298 | 8580 | 8679 | 2321 | -2920 | 12374 | 12924 |
| 101 | 920 | -698 | 7381 | 7471 | 2010 | -2848 | 12011 | 12507 |
| 105A | 920 | -698 | 7381 | 7471 | 2010 | -2848 | 12011 | 12507 |
| 105B | 1163 | -566 | 6842 | 6963 | 2375 | -2834 | 11540 | 12118 |
| 106 | 1163 | -566 | 6842 | 6963 | 2375 | -2834 | 11540 | 12118 |
| 110A | 1163 | -566 | 6842 | 6963 | 2375 | -2834 | 11540 | 12118 |
| 110B | 1377 | -517 | 6263 | 6433 | 2095 | -2425 | 9011 | 9564 |
| 111 | 1377 | -517 | 6263 | 6433 | 2095 | -2425 | 9011 | 9564 |
| 112 | 1382 | -429 | 6247 | 6412 | 1974 | -1685 | 6851 | 7326 |
| 115A | 1382 | -429 | 12247 | 12332 | 1974 | -1685 | 12851 | 13110 |
| 115B | 1671 | -380 | 5409 | 5674 | 2439 | -1312 | 7777 | 8255 |
| 116 | 1671 | -380 | 5409 | 5674 | 2439 | -1312 | 7777 | 8255 |
| 117 | 3417 | -380 | 510 | 3476 | 4659 | -1312 | 4182 | 6397 |
| 118 | 5163 | -380 | -4388 | 6786 | 6553 | -1312 | -8290 | 10648 |
| 119 | 6111 | -380 | -7049 | 9337 | 6653 | -1312 | -10047 | 12121 |
| 120A | 6111 | -380 | -7049 | 9337 | 6653 | -1312 | -10047 | 12121 |
| 120B | 5442 | -266 | -6053 | 8144 | 5704 | -930 | -7881 | 9773 |
| 121 | 5442 | -266 | -6053 | 8144 | 5704 | -930 | -7881 | 9773 |
| 246 | -2120 | -6479 | -310 | 6824 | -11834 | -9801 | -30858 | 34472 |
| 249A | -2120 | -6479 | -310 | 6824 | -11834 | -9801 | -30858 | 34472 |
| 249B | -1536 | -8376 | 2590 | 8901 | -11768 | -11156 | 32974 | 36745 |
| 250 | -1536 | -8376 | 2590 | 8901 | -11768 | -11156 | 32974 | 36745 |
| 251 | -1190 | -8376 | 3941 | 9333 | -10978 | -11156 | 32941 | 36470 |

(1) $SRSS = \sqrt{M_x^2 + M_y^2 + M_z^2}$

(2) The moments are for OLTP w/ RHR Normal Thermal only.

Table 4-8. Moments for the 8-inch Residual Heat Removal Piping Attached to Hot Leg (Unit 2) (Continued)

| Nodes | DW + TE | | | | DW + TE + SSE | | | |
|---|---|---|---|---|---|---|---|---|
| | Moment, ft-lbs | | | | Moment, ft-lbs | | | |
| | $M_x$ | $M_y$ | $M_z$ | SRSS(1) | $M_x$ | $M_y$ | $M_z$ | SRSS(1) |
| 251 | -1190 | -8376 | 3941 | 9333 | -10978 | -11156 | 32941 | 36470 |
| 252 | 3655 | -8376 | 22854 | 24613 | 7235 | -11156 | 32492 | 35107 |
| 253 | 5730 | -8376 | 30961 | 32582 | 6686 | -11156 | 31831 | 34386 |
| 254 | 7517 | -8376 | 33282 | 35133 | 8983 | -11156 | 36458 | 39171 |
| 255A | 7517 | -8376 | 33282 | 35133 | 8983 | -11156 | 36458 | 39171 |
| 255B | 8278 | -6990 | 30527 | 32393 | 9932 | -9582 | 35223 | 37830 |
| 256 | 8278 | -6990 | 30527 | 32393 | 9932 | -9582 | 35223 | 37830 |
| 257 | 1864 | 82 | 4066 | 4474 | 2366 | 1768 | 8294 | 8804 |
| 258 | -3997 | 7153 | -20112 | 21717 | -6559 | 7299 | -32834 | 34269 |
| 260A | -3997 | 7153 | -20112 | 21717 | -6559 | 7299 | -32834 | 34269 |
| 260B | -2996 | 8540 | -21871 | 23670 | -5352 | 8806 | -32447 | 34044 |
| 261 | -2996 | 8540 | -21871 | 23670 | -5352 | 8806 | -32447 | 34044 |
| 262 | 5324 | 8540 | -11063 | 14955 | 5486 | 8806 | -15809 | 18909 |
| 263 | 10402 | 8540 | -4465 | 14180 | 12090 | 8806 | -19119 | 24274 |
| 265A | 10403 | 8540 | -4465 | 14181 | 12091 | 8806 | -19119 | 24275 |
| 265B | 10926 | 7540 | -1922 | 13414 | 12658 | 8888 | -19746 | 25082 |
| 266 | 10926 | 7540 | -1921 | 13413 | 12658 | 8888 | -19745 | 25082 |
| 270 | 9494 | 3022 | 4393 | 10889 | 10384 | 9356 | 28873 | 32078 |

(1) $\text{SRSS} = \sqrt{M_x^2 + M_y^2 + M_z^2}$

(2) The moments are for OLTP w/ RHR Normal Thermal only.

Table 4-9. Moments for the 6-inch RCS Draindown Line Attached to Hot Leg (Unit2)

| Nodes | DW + TE | | | | DW + TE + SSE | | | |
|---|---|---|---|---|---|---|---|---|
| | Moment, ft-lbs | | | | Moment, ft-lbs | | | |
| | $M_x$ | $M_y$ | $M_z$ | SRSS(1) | $M_x$ | $M_y$ | $M_z$ | SRSS(1) |
| 10 | 288 | -39 | 442 | 529 | 454 | -361 | 542 | 794 |
| 7 | -340 | 68 | -409 | 536 | -520 | 418 | -521 | 847 |

(1) $SRSS = \sqrt{M_x^2 + M_y^2 + M_z^2}$

(2) The moments are for OLTP w/ RHR Normal Thermal only.

Table 4-10 Bounding Leakage Rates for the Originally Licensed Thermal Power (OLTP) considering only RHR Normal Thermal

| Line | Unit | Node | Moments | | Net Section Collapse Results | |
|---|---|---|---|---|---|---|
| | | | NOP[4] (in-lbs) | NOP+SSE (in-lbs) | Leakage Flaw Size, 2a (inches) | Leakage Rate (gpm) |
| 6" SI | 1 | 1045 | 7260 | 19550 | 5.230 | 4.600 |
| 6" SI | 2 | 558 | 5480 | 8050 | 5.342 | 4.909 |
| 6" Draindown | 1 | 720 | 11090 | 17920 | 5.246 | 3.941 |
| 6" Draindown | 2 | 7 | 6430 | 10160 | 5.322 | 3.884 |
| 8" RHR | 1 | 2060 | 51410 | 146630 | 6.018 | 6.963 |
| 8" RHR | 2 | 246 | 81890 | 413660 | 4.844 | 3.779 |
| 12" SI | 1 | 185B/ 190 | 343730 | 524660 | 8.878 | 22.422 |
| 12" SI | 2 | 445 | 261.890 | 387420 | 9.200 | 22.632 |
| 6" Capped Nozzle[3] | 1,2 | N/A[1] | 0[2] | 0[2] | 5.420 | 3.740 |

Notes:
1: Not applicable.
2: No loading except pressure (2235 psig) is considered.
3: Piping restraint effect not applicable.
4: NOP = Normal Operating Condition = DW+TH.

Table 4-11 Loads for Uprate Conditions considering RHR Thermal Stratification

| Line | Unit | Node | Forces | | Moments | |
|---|---|---|---|---|---|---|
| | | | Leakage[1] (lbs) | Critical Flaw Size[2] (lbs) | Leakage[1] (in-lbs) | Critical Flaw Size[2] (in-lbs) |
| 6" SI[6] | 1 | 1045 | -368.68 | 1086.66 | 7180.23 | 21045.32 |
| 6" SI | 1 | 1270 | -659.43 | 736.19 | 15004.94 | 18968.52 |
| 12" SI[6] | 1 | 190 | -1962.59 | 5243.32 | 327524.16 | 509258.64 |
| 12" SI | 1 | 910 | -10172.22 | 13731.91 | 520925.40 | 638922.48 |
| 8" RHR[10] | 1 | 2000 | -17063.56 | 22010.32 | 198027.60 | 586646.64 |
| 8" RHR[10] | 1 | 2354 | -9676.03 | 13395.68 | 210368.04 | 384903.96 |
| 8" RHR[6,9] | 1 | 2060 | -18937.3 | 12011.71 | 53102.08 | 389330.52 |
| 6" Draindown[6,9] | 1 | 720 | -2779.48 | 1886.99 | 10565.43 | 47571.04 |
| 6" SI | 2 | 570 | -316.20 | 1157.53 | 10833.93 | 20529.94 |
| 6" SI | 2 | 834 | -292.17 | 731.11 | 12336.26 | 20257.57 |
| 6" SI[7,9] | 2 | 558 | -359.17 | 596.46 | 5234.93 | 10926.00 |
| 12" SI | 2 | 240 | -6803.46 | 15963.99 | 474323.88 | 675871.80 |
| 12" SI[7,9] | 2 | 445 | -2813.77 | 7791.14 | 249803.04 | 410449.32 |
| 8" RHR[10] | 2 | 100 | -16059.03 | 17779.60 | 277176.84 | 379043.64 |
| 8" RHR[10] | 2 | 270 | -23430.19 | 30200.73 | 291160.68 | 709515.60 |
| 8" RHR[7,9] | 2 | 246 | -13093.29 | 22536.71 | 182469.36 | 762461.88 |
| 6" Draindown[7,9] | 2 | 7 | -2477.97 | 2316.43 | 6135.19 | 24841.42 |
| 6" Capped Nozzle[4,5,8] | 1,2 | N/A[3] | 0 | 0 | 0 | 0 |

Notes:

1. DW+TH.
2. |DW|+|TH|+|SSE| except for RHR lines for which it is |DW|+|TH|+ |SSE|+ |STRAT|.
3. Not applicable.
4. Piping restraint effect not applicable.
5. No loading except pressure (2258 psig for critical flaw size and 2235 psig for leakage) is considered.
6. Gave critical leakage values for corresponding lines for Unit 1.
7. Gave critical leakage values for corresponding lines for Unit 2.

8. Gave critical leakage value for capped nozzle for both Units 1 and 2.
9. No data available for the Uprate loads.
10. Thermal loads at hot functional condition and at operating condition are taken conservatively for critical flaw size (larger loads) and leakage (smaller loads) calculations.

Figure 4-1. Schematic of Piping Model and Selected Node Points for the 6-inch Safety Injection Piping Attached to Reactor Pressure Vessel and the Cold Leg (Unit 1 - Loops A and B)

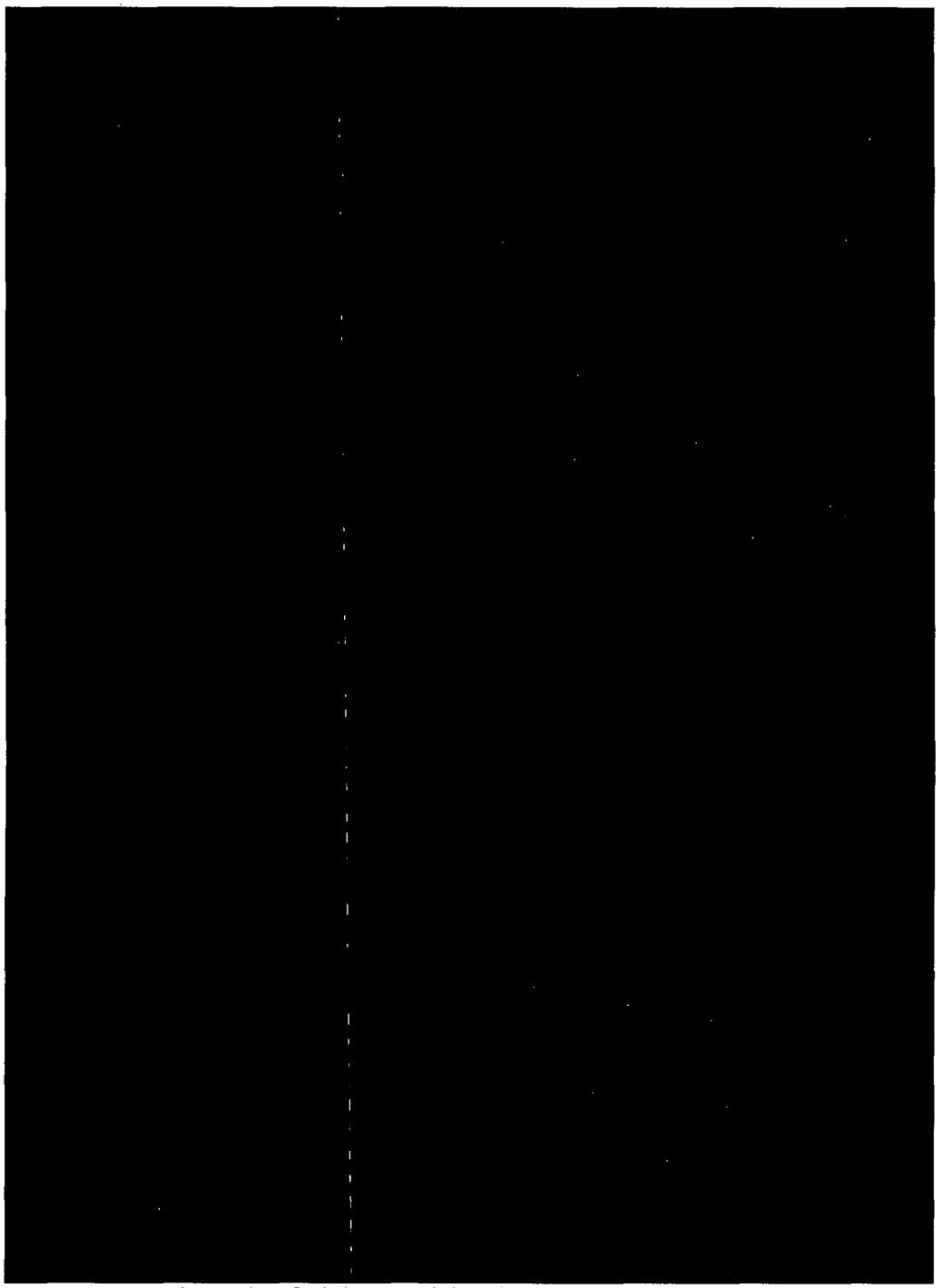

Figure 4-2. Schematic of Piping Model and Selected Node Points for the 6-inch Safety Injection Piping Attached to Reactor Pressure Vessel and the Cold Leg (Unit 2 - Loops A and B)

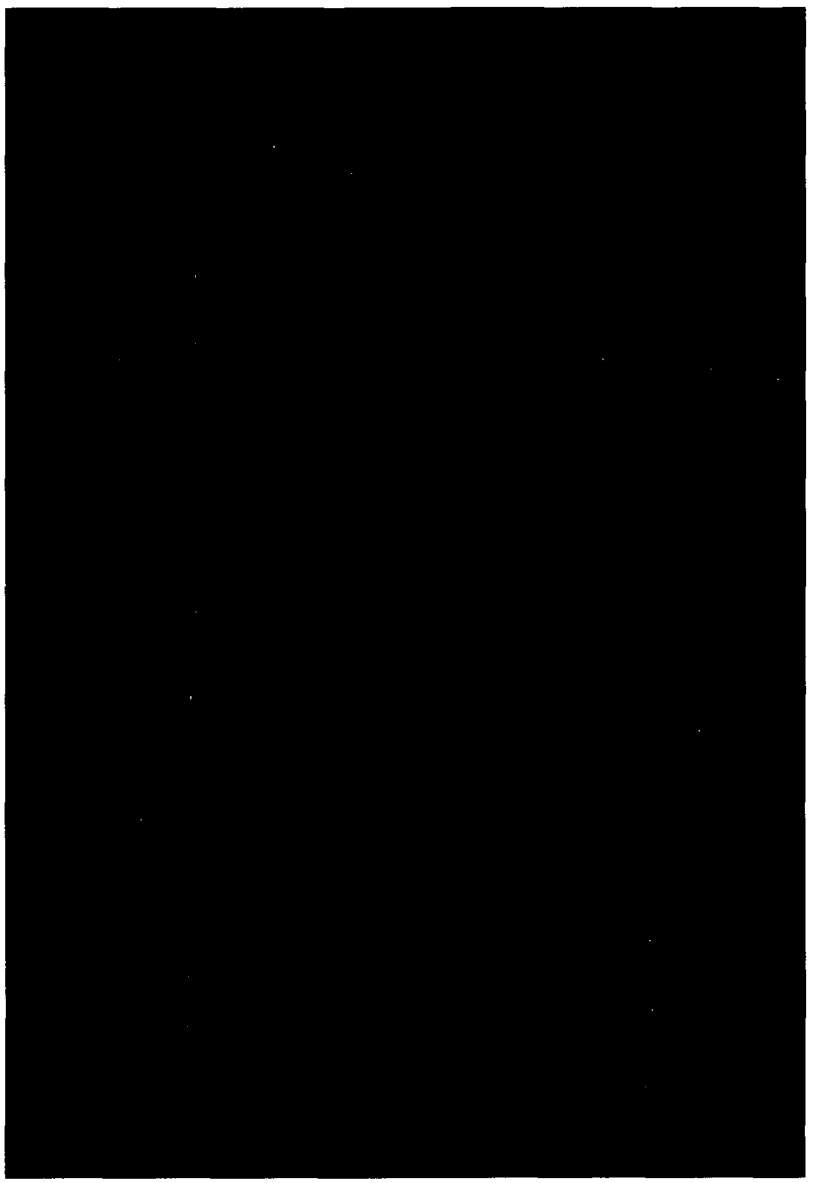

Figure 4-3. Schematic of Piping Model and Selected Node Points for the 12-inch Safety Injection Piping Attached to the Cold Leg (Unit 1 - Loops A and B)

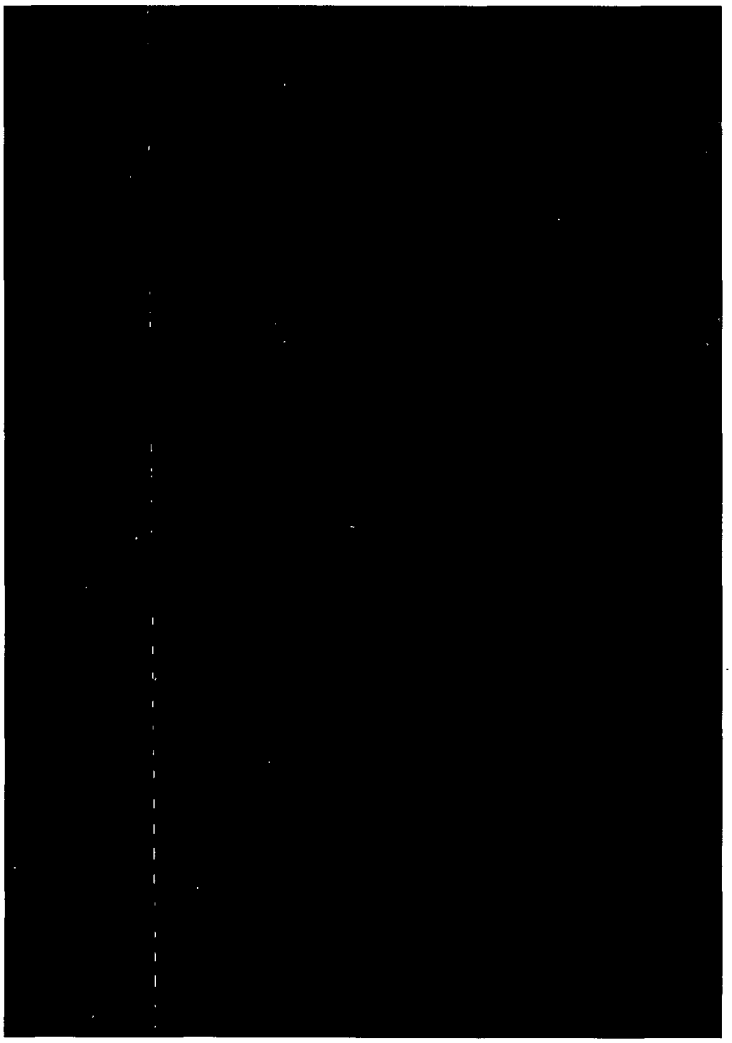

Figure 4-4. Schematic of Piping Model and Selected Node Points for the 12-inch Safety Injection Piping Attached to the Cold Leg (Unit 2 - Loops A and B)

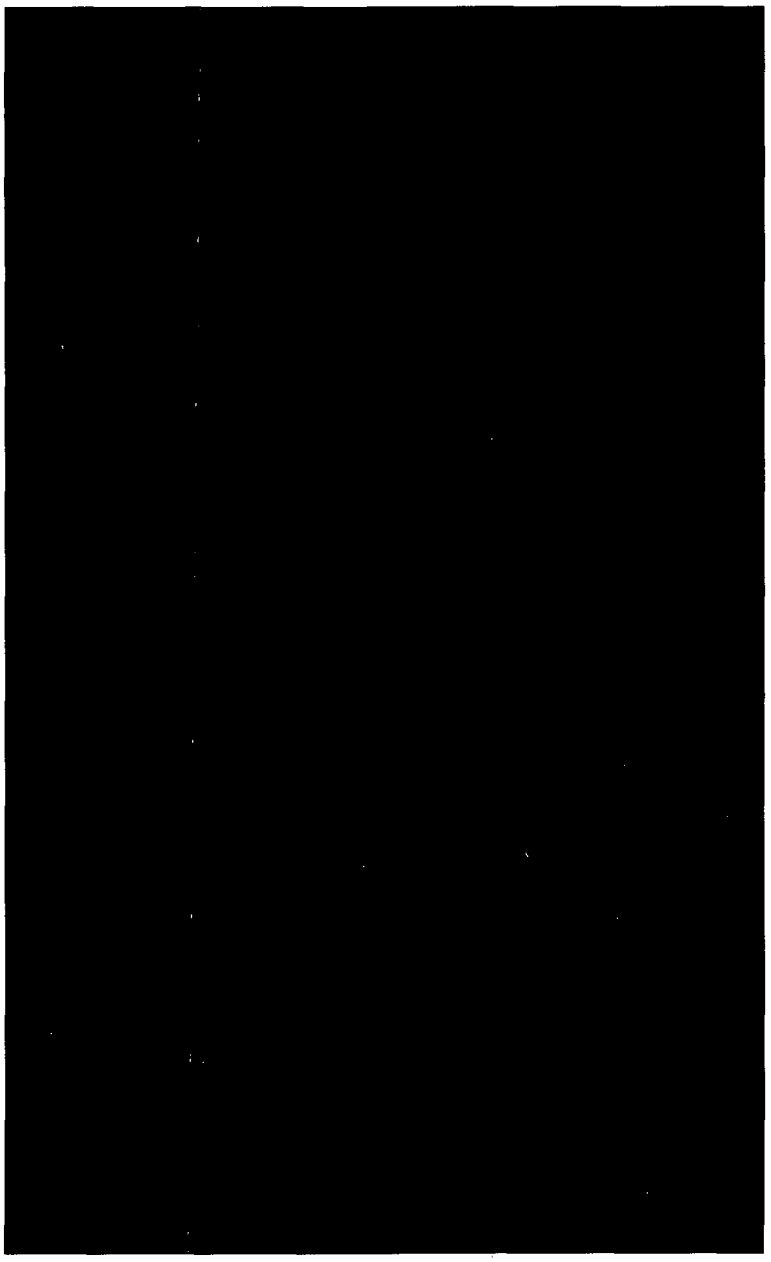

Figure 4-5. Schematic of Piping Model and Selected Node Points for the 8-inch Residual Heat Removal Piping Attached to Hot Leg (Units 1 - Loops A and B)

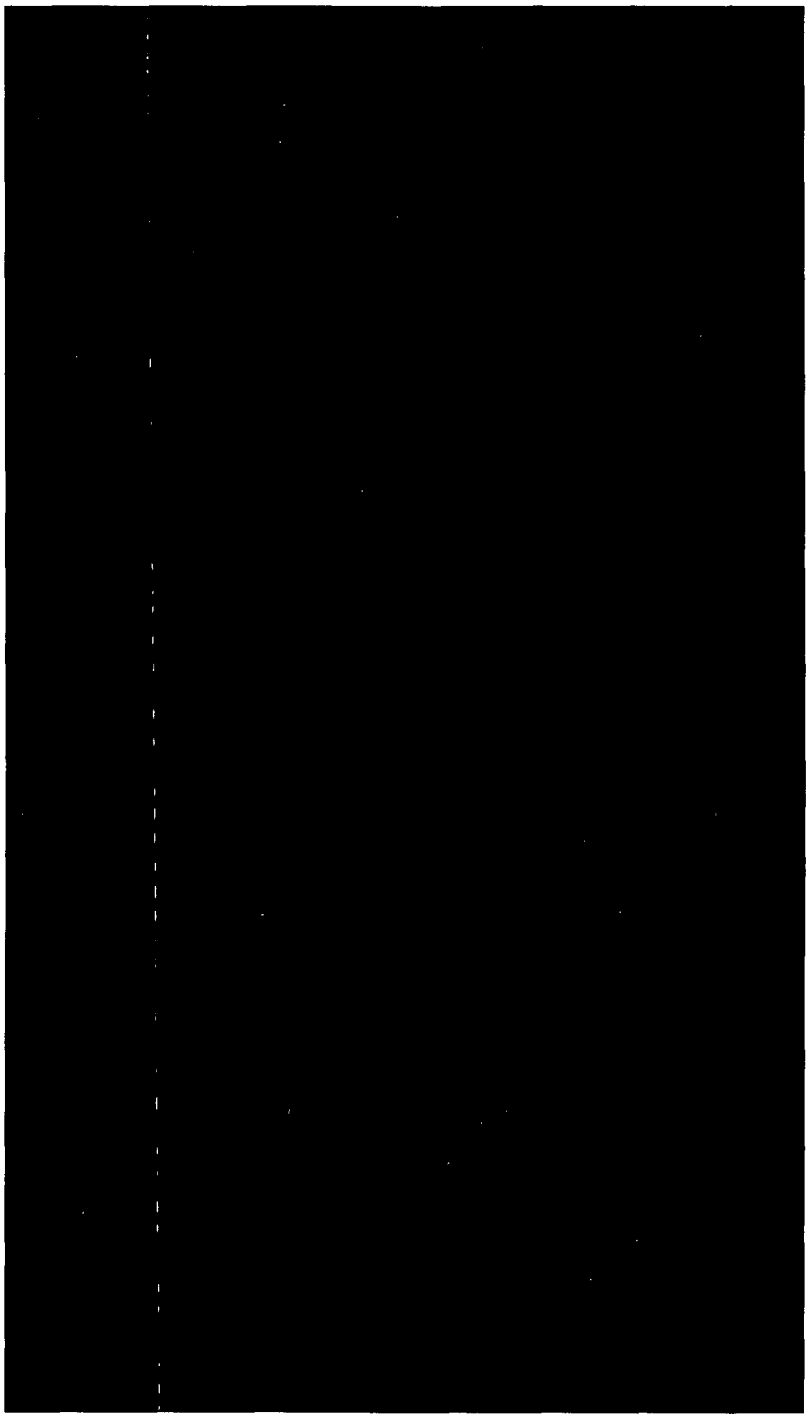

Figure 4-6. Schematic of Piping Model and Selected Node Points for the 8-inch Residual Heat Removal Piping Attached to Hot Leg (Units 2 - Loops A and B)

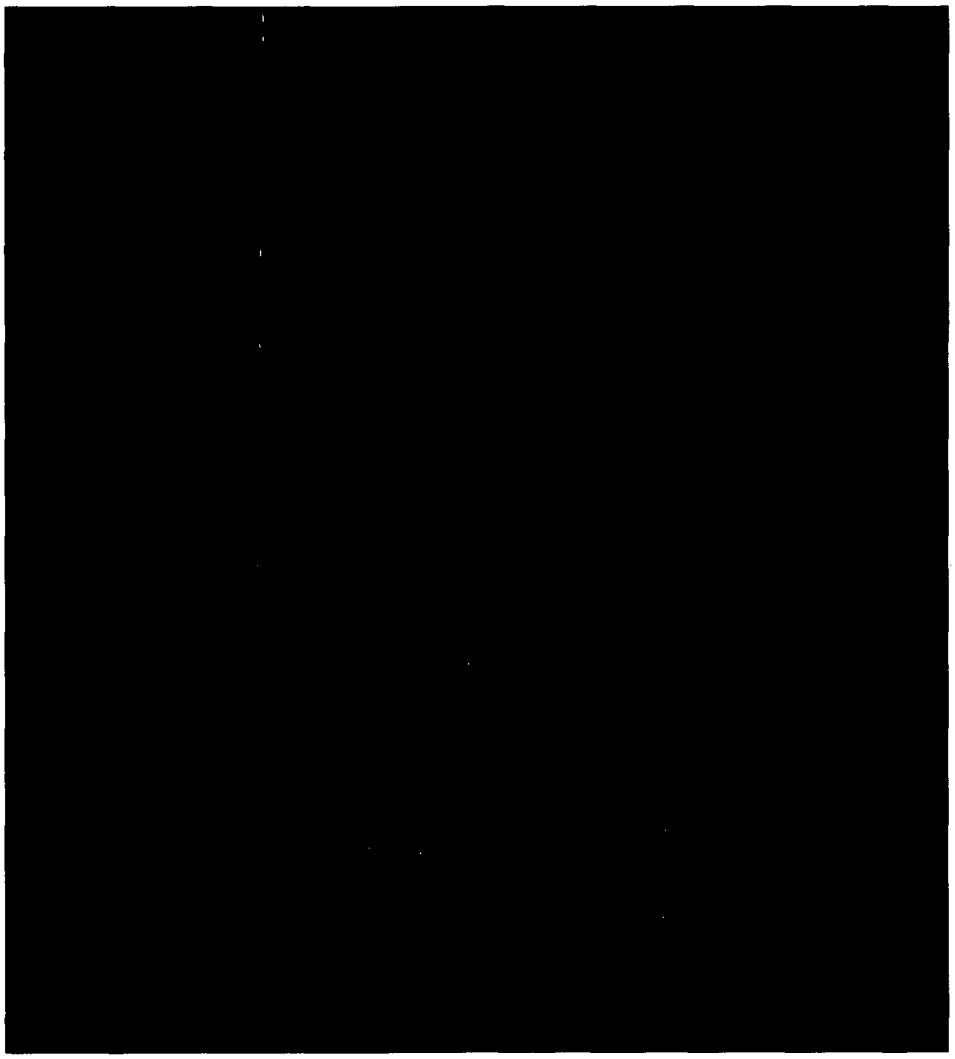

Figure 4-7. Schematic of Piping Model and Selected Node Points for the 6-inch RCS Draindown Line Attached to Hot Leg (Units 1 and 2)

## 5.0 LEAK-BEFORE-BREAK EVALUATION

The LBB approach involves the determination of critical flaw sizes and leakage through flaws. The critical flaw length for a through-wall flaw is that length for which, under a given set of applied stresses, the flaw would become marginally unstable. Similarly, the critical stress is that stress at which a given flaw size becomes marginally unstable. NUREG-1061, Vol. 3 [3] defines required margins of safety on both flaw length and applied stress. Both of these criteria have been examined in this evaluation. Circumferential flaws are more restrictive than postulated axial flaws because the critical flaw sizes for axial flaw are very long since they are affected by only pressure stress and result in large crack opening areas due to out of plane displacements. For this reason, the evaluation presented herein will be based on assumed circumferential flaws.

### 5.1 Evaluation of Critical Flaw Sizes

Critical flaw sizes may be determined using either limit load/net section collapse criterion (NSCC) approach or J-Integral/Tearing Modulus (J/T) methodology. In this evaluation, both methods were used to determine the critical flaw sizes and the most conservative result of the two methods was chosen for a given location.

#### *5.1.1 Critical Flaw Sizes Determined By J-Integral/Tearing Modulus Analysis*

A fracture mechanics analysis for determining the stability of through-wall circumferential flaws in cylindrical geometries such as pipes using the J/T approach is presented in References 21 and 22. This procedure was used for the determination of critical stresses and flaw sizes in the safety injection and RHR lines at Prairie Island, using computer program, **pc-CRACK™** [23] which has been verified under SI's Quality Assurance program.

The expression for the J-integral for a through-wall circumferential crack under tension loading [21] which is applied in this analysis is:

$$J = f_1\left(a_e, \frac{R}{t}\right)\frac{P^2}{E} + \alpha\sigma_o\varepsilon_o c\left(\frac{a}{b}\right)h_1\left(\frac{a}{b}, n, \frac{R}{t}\right)\left[\frac{P}{P_o}\right]^{n+1} \tag{5-1}$$

where

$$f_1\left(a_e, \frac{R}{t}\right) = \frac{a_e F^2\left(\frac{a}{b}, \frac{R}{t}\right)}{4\pi R^2 t^2} \tag{5-2}$$

| | | |
|---|---|---|
| $a_e$ | = | effective crack length including small scale yielding correction |
| R | = | nominal pipe radius |
| t | = | pipe wall thickness |
| F | = | elasticity factor [21, 22] |
| P | = | applied load = $\sigma_\infty$ ($2\pi Rt$); where $\sigma_\infty$ is the remote tension stress in the uncracked section |
| $\alpha$ | = | Ramberg-Osgood material coefficient |
| E | = | elastic modulus |
| $\sigma_o$ | = | yield stress |
| $\varepsilon_o$ | = | yield strain |
| 2a | = | total crack length |
| 2b | = | $2\pi R$ |
| c | = | b-a |
| $h_1$ | = | plasticity factor [21, 22] |
| $P_o$ | = | limit load corresponding to a perfectly plastic material |
| n | = | Ramberg-Osgood strain hardening exponent. |

Similarly, the expression for the J-integral for a through-wall crack under bending loading [22] is given by :

$$J = f_1\left(a_e, \frac{R}{t}\right)\frac{M^2}{E} + \alpha\sigma_o\varepsilon_o c\left(\frac{a}{b}\right)h_1\left(\frac{a}{b}, n, \frac{R}{t}\right)\left[\frac{M}{M_o}\right]^{n+1} \tag{5-3}$$

The parameters in the above equations are the same as the tension loading case except

| | | |
|---|---|---|
| $M$ | = | applied moment = $\sigma_\infty (\pi R^2 t)$ |
| $\sigma_\infty$ | = | remote bending stress in the uncracked section |
| $I$ | = | moment of inertia of the uncracked cylinder about the neutral axis |
| $M_o$ | = | limit moment for a cracked pipe under pure bending corresponding to $n = \infty$ (elastic-perfectly plastic case) |
| | = | $M_o'\left[\mathrm{Cos}\left(\frac{\gamma}{2}\right) - \frac{1}{2}\mathrm{Sin}(\gamma)\right]$ (5-4) |
| $M_o'$ | = | limit moment of the uncracked cylinder = $4\sigma_o R^2 t$ |

The Tearing Modulus (T) is defined by the expression:

$$T = \frac{dJ}{da}\frac{E}{\sigma_f^{\,2}} \tag{5-5}$$

Hence, in calculating T, J from the above expressions is determined as a function of crack size (a) and the slope of the J versus crack size (a) curve is calculated in order to determine T. (The flow stress, $\sigma_f$, is taken as the mean of the yield and ultimate tensile strengths.) The material resistance J-R curve can also be transformed into J-T space in the same manner. The intersection of the applied and the material J-T curves is the point at which instability occurs and the crack size associated with this instability point is the critical crack size.

The piping stresses consist of both tension and bending stresses. The tension stress is due to internal pressure while the bending stress is caused by deadweight, thermal and seismic loads. Because a fracture mechanics model for combined tension and bending loads is not readily available, an alternate analysis is performed to determine the critical flaw length under such loading condition using the tension and bending models separately. For the first case, the stress combination is

assumed to be entirely due to tension and the critical flaw length is determined using the tension model. For the second case, the stress combination is assumed to be entirely due to bending and the critical flaw length is determined as such. The half critical flaw sizes (lengths) obtained with the tension model ($a_t$) and the bending model ($a_b$) are combined to determine the actual half critical flaw size ($a_c$) due to a combined tension and bending stress using linear interpolation, as described by the following equation:

$$a_c = a_t \frac{\sigma_t}{\sigma_b + \sigma_t} + a_b \frac{\sigma_b}{\sigma_b + \sigma_t} \tag{5-6}$$

Where $\sigma_t$ and $\sigma_b$ are the piping tensile and bending stresses respectively.

The critical flaw sizes are determined as a function of applied moment for constant pressure stress and are presented in Tables 5-1 through 5-4. This was done so that the relationship between stress and critical flaw size can be used on a generic basis for both Prairie Island and Kewaunee. In these tables, the critical flaw length is the minimum value determined by two approaches as required by NUREG-1061, Vol. 3. In the first approach, the half critical flaw length is determined with a factor of unity on the normal + SSE stress combination. The leakage flaw total length in this case ($\ell_1$) is equal to the half critical flaw length ($a_c$). In the second approach, critical flaw length is determined with a factor of $\sqrt{2}$ on the normal + SSE stresses. The leakage flaw length in this case ($\ell_2$) is the total flaw length ($2a_c$). The final leakage flaw length is the minimum of $\ell_1$ and $\ell_2$. It was determined that the leakage flaw size based on a factor of unity on the stresses was controlling for all cases and as such are the values shown in Tables 5-1 through 5-4.

The fracture mechanics models used in the determination of the critical flaw sizes (lengths) are limited to flaw sizes of half the circumference of the pipe. For cases where the piping moments/stresses are relatively low, the critical flaw sizes are much greater than half the circumference of the pipe. As can be seen in Tables 5-1 through 5-4 and also Figures 5-2 through 5-5, an extrapolation scheme was used to determine the critical flaw sizes. In order to check the validity of the extrapolation, the critical flaw sizes were also determined by limit load analysis (to be discussed in the next section) and compared to the J/T analysis results. As shown in Figures 5-2

through 5-5, the trending of the extrapolated J/T analysis results and the limit load results is very similar, demonstrating that the extrapolation method used for the J/T analysis is reasonable. Nevertheless, both the J/T analysis and limit load analysis results are presented in this evaluation.

### *5.1.2 Critical Flaw Sizes Determined by Limit Load Analysis*

The methodology provided in NUREG-0800 [4] for calculation of critical flaw sizes by net section collapse (NSC-limit load) analysis was used to determine the critical flaw sizes. This methodology involves constructing a master curve where a stress index, SI, given by

$$SI = S + M P_m \tag{5-7}$$

is plotted as a function of postulated total circumferential through-wall flaw length, L, defined by

$$L = 2 \theta R \tag{5-8}$$

where

$$S = \frac{2 \sigma_f}{\pi} [2 \sin\beta - \sin \theta] \tag{5-9}$$

$$\beta = 0.5 [(\pi - \theta) - \pi (P_m / \sigma_f)], \tag{5-10}$$

| | | |
|---|---|---|
| $\theta$ | = | half angle in radians of the postulated throughwall circumferential flaw, |
| R | = | pipe mean radius, that is, the average between the inner and outer radius, |
| $P_m$ | = | the combined membrane stress, including pressure, deadweight, and seismic components, |
| M | = | the margin associated with the load combination method (that is, absolute or algebraic sum) selected for the analysis. Since the moments were added algebraically, a value of 1.4 recommended in Reference 4 was used. |
| $\sigma_f$ | = | flow stress for austenitic steel pipe material categories. The value of 51 ksi recommended in Reference 4 was used in this case. |

If $\theta + \beta$ from Eqs. (5-9) and (5-10) is greater than $\pi$, then

$$S = \frac{2\sigma_f}{\pi}[\sin\beta], \tag{5-11}$$

where

$$\beta = -\pi (P_m/\sigma_f) \tag{5-12}$$

The critical flaw sizes correspond to the value of $\theta$ that result is S being greater than zero from Eqs. 5-9 and 5-11.

The value of SI used to enter the master curve for base metal and TIG welds is

$$SI = M (P_m + P_b) \tag{5-13}$$

where

| | | |
|---|---|---|
| $P_b$ | = | the combined primary bending stress, including deadweight and seismic components |

The value of SI used to enter the master curve for SMAW and SAW is

$$SI = M (P_m + P_b + P_e) Z \tag{5-14}$$

where

| | | | |
|---|---|---|---|
| $P_e$ | = | combined thermal expansion stress at normal operation, | |
| Z | = | 1.15 [1.0 + 0.013 (OD-4)] for SMAW, | (5-15) |
| Z | = | 1.30 [1.0 + 0.010 (OD-4)] for SAW, | (5-16) |
| OD | = | pipe outer diameter in inches. | |

Since the loads were combined algebraically, a second evaluation was conducted with M = 1. For this case, the leakage size was determined as one half the flaw size based on the master curve. The smaller of the leakage size flaws determined from the M = 1 and M = 1.4 evaluations is the required leakage size flaw based on the limit load analysis.

In this evaluation, the SMAW parameters are used since the piping was welded using this method. The critical flaw sizes were calculated as a function of moments and presented for the various piping lines in Tables 5-5 through 5-8.

## 5.2 Leak Rate Determination

The determination of leak rate is performed using the EPRI program, PICEP [24]. The flow rate equations in PICEP are based on Henry's homogeneous nonequlibrium critical flow model [25]. The program accounts for nonequlibrium "flashing" mass transfer between liquid and vapor phases, fluid friction due to surface roughness and convergent flow paths.

Battelle Columbus and Engineering Mechanics Corporation of Columbus ($Emc^2$) have conducted research to assess the technology used in determining leakage through cracked piping with Stress Corrosion Cracking (SCC) morphology [38]. It has been determined that the crack morphology, characterized by the local roughness, number of flow path turns, and total leakage path length, is significantly different between fatigue cracking and SCC. For fatigue cracks, the flow path is relatively smooth and straight, whereas for SCC, the flow path is relatively rough and consists of many turns. A procedure has been proposed in NUREG/CR-6300 [37] that defines the surface roughness, effective flow path length and number of flow path turns as a function of the ratio of the crack opening displacement (COD, $\delta$) to the global roughness ($\mu_G$) of the flow path. For very tight cracks, there is a relatively longer flow path with many local turns, but the local roughness ($\mu_L$)is relatively lower. For cracks with a larger opening, the roughness is better represented by the global roughness but the number of turns and effective flow path length decrease. Although not confirmed by testing or detailed fluid mechanics analysis, this model is a reasonable representation of the morphology effects on leakage flow due to SCC.

For defining the crack morphology, the model proposed by Battelle is considered that takes into account both global roughness μG and the local roughness μL as illustrated in Figure 5-11 [37].

These are then combined with δ, the COD, by the following set of equations to develop an effective roughness μ.

$$\mu = \begin{cases} \mu_L, & 0.0 \le \dfrac{\delta}{\mu_G} < 0.1 \\ \mu_L + \dfrac{\mu_G - \mu_L}{9.9}\left[\dfrac{\delta}{\mu_G} - 0.1\right], & 0.1 \le \dfrac{\delta}{\mu_G} \le 10 \\ \mu_G, & \dfrac{\delta}{\mu_G} > 10 \end{cases}$$

A similar set of equations is developed to determine the effective number of turns (NT), with the assumption that the number of turns decreases to about 0.1 of the local number of turns, (NL) when the crack opening displacement is equal to or greater than 10 times the global roughness.

$$n_t = \begin{cases} n_{tL}, & 0.0 \le \dfrac{\delta}{\mu_G} < 0.1 \\ n_{tL} - \dfrac{n_{tL}}{11}\left[\dfrac{\delta}{\mu_G} - 0.1\right], & 0.1 \le \dfrac{\delta}{\mu_G} \le 10 \\ 0.1 n_{tL}, & \dfrac{\delta}{\mu_G} > 10 \end{cases}$$

Similarly, the total flow path length is increased due to the crack being skewed relative to the pipe wall and due to the turns within the material, as shown in Figure 5-10. Then, the ratio between the total flow path length La and the pipe wall thickness t is determined by:

$$\frac{L_a}{t} = \begin{cases} K_{G+L}, & 0.0 \le \frac{\delta}{\mu_G} < 0.1 \\ K_{G+L} - \frac{K_{G+L}-K_G}{9.9}\left[\frac{\delta}{\mu_G}-0.1\right], & 0.1 \le \frac{\delta}{\mu_G} \le 10 \\ K_G, & \frac{\delta}{\mu_G} > 10 \end{cases}$$

The EPRI-developed computer program PICEP [24] is not configured to directly include the methods for computing morphology using the interpolation method proposed in NUREG/CR-6300[37]. To determine the effects of crack morphology on leakage flaw sizes, additional calculations can be conducted using PICEP with input revised to simulate SCC morphology.

In PICEP, the number of turns can be simulated by adding an equivalent L/D=26 for 45-degree turns and L/D=50 for 90-degree turns. These equivalent additional lengths are appropriate for use determining pressure drops through typical piping components. However, when the roughness (ε) is increased to be large comparable to the hydraulic diameter (DH), the effect of the number of turns is further amplified since it is multiplied by an increased friction factor (f).

To determine input to PICEP to simulate a crack with both fatigue and Stress Corrosion Cracking morphologies, an equivalent number of turns and equivalent roughness are determined. The method is based on the fact that the flow resistance along a flow path is made up of the friction resistance and the discontinuity (i.e., turns) resistance. The pressure differential is determined by multiplying the sum of the friction (fL/D) and discontinuity (K) loss factors by the velocity pressure in the flow path.

In PICEP, the turns and friction resistance are lumped together.

$$\text{Loss Factor} = f\,(t/D_h + 50N_{90}) \text{ for 90 degree turns}$$

$$= f\,(t/D_h + 26N_{45}) \text{ for 45 degree turns}$$

where,

$f$ = friction factor

$= (2 \log (D_H/2\,\varepsilon) + 1.74)^{-2}$ [24]

$\varepsilon$ = roughness (defined as $\mu$ by Battelle)

t = pipe wall thickness

$N_{90}$, $N_{45}$ = number of 90-degree or 45-degree turns in leak path

$D_h$ = hydraulic diameter = 4 $A/W_p$

A = flow path cross-section area

$W_p$ = wetted perimeter of flow path cross-section area.

($D_h = \pi/2$ COD for an elliptical crack where COD is the center point crack opening displacement)

For flow through a complex crack consisting of a cracked weld followed by a cracked overlay, there will similarly be losses due to friction and turns. To simulate this in PICEP, an equivalent friction factor must be determined that will yield the same friction as for the complex crack case.

$$f_{eq}(t/D_h) = \Sigma\, f_i\, (L_{ai}/D_h)$$

where,

$f_i$ = friction factor for the revised roughness for each crack face

$L_{ai}$ = revised flow path length for each crack face

For input to PICEP, the equation above for the friction factor can be used to solve for an equivalent roughness that will produce the correct loss factor.

The equivalent number of turns can be similarly determined.

$$f\,(50N_{90}) = \Sigma\, N'_i\, L_{ai}\, K_{90}$$

where,

$N'_i$ = number of 90-degree turns per unit flow path length for each crack face

$K_{90}$ = loss coefficient (number of velocity heads) for each 90-degree turn

Thus, the number of turns to be used in a PICEP analysis can be determined by:

$$N_{PICEP\text{-}90} = 0.02\ (\Sigma\ N'_i\ L_{ai}\ K_{90}\ )\ /\ f_{eq}$$

where,

N′ = number of 90° turns per inch predicted for a specific crack morphology

L = total flow path length = t x $K_{G+L}$ (See flow path length equation earlier this Section)

Similarly, the number of 45-degree turns to input in a PICEP run can be determined as:

$$N_{PICEP-45} = N_{PICEP-90} \times \frac{50}{26}$$

In the determination of leak rates using PICEP, the following assumptions are made:

- A plastic zone correction is included. This is consistent with fracture mechanics principles for ductile materials.
- The crack is assumed to be elliptical in shape. This is the most common approach that is available in PICEP for calculations of leakage.
- A sharp-edged entrance loss factor of 0.61 is used (PICEP default).
- The default friction factors of PICEP are utilized.

The parameters used for fatigue morphology are listed below [39] and applied in leakage calculation in Originally Licensed Thermal Power (OLTP) considering only RHR Normal Thermal:

| | | |
|---|---|---|
| $\mu_L$ | = | 0.00197 |
| $\mu$ | = | 0.00197 |
| $N_{90}$ | = | 0 |
| $L_G/t$ | = | 1.000 |
| L/t | = | 1.000 |

, where

| | | |
|---|---|---|
| $\mu_L$ | = | Local roughness, inches |
| $\mu_G$ | = | Global roughness, inches |
| $N_{90}$ | = | Number of 90 degree turns per inch |
| $L_G/t$ | = | Global flow path length to thickness ratio |
| L/t | = | Global plus local flow path length to thickness ratio |

Stress Corrosion Cracking morphology are considered for sensitivity study under Uprate Conditions and RHR Thermal Stratification, even though the piping systems under consideration

are not known to be susceptible to SCC in PWR environment. Normally intergranular stress corrosion cracking (IGSCC) has more adverse morphology, which produces more conservative leakage than transgranular stress corrosion cracking (TGSCC), thus, IGSCC crack morphology is chosen to study the sensitivity of leakage to crack morphology. And since Primary Water Stress Corrosion Cracking, or PWSCC, is a form of IGSCC that occurs in the PWR primary water environment. PWSCC crack morphology parameters [38], shown below, are used for the sensitivity study:

$$\mu_L = 0.00663778$$
$$\mu = 0.0044842$$
$$N_{90} = 150.87$$
$$L_G/t = 1.009$$
$$L/t = 1.243$$

The leakage was calculated at operating temperature and pressure for Originally Licensed Thermal Power (OLTP) considering only RHR Normal Thermal and Uprate Conditions considering RHR Thermal Stratification, using location-unique moments and material properties. For each location, the leakage flaw size was determined based on the information provided in Tables 5-1 through 5-4 for EPFM analysis and also Table 5-5 through 5-8 for net section collapse analysis using the actual moments at each location. The leakage was then determined using the normal operating moment at each location.

## 5.3 Effect of Piping Restraint on LBB Evaluation

In NUREG/CR-6443 [27], a study was performed which showed that restraint of pressure induced bending in a piping system has an effect on LBB analysis results. This was shown to be especially important for small diameter piping such as those being considered for Prairie Island. In this section, an evaluation is performed to assess the impact of the piping restraint on the LBB evaluation.

Recall that the above determination of critical flaw sizes and leakage rates assumes that the pipe is free to displace. With a crack in an unrestraint pipe, there is localized bending of the pipe concentrated in the crack region. This results in a "kink angle" which can be described as a

change in direction of the straight pipe due to the presence of the crack. However, all the piping systems considered in this LBB evaluation are restrained to varying degrees. The opening of the crack and the resulting localized kink angle is resisted by the piping restraints, resulting in a bending moment at the crack location that is in the opposite direction of the kink angle. The presence of the restraint in a flawed piping has two effects.

1) There is a restraint of pressure induced bending for a crack in the piping system. If the pipe is free to displace, a bending moment is developed for a pipe under axial load (resulting from pressure) which is equal to the load times eccentricity (distance from center of the crack plane to the center of the pipe). In a restrained piping system, this induced bending can be restrained resulting in an increased load capacity for the flawed piping (i.e., the critical flaw size increases).

2) The restraint of the bending moment decreases the crack opening displacement and hence reduces the leakage that would have otherwise been calculated.

The effect of these two factors is what effectively introduces a bending moment in the piping system which is in opposite direction to that of the thermal restraint bending moment. This is illustrated in Figure 5-6. The uncracked pipe is shown in 5-6 (a). In 5-6 (b), the piping is shown with a crack that creates the local slope discontinuities.. Here, it is assumed that there is no constraint and the piping freely displaces. In 5-6 (c), the restraint is added, causing a crack-closing moment to occur.

In LBB evaluation, the effects of restraint increasing critical flaw sizes and reducing leakage have compensating effects. However, the exact contribution of each factor cannot be easily quantified in order to determine if the results of the LBB evaluations presented above will be affected. As such, an evaluation is performed using some of the representative piping systems at Prairie Island and Kewaunee to determine the affect of restraint on the LBB evaluation results. To select the lines to use in this analysis, a set of simple criteria was adopted.

1) Compare the similarity of the geometrical configurations of the lines

2) Use thermal anchor stresses as a measure of overall piping system restraint and select the piping lines with the highest thermal stresses at the anchor locations.

Based on the criteria above, it was concluded that all six 8-inch RHR lines are similar enough in geometry that the line with the highest thermal anchor stresses (Prairie Island Unit 1, Loop A) can be conservatively used to represent all the RHR lines. Similar conclusions were reached for the 6-inch SI lines attached to the cold leg, and hence, the Kewaunee, Loop B line was used. The 6-inch draindown line in Prairie Island Unit 2 was used for the evaluation.

The evaluation consists of first modeling the piping lines and then applying a kink angle at all weld locations from the LBB analyses. This process resulted in applied moments at each location that could be used in assessing leakage rate reduction. The three selected piping lines were modeled as PIPE16 elements using the ANSYS computer code [28]. All three models were bounded by two anchors, one of them being the connection to the RCS system. The other was placed at a significant distance away from welds of interest. The piping models used in the analysis are shown in Figures 5-7 through 5-9.

The kink angle was determined using the methodology in NUREG/CR-4572 [29], and is given by:

$$\varphi = \frac{\sigma_f}{E}\left[S_b I_b(\theta_e) + S_t I_t(\theta_e)\right]\left[1 + \alpha'(S_b + S_t)^{n-1}\right] \tag{5-17}$$

where:

$\sigma_f$ = flow stress $\equiv 0.5(\sigma_u+\sigma_y)$ = Average of ultimate and yield strength of the material, ksi

E = Young's modulus in ksi,

$S_b = \sigma_b/\sigma_f$ = normalized bending stress,

$S_t = \sigma_t/\sigma_f$ = normalized tensile stress,

$I_b$ and $I_t$ are compliance functions given in Appendix B of Reference 29,

$\theta_e$ = effective half-crack angle corrected for plastic zone size, in radians, described below,

$\alpha' = \alpha(\sigma_f/\sigma_o)^{n-1}$

$\alpha$ and n are Ramberg-Osgood parameters, described below.

The plastic stress-strain behavior is represented in the Ramberg-Osgood form (Eq. 2.18 in [29]),

$$\frac{\varepsilon}{\varepsilon_o} = \frac{\sigma}{\sigma_o} + \alpha\left(\frac{\sigma}{\sigma_o}\right)^n \tag{5-18}$$

where:

| | | |
|---|---|---|
| $\sigma$ | = | $\sigma_b+\sigma_t$, |
| $\sigma_0$ | = | reference stress used in determining the Ramberg-Osgood constants, usually $\sigma_y$, |
| $\varepsilon_0$ | = | $\sigma_0/E$, |

$\alpha$ and n are material parameters obtained from curve-fitting to tensile test results.

The effective half-crack angle ($\theta_e$) corrected for plastic zone size is (Eq. 2.8 in [29]):

$$\theta_e = \frac{K^2}{\pi R \sigma_f{}^2 \beta} + \theta_o \tag{5-19}$$

where:

| | | |
|---|---|---|
| $\theta_0$ | = | a/R = original crack size, |
| a | = | circumferential crack length, |
| R | = | mean radius of the pipe, |
| K | = | stress intensity factor (Eq. 2.2 in [29]), i.e., |

$$K = \sqrt{\pi R \theta_o}\,(\sigma_t F_t(\theta_o) + \sigma_b F_b(\theta_o)) \tag{5-20}$$

| | | |
|---|---|---|
| $F_t$ | = | geometry factor for tension (See Appendix A of Reference 29), |
| $F_b$ | = | geometry factor for bending (See Appendix A of Reference 29), |

$\beta$ = 2, for plane stress condition, parameter in Irwin plastic zone correction (Eq. 2.4 in [29])

The kink angle was applied individually at all weld locations from the LBB analysis on the piping lines considered in the analysis. At each weld location, the kink angle is applied in four different directions (0°, 45°, 90°, and 135°) simulating different possible locations of a crack at that location.

The resulting moments due to the introduction of the kink angles at the various weld locations on the various lines is summarized in Tables 5-18 through 5-20. These moments act in the opposite direction to the thermal restraint moments and were therefore subtracted from the moments used in calculating the leakage rate. The resulting leakage rates for the three lines considered in this analysis are shown in Tables 5-21 through 5-23. In comparing these results to those presented in Tables 5-9 through 5-17, it can be seen that the effect of the restraint did not change the leakage rate significantly for the 6-inch piping. However, the leakage for the 8-inch pipe was reduced by approximately 13%. This is a conservative estimate of leakage reduction since no credit was taken for the effects of restraint on increasing the critical flaw sizes. These results are consistent with the conclusions in a similar study in Reference 33.

## 5.4 LBB Evaluation Results and Discussions

### *5.4.1 Originally Licensed Thermal Power (OLTP) considering only RHR Normal Thermal*

Tables 5-9 through 5-17 show the predicted leakage for the leakage flaw length for each location under Originally Licensed Thermal Power (OLTP) considering only RHR Normal Thermal using fatigue morphology. In all cases, the leakage for cracks determined with net section collapse analyses was less than the leakage for cracks determined using J/T analysis. The leakage associated with net section collapse analyses is therefore conservatively used in the LBB evaluation.

It can be seen from Tables 5-9 through 5-17 that the limiting leakage is obtained from the limit load evaluation. Without the consideration of piping restraint effect, the predicted leakage range for all the lines considered in this evaluation are summarized below.

| | | |
|---|---|---|
| 6-inch Safety Injection Attached to RPV and Cold Leg | Unit 1 | 4.60 – 5.27 gpm |
| | Unit 2 | 4.91 – 5.71 gpm |
| 6-inch Draindown Line Attached to Hot Leg | Unit 1 | 3.94 – 3.97 gpm |
| | Unit 2 | 3.88 – 3.90 gpm |
| 8-inch RHR Line Attached to Hot Leg | Unit 1 | 6.96 – 11.20 gpm |
| | Unit 2 | 3.78 – 11.73 gpm |
| 12-inch Safety Injection Line Attached to Cold Leg | Unit 1 | 22.42 – 26.98 gpm |
| | Unit 2 | 22.63 – 26.67 gpm |
| 6-inch Hot Leg Capped Nozzles | Units 1/2 | 3.74 gpm |

The piping restraint has no significant impact on the predicted leakages for the 6-inch safety injection and draindown lines. At the worst location, piping restraint produced about 13% reduction of the leak rate on the 8-inch RHR line. The minimum leakage is 3.78 gpm associated with the 8-inch RHR piping without the consideration of the piping restraint effect. If this effect is taken into account, it is expected that the leakage would reduce to 3.4 gpm. This is well above the required leak detection of 2.0 gpm for Prairie Island as discussed in Section 1.3 of this report thereby justifying LBB for all the piping considered in this evaluation.

### *5.4.2 Uprate Conditions considering RHR Thermal Stratification*

Table 5-24 and Table 5-25 show the predicted leakage under Uprate Conditions considering RHR Thermal Stratification using fatigue morphology and PWSCC morphology, respectively. Note that the leak rates calculated by PICEP using fatigue crack morphology are given at a default pipe outlet temperature of 200°F whereas, in general the sump where the leaked fluid is collected temperature is at 120 °F. Therefore, the fluid collected at the sump will be slightly less than that exiting from the pipe. This is incorporated in Table 5-24. Also, a 13% reduction of the leak rate due to piping restraint is considered for all the lines for the leakage at the sump temperature.

As shown in Table 5-24, the minimum leakage is 2.44 gpm associated with the 8-inch RHR piping without the consideration of the piping restraint effect. If this effect is taken into account, it is expected that the leakage would reduce to 2.12 gpm. This is well above the 2.0 gpm required leakage detection at Prairie Island. Therefore, LBB is still applicable under Uprate Conditions considering RHR Thermal Stratification load for all the piping considered in this report.

Hypothetical flaws due to PWSCC morphology have also been evaluated, with the leakage results reported in Table 5-25. Comparing Table 5-25 with Table 5-24, it shows that using the PWSCC morphology, leakage reduced to as low as 22% of the leakage using fatigue morphology. It is recognized that there have been some instances of SCC in recent PWR plant operations. However, it is highly unlikely that the RCS-attached piping systems at PI would be affected. There are no Alloy 82/182 weldments in the piping being evaluated for LBB in this report. The occurrence of TGSCC such as that which has occurred in CEDMs at Palisades is not expected at PI since the water in the RCS-attached lines is free to communicate with the RCS such that high levels of oxidants cannot concentrate. On the other hand, the piping systems at all nuclear plants are affected by cyclic stresses due to normal operating pressure and thermal expansion loadings. Because these stresses could potentially contribute to growth of cracks, fatigue crack growth was addressed in Section 6.0. It was shown that the current Section XI ISI program at PI can be used to assure that growth of any potential cracks in the subject lines can be readily detected.

Since SCC cracks are of such a low probability and the only credible growth mechanism is due to cyclic stresses and fatigue crack growth, fatigue crack morphology has typically been the basis of LBB evaluations.

Table 5-1. Leakage Flaw Size Versus Stress Determined by J/T Analysis for 6-inch Safety Injection Lines Attached to RCS Cold Leg (Temperature = 550°F)

| **Total Stress, $\sigma_T$, ksi** | **Bending Stress, $\sigma_b$, ksi** | **Tension Stress, $\sigma_t$, ksi** | **Bending Moment, in-kips** | **Leakage Flaw Size** (a), inches** |
|---|---|---|---|---|
| 3.55 | 0.00 | 3.55 | 0.0 | 2.81* |
| 3.83 | 0.28 | 3.55 | 5.0 | 2.79* |
| 4.11 | 0.56 | 3.55 | 10.0 | 2.77* |
| 5.24 | 1.69 | 3.55 | 30.0 | 2.69* |
| 6.36 | 2.81 | 3.55 | 50.0 | 2.60* |
| 7.48 | 3.93 | 3.55 | 70.0 | 2.52* |
| 8.60 | 5.05 | 3.55 | 90.0 | 2.44* |
| 9.17 | 5.62 | 3.55 | 100.0 | 2.40* |
| 9.73 | 6.18 | 3.55 | 110.0 | 2.36* |
| 10.29 | 6.74 | 3.55 | 120.0 | 2.32* |
| 10.85 | 7.30 | 3.55 | 130.0 | 2.27* |
| 11.0 | 7.45 | 3.55 | 132.7 | 2.26* |
| 12.0 | 8.45 | 3.55 | 150.5 | 2.19 |
| 13.0 | 9.45 | 3.55 | 168.3 | 2.12 |
| 14.0 | 10.45 | 3.55 | 186.1 | 2.04 |

* Linearly extrapolated values
** Leakage flaw size (a) is one half the total flaw length.

Table 5-2. Leakage Flaw Size Versus Stress Determined by J/T Analysis for 12-inch Safety Injection Lines Attached to RCS Cold Leg (Temperature = 550°F)

| Total Stress, $\sigma_T$, ksi | Bending Stress, $\sigma_b$, ksi | Tension Stress, $\sigma_t$, ksi | Bending Moment, in-kips | Leakage Flaw Size** (a), inches |
|---|---|---|---|---|
| 3.82 | 0.00 | 3.82 | 0.00 | 5.39* |
| 4.23 | 0.41 | 3.82 | 50.00 | 5.32* |
| 4.63 | 0.82 | 3.82 | 100.00 | 5.26* |
| 5.45 | 1.63 | 3.82 | 200.00 | 5.14* |
| 6.27 | 2.45 | 3.82 | 300.00 | 5.02* |
| 7.08 | 3.26 | 3.82 | 400.00 | 4.90* |
| 7.90 | 4.08 | 3.82 | 500.00 | 4.78* |
| 8.71 | 4.90 | 3.82 | 600.00 | 4.66* |
| 9.53 | 5.71 | 3.82 | 700.00 | 4.54* |
| 10.35 | 6.53 | 3.82 | 800.00 | 4.42* |
| 11.00 | 7.18 | 3.82 | 880.00 | 4.32* |
| 12.00 | 8.18 | 3.82 | 1002.54 | 4.18 |
| 13.00 | 9.18 | 3.82 | 1125.07 | 4.03 |
| 14.00 | 10.18 | 3.82 | 1247.60 | 3.89 |
| 14.50 | 10.68 | 3.82 | 1308.86 | 3.82 |

* Linearly extrapolated values
** Leakage flaw size (a) is one half the total flaw length.

Table 5-3. Leakage Flaw Size Versus Stress Determined by J/T Analysis for 8-inch RHR Lines Attached to RCS Hot Leg (Temperature = 607.4°F)

| Total Stress, $\sigma_T$, ksi | Bending Stress, $\sigma_b$, ksi | Tension Stress, $\sigma_t$, ksi | Bending Moment, in-kips | Leakage Flaw Size** (a), inches |
|---|---|---|---|---|
| 4.32 | 0.00 | 4.32 | 0.00 | 3.63* |
| 5.02 | 0.70 | 4.32 | 25.00 | 3.56* |
| 5.72 | 1.40 | 4.32 | 50.00 | 3.49* |
| 6.14 | 1.82 | 4.32 | 65.00 | 3.44* |
| 6.50 | 2.18 | 4.32 | 77.81 | 3.40* |
| 8.00 | 3.68 | 4.32 | 131.28 | 3.25* |
| 9.00 | 4.68 | 4.32 | 166.93 | 3.14* |
| 10.00 | 5.68 | 4.32 | 202.57 | 3.04* |
| 11.00 | 6.68 | 4.32 | 238.22 | 2.93 |
| 11.50 | 7.18 | 4.32 | 256.04 | 2.88 |
| 12.00 | 7.68 | 4.32 | 273.87 | 2.83 |
| 12.50 | 8.18 | 4.32 | 291.69 | 2.78 |
| 14.00 | 9.68 | 4.32 | 345.16 | 2.63 |
| 15.00 | 10.68 | 4.32 | 380.80 | 2.54 |
| 16.50 | 12.18 | 4.32 | 434.27 | 2.41 |
| 17.50 | 13.18 | 4.32 | 469.92 | 2.32 |
| 18.00 | 13.68 | 4.32 | 487.74 | 2.28 |

* Linearly extrapolated values
** Leakage flaw size (a) is one half the total flaw length.

Table 5-4. Leakage Flaw Size Versus Stress Determined by J/T Analysis for 6-inch Draindown Lines and Nozzles Attached to RCS Hot Leg (Temperature = 607.4°F)

| Total Stress, $\sigma_T$, ksi | Bending Stress, $\sigma_b$, ksi | Tension Stress, $\sigma_t$, ksi | Bending Moment, in-kips | Leakage Flaw Size** (a), inches |
|---|---|---|---|---|
| 3.55 | 0.00 | 3.55 | 0.0 | 2.89* |
| 3.83 | 0.28 | 3.55 | 5.0 | 2.87* |
| 4.11 | 0.56 | 3.55 | 10.0 | 2.85* |
| 5.24 | 1.69 | 3.55 | 30.0 | 2.75* |
| 6.36 | 2.81 | 3.55 | 50.0 | 2.65* |
| 7.48 | 3.93 | 3.55 | 70.0 | 2.56* |
| 8.60 | 5.05 | 3.55 | 90.0 | 2.46* |
| 9.17 | 5.62 | 3.55 | 100.0 | 2.41* |
| 9.73 | 6.18 | 3.55 | 110.0 | 2.36* |
| 10.29 | 6.74 | 3.55 | 120.0 | 2.31* |
| 10.85 | 7.30 | 3.55 | 130.0 | 2.27* |
| 11.00 | 7.45 | 3.55 | 132.7 | 2.25 |
| 12.00 | 8.45 | 3.55 | 150.5 | 2.17 |
| 13.00 | 9.45 | 3.55 | 168.3 | 2.09 |

* Linearly extrapolated values.
** Leakage flaw size (a) is one half the total flaw length.

Table 5-5. Leakage Flaw Size Versus Stress Determined by Limit Load for 6-inch Safety Injection Lines Attached to RCS Cold Leg (Temperature = 550°F)

| Moment, in-kips | Leakage Flaw Size (a)*, inches |
|---|---|
| 0 | 2.710 |
| 18.6 | 2.619 |
| 37.2 | 2.534 |
| 55.8 | 2.452 |
| 74.5 | 2.377 |
| 93.1 | 2.304 |
| 111.7 | 2.236 |
| 130.3 | 2.170 |
| 148.9 | 2.106 |
| 167.5 | 2.044 |
| 186.1 | 1.986 |

* Leakage flaw size (a) is one half the total flaw length.

Table 5-6. Leakage Flaw Size Versus Stress Determined by Limit Load for 12-inch Safety Injection Lines Attached to RCS Cold Leg (Temperature = 550°F)

| Moment, in-kips | Leakage Flaw Size (a)*, inches |
|---|---|
| 0.0 | 5.111 |
| 130.9 | 4.926 |
| 261.8 | 4.753 |
| 392.7 | 4.594 |
| 523.5 | 4.440 |
| 654.4 | 4.295 |
| 785.3 | 4.157 |
| 916.2 | 4.023 |
| 1047.1 | 3.895 |
| 1178.0 | 3.770 |
| 1308.9 | 3.650 |

* Leakage flaw size (a) is one half the total flaw length.

Table 5-7. Leakage Flaw Size Versus Stress Determined by Limit Load for 8-inch RHR Lines Attached to RCS Hot Leg (Temperature = 607.4°F)

| Moment, in-kips | Leakage Flaw Size (a)*, inches |
|---|---|
| 0.0 | 3.414 |
| 47.4 | 3.274 |
| 94.8 | 3.143 |
| 142.2 | 3.020 |
| 189.6 | 2.903 |
| 237.0 | 2.795 |
| 284.4 | 2.689 |
| 331.8 | 2.588 |
| 379.2 | 2.491 |
| 426.6 | 2.396 |
| 474.0 | 2.306 |

* Leakage flaw size (a) is one half the total flaw length.

Table 5-8. Leakage Flaw Size Versus Stress Determined by Limit Load for 6-inch Draindown Lines and Nozzles Attached to RCS Hot Leg (Temperature = 607.4°F)

| Moment, in-kips | Leakage Flaw Size (a)*, inches |
|---|---|
| 0 | 2.710 |
| 16.8 | 2.628 |
| 33.7 | 2.549 |
| 50.5 | 2.475 |
| 67.3 | 2.406 |
| 84.1 | 2.339 |
| 100.9 | 2.275 |
| 117.8 | 2.214 |
| 134.6 | 2.155 |
| 151.4 | 2.098 |
| 168.2 | 2.042 |

* Leakage flaw size (a) is one half the total flaw length.

Table 5-9. Predicted Leakage Rates for 6-inch Safety Injection lines Attached to Reactor Pressure Vessel and RCS Cold Leg (Unit 1)

| Node | Moments | | EPFM Results | | Net Section Collapse Results | |
|---|---|---|---|---|---|---|
| | NOP in-kips | NOP+SSE in-kips | Leakage Flaw Size** (a), inches | Leakage Rate, gpm | Leakage Flaw Size** (a), inches | Leakage Rate, gpm |
| 1621* | 8.78 | 19.87 | 2.730 | 5.733 | 2.613 | 4.714 |
| 1622* | 8.27 | 16.55 | 2.743 | 5.810 | 2.629 | 4.801 |
| 1630* | 17.34 | 28.18 | 2.696 | 6.217 | 2.575 | 5.104 |
| 1640A* | 18.55 | 30.55 | 2.686 | 6.230 | 2.565 | 5.108 |
| 1640B* | 17.88 | 33.78 | 2.672 | 6.038 | 2.550 | 4.929 |
| 1645* | 16.33 | 32.52 | 2.678 | 5.945 | 2.556 | 4.858 |
| 1646* | 17.46 | 34.03 | 2.671 | 5.989 | 2.549 | 4.887 |
| 1045* | 7.26 | 12.02 | 2.762 | 5.879 | 2.651 | 4.902 |
| 1040* | 3.86 | 8.34 | 2.777 | 5.676 | 2.669 | 4.757 |
| 1025 | 2.64 | 3.95 | 2.795 | 5.722 | 2.691 | 4.819 |
| 1027 | 2.77 | 4.32 | 2.794 | 5.721 | 2.689 | 4.817 |
| 1030 | 3.02 | 5.04 | 2.791 | 5.718 | 2.685 | 4.812 |
| 1031 | 3.30 | 5.87 | 2.787 | 5.715 | 2.681 | 4.804 |
| 1039A | 3.30 | 5.87 | 2.787 | 5.715 | 2.681 | 4.804 |
| 1039B | 5.44 | 14.08 | 2.753 | 5.620 | 2.641 | 4.663 |
| 1040 | 5.44 | 14.08 | 2.753 | 5.620 | 2.641 | 4.663 |
| 1045 | 7.26 | 19.55 | 2.731 | 5.597 | 2.615 | 4.600 |
| 1236 | 3.35 | 8.56 | 2.776 | 5.616 | 2.668 | 4.704 |
| 1238 | 3.70 | 8.53 | 2.776 | 5.652 | 2.668 | 4.735 |
| 1250 | 4.02 | 8.78 | 2.775 | 5.675 | 2.667 | 4.753 |
| 1259 | 4.39 | 9.38 | 2.773 | 5.689 | 2.664 | 4.762 |

Table 5-9. Predicted Leakage Rates for 6-inch Safety Injection lines Attached to Reactor Pressure Vessel and RCS Cold Leg (Unit 1) (Continued)

| Node | Moments | | EPFM Results | | Net Section Collapse Results | |
|---|---|---|---|---|---|---|
| | NOP in-kips | NOP+SSE in-kips | Leakage Flaw Size** (a), inches | Leakage Rate, gpm | Leakage Flaw Size** (a), inches | Leakage Rate, gpm |
| 1260A | 4.39 | 9.38 | 2.773 | 5.689 | 2.664 | 4.762 |
| 1260B | 8.22 | 12.86 | 2.758 | 5.945 | 2.647 | 4.951 |
| 1265 | 8.22 | 12.86 | 2.758 | 5.945 | 2.647 | 4.951 |
| 1270 | 15.14 | 19.04 | 2.733 | 6.392 | 2.617 | 5.272 |

Notes:

* These nodes are on the safety injection lines attached to the reactor pressure vessel.

** Leakage flaw size (a) is one half the total flaw length.

*** OLTP and RHR Normal Thermal Only.

Table 5-10. Predicted Leakage Rates for 12-inch Safety Injection Lines Attached to RCS Cold Leg (Unit 1)

| Node | Moments | | EPFM Results | | Net Section Collapse Results | |
|---|---|---|---|---|---|---|
| | NOP in-kips | NOP+SSE in-kips | Leakage Flaw Size* (a), inches | Leakage Rate, gpm | Leakage Flaw Size* (a), inches | Leakage Rate, gpm |
| 175 | 334.54 | 376.70 | 4.930 | 33.189 | 4.613 | 25.643 |
| 180 | 347.18 | 423.67 | 4.874 | 32.289 | 4.558 | 24.946 |
| 185A | 356.95 | 462.50 | 4.827 | 31.532 | 4.512 | 24.360 |
| 185B | 343.73 | 524.66 | 4.752 | 29.113 | 4.439 | 22.422 |
| 190 | 343.73 | 524.66 | 4.752 | 29.113 | 4.439 | 22.422 |
| 855 | 650.48 | 812.24 | 4.405 | 32.866 | 4.129 | 26.124 |
| 860A | 650.47 | 812.24 | 4.405 | 32.865 | 4.129 | 26.124 |
| 860B | 684.59 | 846.11 | 4.364 | 33.023 | 4.095 | 26.378 |
| 865 | 684.59 | 846.11 | 4.364 | 33.023 | 4.095 | 26.378 |
| 870 | 451.74 | 566.00 | 4.702 | 32.569 | 4.393 | 25.254 |
| 875 | 263.66 | 341.63 | 4.973 | 30.841 | 4.656 | 23.810 |
| 880 | 275.23 | 323.44 | 4.995 | 31.966 | 4.678 | 24.712 |
| 885 | 504.66 | 574.86 | 4.691 | 34.705 | 4.383 | 26.985 |
| 890A | 504.68 | 574.88 | 4.691 | 34.706 | 4.383 | 26.985 |
| 890B | 513.82 | 617.21 | 4.640 | 33.707 | 4.336 | 26.270 |
| 895 | 513.82 | 617.21 | 4.640 | 33.707 | 4.336 | 26.270 |
| 897 | 520.49 | 637.26 | 4.616 | 33.353 | 4.314 | 26.005 |
| 905A | 520.46 | 637.24 | 4.616 | 14.995 | 4.314 | 26.005 |
| 905B | 545.80 | 662.82 | 4.585 | 33.600 | 4.286 | 26.252 |
| 910 | 545.80 | 662.82 | 4.585 | 33.600 | 4.286 | 26.252 |

* Leakage flaw size (a) is one half the total flaw length.

*** OLTP and RHR Normal Thermal only.

Table 5-11. Predicted Leakage Rates for 8-inch RHR Lines Attached to RCS Hot Leg (Unit 1)

| Node | Moments | | EPFM Results | | Net Section Collapse Results | |
|---|---|---|---|---|---|---|
| | NOP in-kips | NOP+SSE in-kips | Leakage Flaw Size* (a), inches | Leakage Rate, gpm | Leakage Flaw Size* (a), inches | Leakage Rate, gpm |
| 2000 | 191.71 | 220.94 | 2.983 | 12.963 | 2.832 | 10.770 |
| 2005 | 153.86 | 174.83 | 3.118 | 13.178 | 2.940 | 10.640 |
| 2010A | 153.86 | 174.83 | 3.118 | 13.178 | 2.940 | 10.640 |
| 2010B | 151.93 | 169.54 | 3.133 | 13.306 | 2.953 | 10.730 |
| 2015 | 151.93 | 169.54 | 3.133 | 13.306 | 2.953 | 10.730 |
| 2020A | 151.93 | 169.54 | 3.133 | 13.306 | 2.953 | 10.730 |
| 2020B | 125.93 | 143.96 | 3.208 | 13.037 | 3.016 | 10.345 |
| 2025 | 125.93 | 143.96 | 3.208 | 13.037 | 3.016 | 10.345 |
| 2030 | 59.23 | 80.32 | 3.395 | 11.758 | 3.183 | 9.099 |
| 2035 | 201.54 | 235.61 | 2.940 | 12.742 | 2.798 | 10.702 |
| 2040A | 201.54 | 235.61 | 2.940 | 12.742 | 2.798 | 10.702 |
| 2040B | 236.90 | 268.52 | 2.844 | 12.791 | 2.725 | 11.066 |
| 2045 | 236.90 | 268.52 | 2.844 | 12.791 | 2.725 | 11.066 |
| 2050 | 195.89 | 212.72 | 3.007 | 13.547 | 2.850 | 11.200 |
| 2055 | 97.15 | 159.71 | 3.162 | 10.817 | 2.977 | 8.627 |
| 2060 | 51.41 | 146.63 | 3.200 | 8.866 | 3.009 | 6.963 |
| 2070A | 51.41 | 146.63 | 3.200 | 8.866 | 3.009 | 6.963 |
| 2070B | 55.81 | 145.12 | 3.205 | 9.153 | 3.013 | 7.189 |
| 2075 | 55.81 | 145.12 | 3.205 | 9.153 | 3.013 | 7.189 |
| 2324 | 119.22 | 236.21 | 2.938 | 9.104 | 2.797 | 7.600 |

Table 5-11. Predicted Leakage Rates for 8-inch RHR Lines Attached to RCS Hot Leg (Unit 1) (Continued)

| Node | Moments | | EPFM Results | | Net Section Collapse Results | |
|---|---|---|---|---|---|---|
| | NOP in-kips | NOP+SSE in-kips | Leakage Flaw Size* (a), inches | Leakage Rate, gpm | Leakage Flaw Size* (a), inches | Leakage Rate, gpm |
| 2326 | 122.40 | 231.84 | 2.951 | 9.398 | 2.807 | 7.823 |
| 2328A | 122.40 | 231.84 | 2.951 | 9.398 | 2.807 | 7.823 |
| 2328B | 114.43 | 202.02 | 3.039 | 10.085 | 2.875 | 8.222 |
| 2330 | 98.92 | 163.40 | 3.151 | 10.762 | 2.968 | 8.603 |
| 2332 | 74.28 | 128.34 | 3.254 | 10.769 | 3.056 | 8.460 |
| 2334 | 73.92 | 128.93 | 3.252 | 10.724 | 3.054 | 8.427 |
| 2336 | 95.71 | 143.03 | 3.211 | 11.397 | 3.018 | 9.003 |
| 2338 | 106.92 | 147.92 | 3.196 | 11.807 | 3.006 | 9.365 |
| 2340A | 106.92 | 147.92 | 3.196 | 11.807 | 3.006 | 9.365 |
| 2340B | 105.91 | 140.45 | 3.218 | 12.059 | 3.025 | 9.535 |
| 2342 | 105.91 | 140.45 | 3.218 | 12.059 | 3.025 | 9.535 |
| 2344 | 95.90 | 137.40 | 3.227 | 11.628 | 3.033 | 9.181 |
| 2346A | 95.90 | 137.40 | 3.227 | 11.628 | 3.033 | 9.181 |
| 2346B | 98.71 | 151.66 | 3.186 | 11.218 | 2.997 | 8.907 |
| 2348 | 98.71 | 151.66 | 3.186 | 11.218 | 2.997 | 8.907 |
| 2350A | 98.71 | 151.66 | 3.186 | 11.218 | 2.997 | 8.907 |
| 2350B | 103.20 | 158.90 | 3.164 | 11.163 | 2.979 | 8.905 |
| 2352 | 103.20 | 158.90 | 3.164 | 11.163 | 2.979 | 8.905 |
| 2354 | 106.54 | 166.88 | 3.141 | 11.009 | 2.959 | 8.827 |

* Leakage flaw size (a) is one half the total flaw length.

*** OLTP and RHR Normal Thermal only.

Table 5-12. Predicted Leakage Rates for 6-inch Draindown Lines Attached to RCS Hot Leg (Unit 1)

| Node | Moments | | EPFM Results | | Net Section Collapse Results | |
|---|---|---|---|---|---|---|
| | NOP in-kips | NOP+SSE in-kips | Leakage Flaw Size* (a), inches | Leakage Rate, gpm | Leakage Flaw Size* (a), inches | Leakage Rate, gpm |
| 730 | 12.80 | 20.63 | 2.794 | 5.367 | 2.610 | 3.970 |
| 720 | 11.09 | 17.92 | 2.808 | 5.336 | 2.623 | 3.941 |

* Leakage flaw size (a) is one half the total flaw length.

*** OLTP and RHR Normal Thermal only.

Table 5-13. Predicted Leakage Rates for 6-inch Safety Injection Lines Attached to Reactor Pressure Vessel and RCS Cold Leg (Unit 2)

| | Moments | | EPFM Results | | Net Section Collapse Results | |
|---|---|---|---|---|---|---|
| Node | NOP in-kips | NOP+SSE in-kips | Leakage Flaw Size** (a), inches | Leakage Rate, gpm | Leakage Flaw Size** (a), inches | Leakage Rate, gpm |
| 695* | 14.80 | 25.38 | 2.707 | 6.092 | 2.588 | 5.005 |
| 690* | 38.47 | 57.97 | 2.572 | 6.815 | 2.443 | 5.511 |
| 685B* | 38.47 | 57.97 | 2.572 | 6.815 | 2.443 | 5.511 |
| 685A* | 40.14 | 60.98 | 2.559 | 6.823 | 2.431 | 5.521 |
| 680* | 40.14 | 60.98 | 2.559 | 6.823 | 2.431 | 5.521 |
| 670* | 39.29 | 62.20 | 2.554 | 6.695 | 2.426 | 5.416 |
| 552* | 29.68 | 37.81 | 2.656 | 6.958 | 2.531 | 5.675 |
| 551* | 25.86 | 33.67 | 2.673 | 6.788 | 2.550 | 5.557 |
| 550B* | 25.86 | 33.67 | 2.673 | 6.788 | 2.550 | 5.557 |
| 550A* | 29.69 | 37.03 | 2.659 | 6.995 | 2.535 | 5.708 |
| 548* | 29.69 | 37.03 | 2.659 | 6.995 | 2.535 | 5.708 |
| 558 | 5.48 | 8.05 | 2.778 | 5.852 | 2.671 | 4.909 |
| 560 | 6.30 | 8.86 | 2.775 | 5.902 | 2.667 | 4.947 |
| 562 | 7.94 | 10.43 | 2.768 | 6.010 | 2.659 | 5.029 |
| 564 | 9.61 | 12.16 | 2.761 | 6.114 | 2.651 | 5.102 |
| 566A | 9.61 | 12.16 | 2.761 | 6.114 | 2.651 | 5.102 |
| 566B | 10.98 | 13.99 | 2.754 | 6.181 | 2.642 | 5.141 |
| 568 | 10.98 | 13.99 | 2.754 | 6.181 | 2.642 | 5.141 |
| 570 | 11.29 | 15.13 | 2.749 | 6.167 | 2.636 | 5.118 |
| 826 | 10.66 | 12.80 | 2.759 | 6.195 | 2.647 | 5.165 |
| 828 | 11.94 | 14.41 | 2.752 | 6.261 | 2.640 | 5.205 |

Table 5-13. Predicted Leakage Rates for 6-inch Safety Injection Lines Attached to Reactor Pressure Vessel and RCS Cold Leg (Unit 2) (Continued)

| Node | Moments | | EPFM Results | | Net Section Collapse Results | |
|---|---|---|---|---|---|---|
| | NOP in-kips | NOP+SSE in-kips | Leakage Flaw Size** (a), inches | Leakage Rate, gpm | Leakage Flaw Size** (a), inches | Leakage Rate, gpm |
| 830A | 11.94 | 14.41 | 2.752 | 6.261 | 2.640 | 5.205 |
| 830B | 12.83 | 15.59 | 2.747 | 6.303 | 2.634 | 5.228 |
| 832 | 12.83 | 15.59 | 2.747 | 6.303 | 2.634 | 5.228 |
| 834 | 12.92 | 15.77 | 2.746 | 6.305 | 2.633 | 5.229 |

Notes:

* These nodes are on the safety injection lines attached to the reactor pressure vessel.

** Leakage flaw size (a) is one half the total flaw length.

*** OLTP and RHR Normal Thermal only.

Table 5-14. Predicted Leakage Rates for 12-inch Safety Injection Lines Attached to RCS Cold Leg (Unit 2)

| Node | Moments | | EPFM Results | | Net Section Collapse Results | |
|---|---|---|---|---|---|---|
| | NOP in-kips | NOP+SSE in-kips | Leakage Flaw Size* (a), inches | Leakage Rate, gpm | Leakage Flaw Size* (a), inches | Leakage Rate, gpm |
| 225 | 644.86 | 780.17 | 4.444 | 33.713 | 4.162 | 26.673 |
| 230A | 644.86 | 780.17 | 4.444 | 33.713 | 4.162 | 26.673 |
| 230B | 581.20 | 728.98 | 4.505 | 32.898 | 4.216 | 25.906 |
| 235 | 581.20 | 728.98 | 4.505 | 32.898 | 4.216 | 25.906 |
| 240 | 497.27 | 637.96 | 4.615 | 32.325 | 4.313 | 25.182 |
| 436 | 328.09 | 457.28 | 4.833 | 30.406 | 4.518 | 23.470 |
| 440A | 328.09 | 457.28 | 4.833 | 30.406 | 4.518 | 23.470 |
| 440B | 307.99 | 438.73 | 4.856 | 30.048 | 4.540 | 23.182 |
| 441 | 307.99 | 438.73 | 4.856 | 30.048 | 4.540 | 23.182 |
| 445 | 261.89 | 387.42 | 4.917 | 29.388 | 4.600 | 22.632 |

* Leakage flaw size (a) is one half the total flaw length.

*** OLTP and RHR Normal Thermal only.

Table 5-15. Predicted Leakage Rates for 8-inch RHR Lines Attached to RCS Hot Leg (Unit 2)

| Node | Moments | | EPFM Results | | Net Section Collapse Results | |
|---|---|---|---|---|---|---|
| | NOP in-kips | NOP+SSE in-kips | Leakage Flaw Size* (a), inches | Leakage Rate, gpm | Leakage Flaw Size* (a), inches | Leakage Rate, gpm |
| 100 | 104.15 | 155.09 | 3.176 | 11.367 | 2.989 | 9.053 |
| 101 | 89.65 | 150.08 | 3.190 | 10.797 | 3.001 | 8.558 |
| 105A | 89.65 | 150.08 | 3.190 | 10.797 | 3.001 | 8.558 |
| 105B | 83.56 | 145.42 | 3.204 | 10.645 | 3.012 | 8.408 |
| 106 | 83.56 | 145.42 | 3.204 | 10.645 | 3.012 | 8.408 |
| 110A | 83.56 | 145.42 | 3.204 | 10.645 | 3.012 | 8.408 |
| 110B | 77.20 | 114.77 | 3.294 | 11.502 | 3.092 | 8.983 |
| 111 | 77.20 | 114.77 | 3.294 | 11.502 | 3.092 | 8.983 |
| 112 | 76.94 | 87.91 | 3.372 | 12.609 | 3.162 | 9.775 |
| 115A | 147.98 | 157.32 | 3.169 | 13.669 | 2.983 | 10.956 |
| 115B | 68.09 | 99.06 | 3.340 | 11.590 | 3.132 | 8.971 |
| 116 | 68.09 | 99.06 | 3.340 | 11.590 | 3.132 | 8.971 |
| 117 | 41.71 | 76.76 | 3.405 | 10.745 | 3.193 | 8.288 |
| 118 | 81.43 | 127.78 | 3.255 | 11.201 | 3.058 | 8.811 |
| 119 | 112.04 | 145.45 | 3.204 | 12.186 | 3.012 | 9.663 |
| 120A | 112.04 | 145.45 | 3.204 | 12.186 | 3.012 | 9.663 |
| 120B | 97.73 | 117.28 | 3.286 | 12.611 | 3.085 | 9.892 |
| 121 | 97.73 | 117.28 | 3.286 | 12.611 | 3.085 | 9.892 |
| 246 | 81.89 | 413.66 | 2.459 | 3.994 | 2.422 | 3.779 |
| 249A | 81.89 | 413.66 | 2.459 | 3.994 | 2.422 | 3.779 |
| 249B | 106.81 | 440.94 | 2.392 | 4.139 | 2.369 | 4.006 |
| 250 | 106.81 | 440.94 | 2.392 | 4.139 | 2.369 | 4.006 |
| 251 | 112.00 | 437.64 | 2.400 | 4.292 | 2.375 | 4.146 |

Table 5-15. Predicted Leakage Rates for 8-inch RHR Lines Attached to RCS Hot Leg (Unit 2) (Continued)

| Node | Moments | | EPFM Results | | Net Section Collapse Results | |
|---|---|---|---|---|---|---|
| | NOP in-kips | NOP+SSE in-kips | Leakage Flaw Size* (a), inches | Leakage Rate, gpm | Leakage Flaw Size* (a), inches | Leakage Rate, gpm |
| 251 | 112.00 | 437.64 | 2.400 | 4.292 | 2.375 | 4.146 |
| 252 | 295.36 | 421.28 | 2.440 | 9.245 | 2.407 | 8.829 |
| 253 | 390.98 | 412.63 | 2.462 | 12.338 | 2.424 | 11.728 |
| 254 | 421.60 | 470.05 | 2.324 | 11.079 | 2.313 | 10.930 |
| 255A | 421.60 | 470.05 | 2.324 | 11.079 | 2.313 | 10.930 |
| 255B | 388.72 | 453.96 | 2.362 | 10.747 | 2.344 | 10.501 |
| 256 | 388.72 | 453.96 | 2.362 | 10.747 | 2.344 | 10.501 |
| 257 | 53.69 | 105.65 | 3.320 | 10.444 | 3.115 | 8.083 |
| 258 | 260.60 | 411.23 | 2.465 | 8.573 | 2.427 | 8.131 |
| 260A | 260.60 | 411.23 | 2.465 | 8.573 | 2.427 | 8.131 |
| 260B | 284.04 | 408.53 | 2.472 | 9.322 | 2.432 | 8.829 |
| 261 | 284.04 | 408.53 | 2.472 | 9.322 | 2.432 | 8.829 |
| 262 | 179.46 | 226.91 | 2.965 | 12.125 | 2.818 | 10.105 |
| 263 | 170.16 | 291.29 | 2.779 | 9.279 | 2.675 | 8.134 |
| 265A | 170.16 | 291.30 | 2.779 | 9.279 | 2.675 | 8.133 |
| 265B | 160.97 | 300.98 | 2.753 | 8.669 | 2.654 | 7.635 |
| 266 | 160.96 | 300.98 | 2.753 | 8.669 | 2.654 | 7.634 |
| 270 | 130.67 | 384.94 | 2.531 | 5.652 | 2.480 | 5.262 |

* Leakage flaw size (a) is one half the total flaw length.

*** OLTP and RHR Normal Thermal only.

Table 5-16. Predicted Leakage Rates for 6-inch Draindown Lines Attached to RCS Hot Leg (Unit 2)

| Node | Moments | | EPFM Results | | Net Section Collapse Results | |
|---|---|---|---|---|---|---|
| | NOP in-kips | NOP+SSE in-kips | Leakage Flaw Size* (a), inches | Leakage Rate, gpm | Leakage Flaw Size* (a), inches | Leakage Rate, gpm |
| 10 | 6.35 | 9.53 | 2.848 | 5.264 | 2.664 | 3.899 |
| 7 | 6.43 | 10.16 | 2.845 | 5.245 | 2.661 | 3.884 |

* Leakage flaw size (a) is one half the total flaw length.

*** OLTP and RHR Normal Thermal only.

Table 5-17. Predicted Leakage Rates for 6-inch Nozzles Attached to RCS Hot Leg (Units 1 and 2)

| Node | Moments | | EPFM Results | | Net Section Collapse Results | |
|---|---|---|---|---|---|---|
| | NOP in-kips | NOP+SSE in-kips | Leakage Flaw Size* (a), inches | Leakage Rate, gpm | Leakage Flaw Size* (a), inches | Leakage Rate, gpm |
| N/A | 0 | 0 | 2.894 | 5.073 | 2.710 | 3.740 |

* Leakage flaw size (a) is one half the total flaw length.

*** OLTP and RHR Normal Thermal only.

Table 5-18. Moments Due to Kink Angle Restraint Effects for 6-inch Safety Injection Line Attached to RCS Cold Leg

| Node | Crack Orientation (Degrees) | $M_x$ [in-kips] | $M_y$ [in-kips] | $M_z$ [in-kips] | SRSS [in-kips] | Limiting Load Reduction Moment [in-kips] |
|---|---|---|---|---|---|---|
| 280 | 0 | -0.019 | -0.565 | -0.157 | 0.587 | 0.587 |
| | 45 | -0.068 | -0.492 | 0.230 | 0.547 | |
| | 90 | -0.078 | -0.105 | 0.157 | 0.204 | |
| | 135 | -0.042 | -0.178 | -0.230 | 0.294 | |
| 275B | 0 | -0.011 | -0.516 | -0.141 | 0.535 | 0.535 |
| | 45 | -0.048 | -0.447 | 0.210 | 0.496 | |
| | 90 | -0.057 | -0.096 | 0.141 | 0.180 | |
| | 135 | -0.033 | -0.164 | -0.210 | 0.269 | |
| 275A | 0 | -0.057 | -0.478 | 0.046 | 0.484 | 0.487 |
| | 45 | -0.107 | -0.392 | 0.040 | 0.408 | |
| | 90 | -0.094 | -0.398 | -0.046 | 0.412 | |
| | 135 | -0.026 | -0.484 | -0.040 | 0.487 | |

Note: Based on Kewaunee Loop B line.

Table 5-19. Moments Due to Kink Angle Restraint Effects for 6-inch Draindown Line Attached to RCS Hot Leg

| Node | Crack Orientation (Degrees) | $M_x$ [in-kips] | $M_y$ [in-kips] | $M_z$ [in-kips] | SRSS [in-kips] | Limiting Load Reduction Moment [in-kips] |
|---|---|---|---|---|---|---|
| 7 | 0 | 0.46 | -0.34 | -0.06 | 0.57 | 0.57 |
| | 45 | 0.34 | -0.26 | 0.14 | 0.45 | |
| | 90 | 0.03 | -0.06 | 0.06 | 0.09 | |
| | 135 | -0.31 | -0.14 | -0.14 | 0.36 | |
| 10 | 0 | 0.34 | -0.26 | -0.05 | 0.43 | 0.43 |
| | 45 | 0.26 | -0.21 | 0.10 | 0.34 | |
| | 90 | 0.02 | -0.06 | 0.05 | 0.08 | |
| | 135 | -0.23 | -0.11 | -0.10 | 0.27 | |

Note: Based on Prairie Island Unit 2 line.
OLTP and RHR Normal Thermal only.

Table 5-20. Moments Due to Kink angle Restraint Effects for 8-inch RHR Lines Attached to RCS Hot Leg

| Node | Crack Orientation (Degrees) | $M_x$ [in-kips] | $M_y$ [in-kips] | $M_z$ [in-kips] | SRSS [in-kips] | Limiting Load Reduction Moment [in-kips] |
|---|---|---|---|---|---|---|
| 2000 | 0 | 8.02 | -34.58 | 4.32 | 35.77 | 35.77 |
| | 45 | 2.93 | -20.83 | 9.43 | 23.05 | |
| | 90 | -3.85 | -15.72 | -4.32 | 16.76 | |
| | 135 | -8.41 | -29.48 | -9.43 | 32.08 | |
| 2010A | 0 | 6.33 | -23.46 | 3.84 | 24.59 | 24.59 |
| | 45 | 1.86 | -14.34 | 5.28 | 15.38 | |
| | 90 | -3.69 | -12.93 | -3.84 | 13.97 | |
| | 135 | -7.08 | -22.05 | -5.28 | 23.73 | |
| 2010B | 0 | 1.64 | -21.86 | 7.17 | 23.05 | 24.91 |
| | 45 | 3.34 | -10.12 | 4.53 | 11.59 | |
| | 90 | 3.07 | -12.77 | -7.17 | 14.96 | |
| | 135 | 1.03 | -24.47 | -4.53 | 24.91 | |
| 2020B | 0 | 0.07 | -19.21 | 0.00 | 19.21 | 19.21 |
| | 45 | -1.81 | -12.07 | 7.14 | 14.15 | |
| | 90 | -2.66 | -4.97 | 0.00 | 5.62 | |
| | 135 | -1.94 | -12.07 | -7.14 | 14.16 | |
| 2040A | 0 | -0.15 | -16.57 | 0.25 | 16.58 | 16.58 |
| | 45 | 0.10 | -10.09 | 6.22 | 11.87 | |
| | 90 | 0.28 | -4.12 | -0.25 | 4.14 | |
| | 135 | 0.30 | -10.59 | -6.22 | 12.29 | |
| 2040B | 0 | -0.20 | -20.16 | -0.20 | 20.16 | 20.16 |
| | 45 | -0.59 | -13.97 | 6.39 | 15.37 | |
| | 90 | -0.63 | -7.38 | 0.20 | 7.40 | |
| | 135 | -0.32 | -13.57 | -6.39 | 15.00 | |

Table 5-20. Moments Due to Kink Angle Restraint Effects for 8-inch RHR Lines Attached to RCS Hot Leg (Continued)

| Node | Crack Orientation (Degrees) | $M_x$ [in-kips] | $M_y$ [in-kips] | $M_z$ [in-kips] | SRSS [in-kips] | Limiting Load Reduction Moment [in-kips] |
|---|---|---|---|---|---|---|
| 2070A | 0 | 0.50 | -4.75 | 1.79 | 5.08 | 7.03 |
| | 45 | 1.18 | -3.46 | -0.50 | 3.68 | |
| | 90 | 1.21 | -5.71 | -1.79 | 6.10 | |
| | 135 | 0.50 | -7.00 | 0.50 | 7.03 | |
| 2070B | 0 | 1.61 | -4.13 | 0.39 | 4.45 | 4.45 |
| | 45 | 1.89 | -2.91 | 0.84 | 3.56 | |
| | 90 | 1.05 | -2.49 | -0.39 | 2.71 | |
| | 135 | -0.42 | -3.71 | -0.84 | 3.81 | |

Note: Based on Prairie Island Unit 1 Loop A line.
OLTP and RHR Normal Thermal only.

Table 5-21. Leakage Flaw Size and Leakages for 6-inch Safety Injection Line Attached to RCS Cold Leg Considering Restraint Effect

| Node | Leakage Results without Restraint Effects | | | | Leakage Results with Restraint Effects | | | |
|---|---|---|---|---|---|---|---|---|
| | EPFM | | Limit Load | | EPFM | | Limit Load | |
| | Leakage Flaw Size (a)* | Flow Rate | Leakage Flaw Size (a)* | Leakage Flow Rate | Leakage Flaw Size (a)* | Flow Rate | Leakage Flaw Size (a)* | Flow Rate |
| | (in) | (gpm) | (in) | (gpm) | (in) | (gpm) | (in) | (gpm) |
| 280 | 2.720 | 6.397 | 2.603 | 5.270 | 2.720 | 6.340 | 2.603 | 5.221 |
| 275B | 2.722 | 6.374 | 2.604 | 5.251 | 2.722 | 6.321 | 2.604 | 5.206 |
| 275A | 2.735 | 6.293 | 2.619 | 5.189 | 2.735 | 6.245 | 2.619 | 5.148 |

Note: Based on evaluating Kewaunee Loop B line.

* Leakage flaw size (a) is one half the total flaw length.

Table 5-22. Leakage Flaw Size and Leak Rates for 8-inch RHR Line Attached to RCS Hot Leg Considering Restraint Effects

| Node | Leakage Results without Restraint Effects | | | | Leakage Results with Restraint Effects | | | |
|---|---|---|---|---|---|---|---|---|
| | EPFM | | Limit Load | | EPFM | | Limit Load | |
| | Leakage Flaw Size (a)* | Flow Rate | Leakage Flaw Size (a)* | Leakage Flow Rate | Leakage Flaw Size (a)* | Flow Rate | Leakage Flaw Size (a)* | Flow Rate |
| | (in) | (gpm) | (in) | (gpm) | (in) | (gpm) | (in) | (gpm) |
| 2000 | 2.983 | 12.963 | 2.832 | 10.770 | 2.983 | 11.316 | 2.832 | 9.378 |
| 2010A | 2.118 | 13.178 | 2.940 | 10.640 | 3.118 | 11.884 | 2.940 | 9.571 |
| 2010B | 3.133 | 13.306 | 2.953 | 10.730 | 3.133 | 11.975 | 2.953 | 9.631 |
| 2020B | 3.208 | 13.037 | 3.016 | 10.345 | 3.208 | 11.959 | 3.016 | 9.466 |
| 2040A | 2.940 | 12.742 | 2.798 | 10.940 | 2.940 | 11.980 | 2.798 | 10.051 |
| 2040B | 2.844 | 12.791 | 2.725 | 11.066 | 2.844 | 11.955 | 2.725 | 10.334 |
| 2070A | 3.200 | 8.866 | 3.009 | 6.963 | 3.200 | 8.491 | 3.009 | 6.659 |
| 2070B | 3.205 | 9.153 | 3.013 | 7.189 | 3.205 | 8.911 | 3.013 | 6.992 |

Note:

* Leakage flaw size (a) is one half the total flaw length.

** Based on Prairie Island Loop A line.

*** OLTP and RHR Normal Thermal only.

Table 5-23. Leakage Flaw Size and Leak Rates for 6-inch Draindown Line Attached to RCS Hot Leg Considering Restraint Effects

| Node | Leakage Results without Restraint Effects | | | | Leakage Results with Restraint Effects | | | |
|---|---|---|---|---|---|---|---|---|
| | EPFM | | Limit Load | | EPFM | | Limit Load | |
| | Leakage Flaw Size (a)* | Flow Rate | Leakage Flaw Size (a)* | Leakage Flow Rate | Leakage Flaw Size (a)* | Flow Rate | Leakage Flaw Size (a)* | Flow Rate |
| | (in) | (gpm) | (in) | (gpm) | (in) | (gpm) | (in) | (gpm) |
| 7 | 2.845 | 5.245 | 2.661 | 3.884 | 2.845 | 5.195 | 2.661 | 3.845 |
| 10 | 2.848 | 5.264 | 2.664 | 3.899 | 2.848 | 5.226 | 2.664 | 3.869 |

Note:

* Leakage flaw size (a) is one half the total flaw length.

** Based on Prairie Island Unit 2 line.

*** OLTP and RHR Normal Thermal only.

Table 5-24. Updated Leak Rates under Uprate Conditions with RHR Thermal Stratification using Fatigue Crack Morphology

| Line | Unit | Node | Leak Rate (gpm) at 200°F[1] | Leak Rate (gpm) at 120°F[2] | Adjusted Leak Rate (gpm) at 120°F[3] |
|---|---|---|---|---|---|
| 6" SI | 1 | 1045 | 4.580 | 4.463 | 3.882 |
| 6" SI | 1 | 1270 | 5.325 | 5.188 | 4.514 |
| 12" SI | 1 | 190 | 22.494 | 21.916 | 19.067 |
| 12" SI | 1 | 910 | 24.750 | 24.114 | 20.979 |
| 8" RHR | 1 | 2000 | 3.442 | 3.354 | 2.918 |
| 8" RHR | 1 | 2354 | 6.862 | 6.685 | 5.816 |
| 8" RHR | 1 | 2060 | 2.673 | 2.604 | 2.265 |
| 6" Draindown | 1 | 720 | 3.158 | 3.077 | 2.677 |
| 6" SI | 2 | 570 | 4.911 | 4.785 | 4.163 |
| 6" SI | 2 | 834 | 5.094 | 4.963 | 4.318 |
| 6" SI | 2 | 558 | 4.858 | 4.734 | 4.118 |
| 12" SI | 2 | 240 | 22.584 | 22.003 | 19.143 |
| 12" SI | 2 | 445 | 21.353 | 20.804 | 18.099 |
| 8" RHR | 2 | 100 | 9.247 | 9.009 | 7.838 |
| 8" RHR | 2 | 270 | 3.866 | 3.767 | 3.277 |
| 8" RHR | 2 | 246 | 2.504 | 2.440 | 2.123 |
| 6" Draindown | 2 | 7 | 3.446 | 3.358 | 2.921 |
| 6" Capped Nozzle | 1,2 | N/A[4] | 4.217 | 4.109 | 3.575 |

Notes:

1. PICEP default outlet fluid temperature.
2. Sump temperature at which the fluid from the cracked pipe is collected.
3. Includes a 13 % decrease (maximum decrease as calculated in Reference 1) in leak rate due to the effect of piping restraint.
4. Uprate Conditions with RHR Thermal Stratification.

Table 5-25. Updated Leak Rates under Uprate Conditions with RHR Thermal Stratification using PWSCC Crack Morphology

| Line | Unit | Node | Leak Rate (gpm) at 200°F[1] | Leak Rate (gpm) at 120°F[2] | Adjusted Leak Rate (gpm) at 120°F[3] |
|---|---|---|---|---|---|
| 6" SI | 1 | 1045 | 1.454 | 1.416 | 1.232 |
| 6" SI | 1 | 1270 | 1.630 | 1.588 | 1.382 |
| 12" SI | 1 | 190 | 4.945 | 4.817 | 4.191 |
| 12" SI | 1 | 910 | 5.293 | 5.157 | 4.487 |
| 8" RHR | 1 | 2000 | 0.971 | 0.946 | 0.823 |
| 8" RHR | 1 | 2354 | 1.751 | 1.706 | 1.484 |
| 8" RHR | 1 | 2060 | 0.816 | 0.795 | 0.691 |
| 6" Draindown | 1 | 720 | 0.971 | 0.946 | 0.823 |
| 6" SI | 2 | 570 | 1.521 | 1.482 | 1.290 |
| 6" SI | 2 | 834 | 1.570 | 1.529 | 1.330 |
| 6" SI | 2 | 558 | 1.513 | 1.474 | 1.282 |
| 12" SI | 2 | 240 | 4.899 | 4.773 | 4.152 |
| 12" SI | 2 | 445 | 4.775 | 4.652 | 4.047 |
| 8" RHR | 2 | 100 | 2.268 | 2.210 | 1.922 |
| 8" RHR | 2 | 270 | 1.045 | 1.018 | 0.886 |
| 8" RHR | 2 | 246 | 0.732 | 0.713 | 0.621 |
| 6" Draindown | 2 | 7 | 1.041 | 1.014 | 0.882 |
| 6" Capped Nozzle | 1,2 | N/A[4] | 1.239 | 1.207 | 1.050 |

Notes:

1. PICEP default outlet fluid temperature.
2. Sump temperature at which the fluid from the cracked pipe is collected.
3. Includes a 13% decrease (maximum decrease as calculated in Reference 1) in leak rate due to the effect of piping restraint.
4. Uprate Conditions with RHR Thermal Stratification.

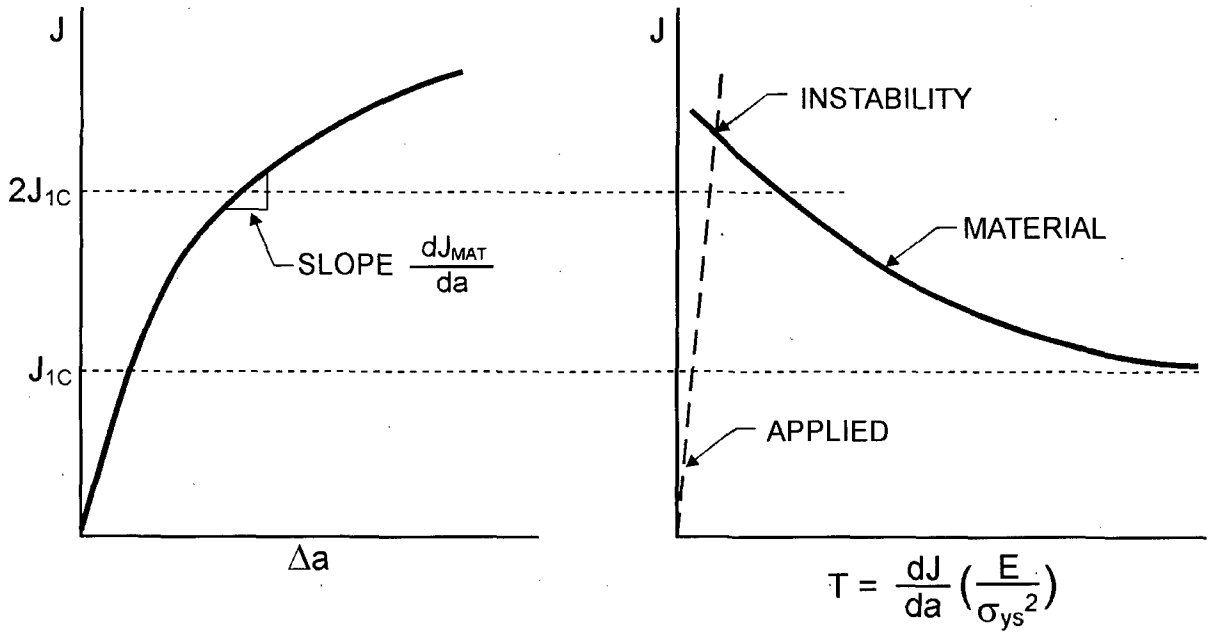


93220r0

Note: Linear extrapolation used to determine $T_{material}$ for J values greater than 2 $J_{IC}$

Figure 5-1. J-Integral/Tearing Modulus Concept for Determination of Instability During Ductile Tearing

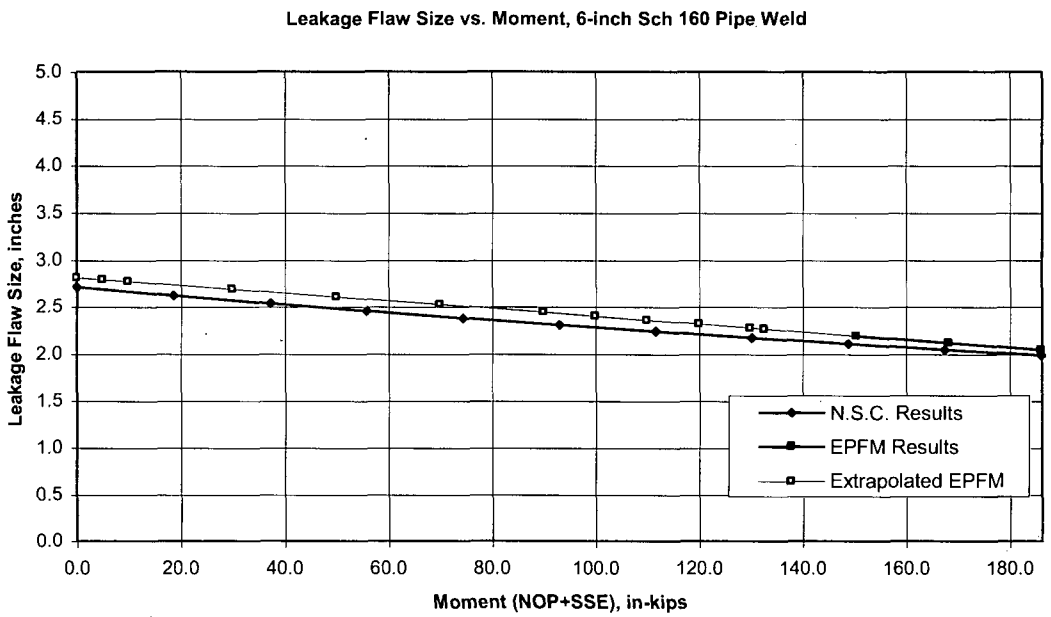


Note: Leakage flaw size (a) is one half the total flaw length.

Figure 5-2. Leakage Flaw Size Versus Moment for 6-inch Schedule 160 Pipe Weld Determined by J/T and Limit Load Analyses

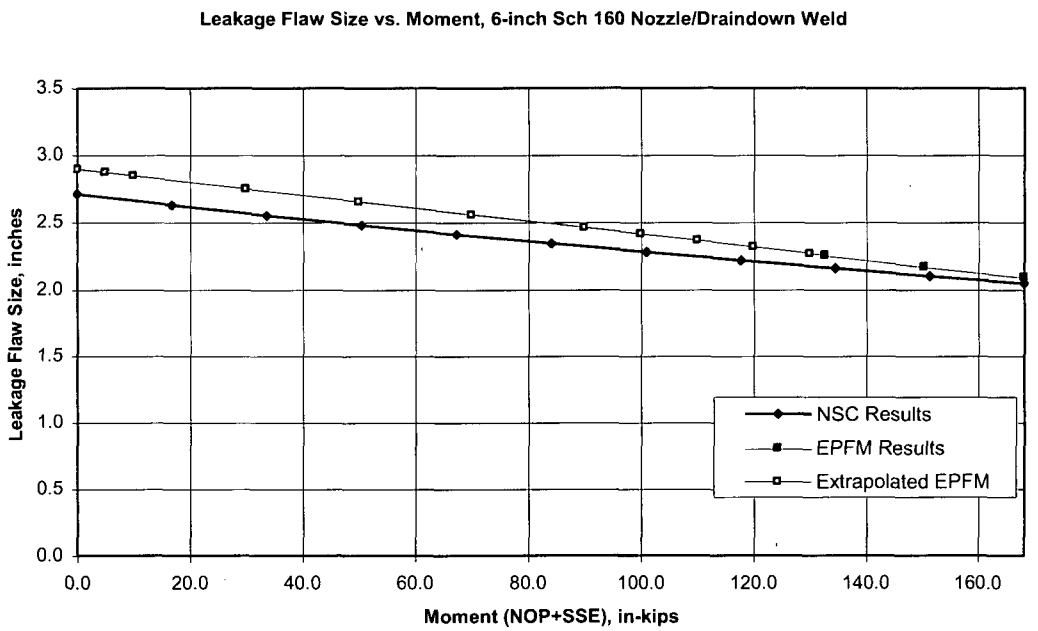


Note: Leakage flaw size (a) is one half the total flaw length.

Figure 5-3. Leakage Flaw Size Versus Moment for 6-inch Schedule 160 Nozzle/Draindown Weld Determined by J/T and Limit Load Analyses

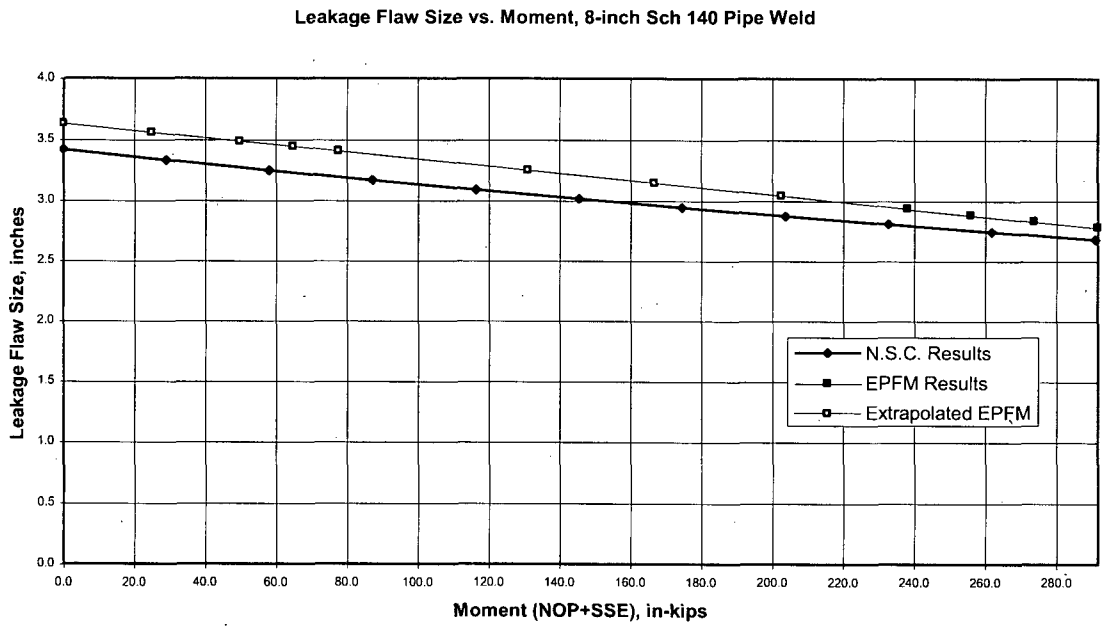


Note: Leakage flaw size (a) is one half the total flaw length.

Figure 5-4. Leakage Flaw Size Versus Moment for 8-inch Schedule 140 Pipe Weld Determined by J/T and Limit Load Analyses

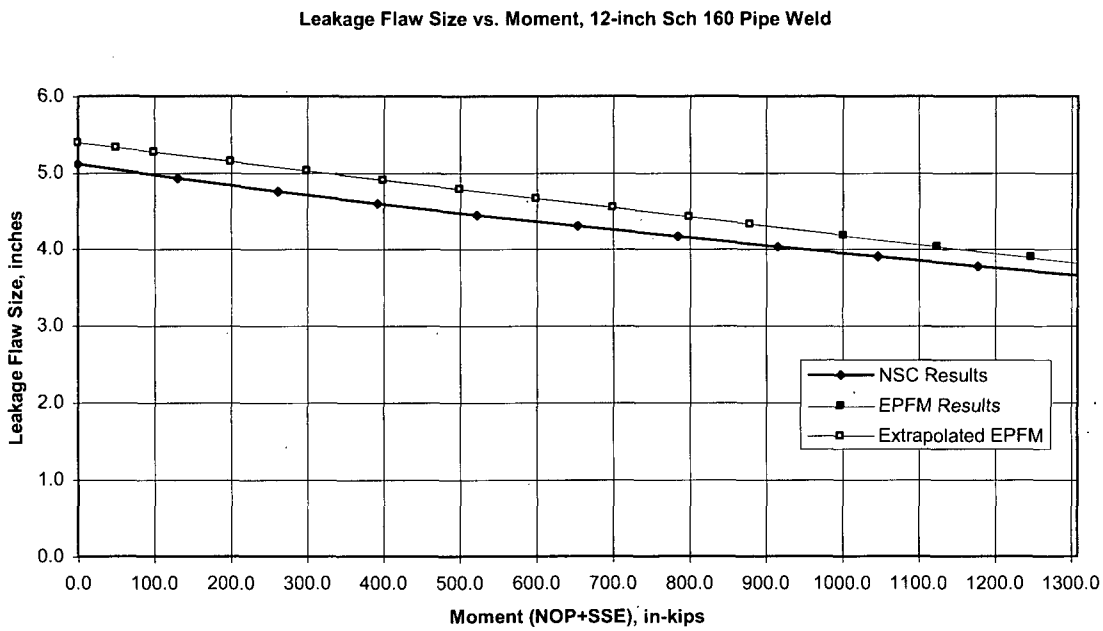


Note: Leakage flaw size (a) is one half the total flaw length.

Figure 5-5. Leakage Flaw Size Versus Moment for 12-inch Schedule 160 Pipe Weld Determined by J/T and Limit Load Analyses

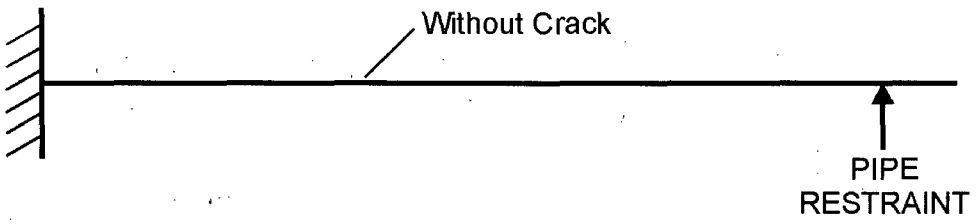


a) Uncracked piping.

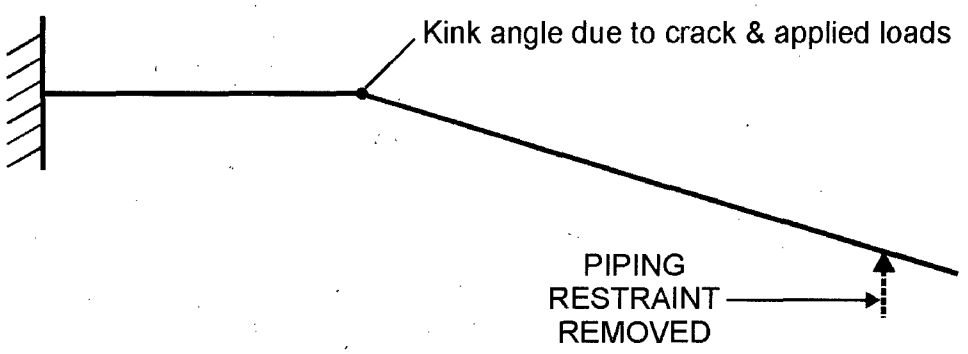


b) Cracked pipe without restraint.

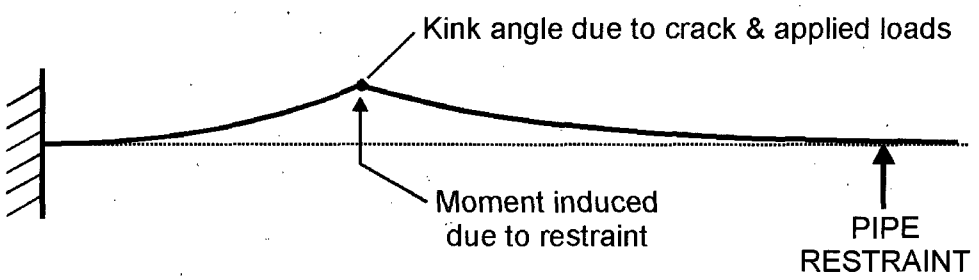


00034r0

c) Cracked pipe with restraint.

Figure 5-6. Depiction of Restraint Effect on Cracked Piping

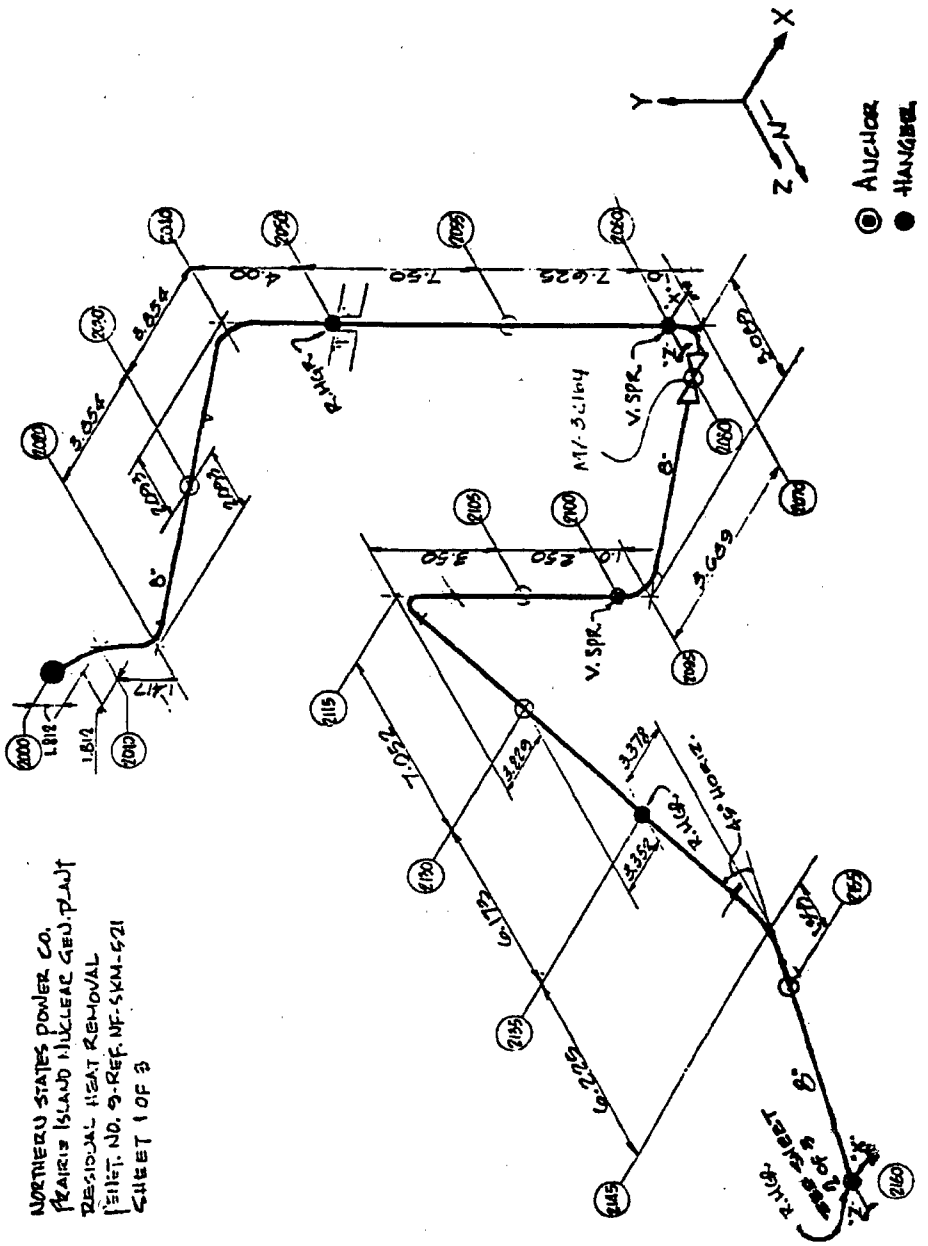


Note: For evaluation of restraint, piping evaluated between Node 2000 and an assumed anchor located at Node 2160.

Figure 5-7. Schematic of Piping Layout Used to Determine the Effect of Restraint on LBB Evaluation (8-inch RHR Line - Prairie Island Unit 1, Loop A)

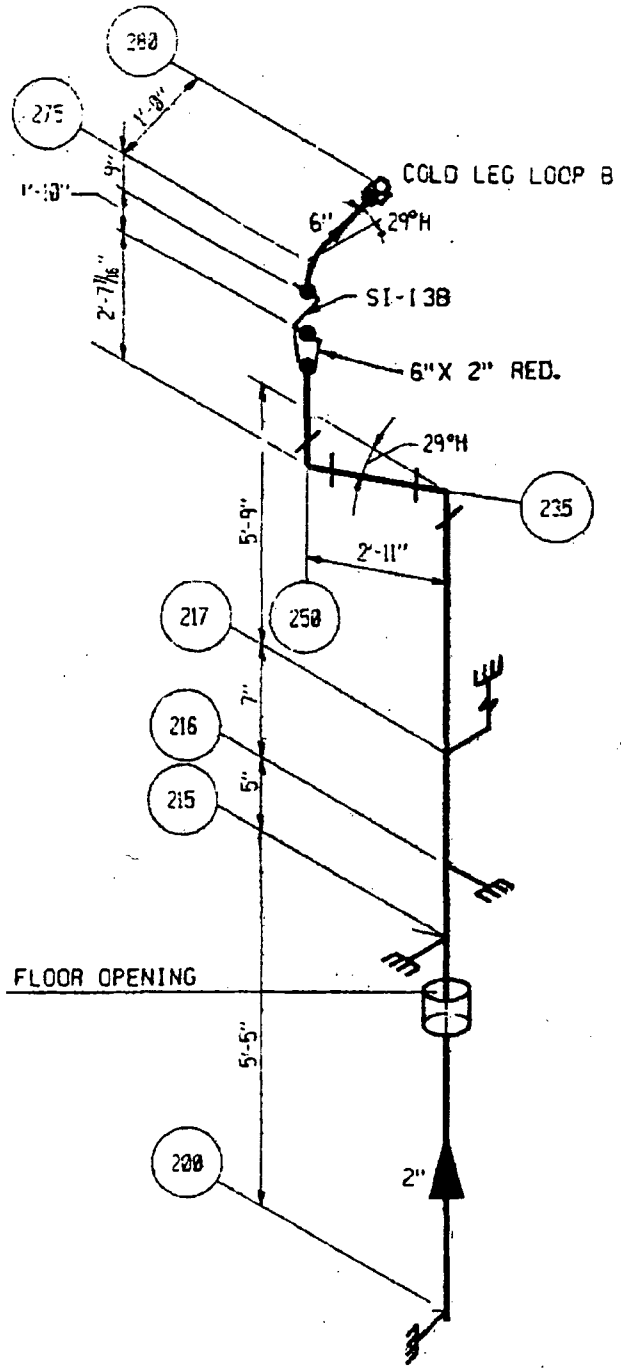


Note: For evaluation of restraint, piping evaluated between Node 280 and an assumed anchor located at Node 200.

Figure 5-8. Schematic of Piping Layout Used to Determine the Effect of Restraint on LBB Evaluation (6-inch Safety Injection Line – Kewaunee, Loop B)

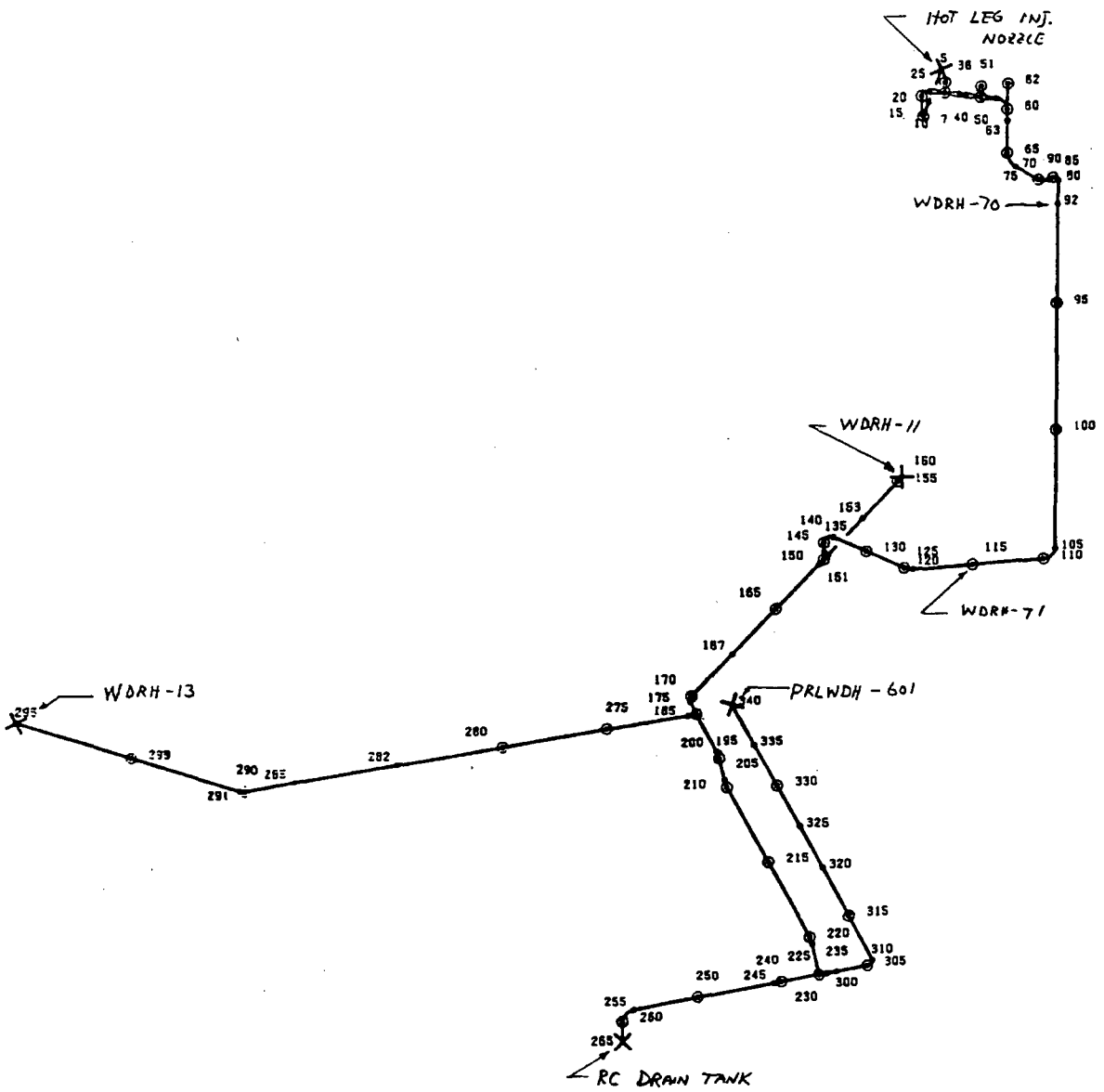


Note: For evaluation of restraint, piping evaluated between Node 5 and an assumed anchor located at Node 150.

Figure 5-9. Schematic of Piping Layout Used to Determine the Effect of Restraint on LBB Evaluation (6-inch Draindown Line – Prairie Island Unit 2)

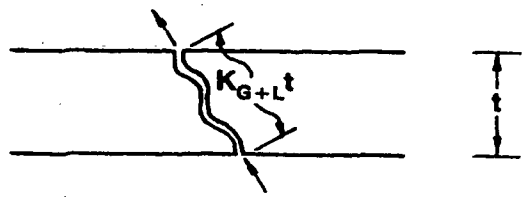


**Small COD**

Figure 5-10. Flow Path Deviation As Affected by Roughness and Crack Opening Displacement

**Large COD**

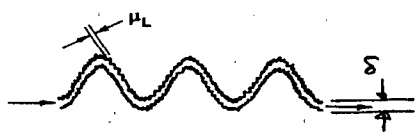


**Small COD**

Figure 5-11. Roughness Depiction for Small and Large Crack Opening Displacements

## 6.0 EVALUATION OF FATIGUE CRACK GROWTH OF SURFACE FLAWS

In accordance with the NRC criteria [3] set forth in Section 2 of this report, the growth of postulated surface cracks by fatigue is evaluated to demonstrate that such growth is insignificant for the plant life, when initial flaw sizes meeting ASME Code Section XI IWB-3514 acceptance standards [30] are postulated. The crack growth analysis is performed for the locations with the maximum stresses. The evaluation is performed using bounding stresses from Prairie Island Units 1 and 2 and Kewaunee.

### 6.1 Plant Transients

Since Prairie Island RCS attached piping lines were designed to the requirements of ANSI B31.1, no specific line unique transients exist in the design basis. Hence, transient information specific only to this LBB evaluation is developed to perform the crack growth evaluation. The transients used in the evaluation consist of those for the reactor pressure vessel [11[PJ1]] (specified in the Plant Technical Specification) and additional transients specific to the operation of these systems. The plant transients used in this evaluation are presented in Table 6-1. These are consistent with the original design of the reactor pressure vessel [11] except that the number of heatup/cooldown cycles was modified from [redacted] to account for future potential license renewal. The pressure change due to normal fluctuations is assumed for those events with no significant pressure change defined. Table 6-2 shows the additional thermal transients assumed for the systems. Accumulator blowdown transient was not evaluated, since this transient has never occurred at Prairie Island and hence is considered as a very unlikely event. Although there was a safety injection transient in Unit 1 due to tube rupture in 1979, there have been no inadvertent safety injections since. This transient is therefore also considered unlikely and was not evaluated. There are no local piping system transients for the 6-inch draindown line and the 6-inch hot leg nozzles.

For crack growth analysis, the design basis transients are combined into load set pairs to give the largest pressure and temperature ranges. The combined transients and the associated number of cycles are shown in Table 6-3 for the hot leg and Table 6-4 for the cold leg. They are in order of

decreasing $\Delta T$ except for the test events. For purposes of this analysis, the test events in Table 6-1 and the Table 6-2 transients are treated as standalone events and not combined with the normal system transients.

## 6.2 Stresses for Crack Growth Evaluation

The axial stresses due to pressure and thermal loads are calculated as described below. For pressure loads, P, the axial stress is calculated as:

$$\sigma_p = P\frac{D_i^2}{D_o^2 - D_i^2}$$

where $D_o$ is the outside diameter and $D_i$ is the inside diameter of the pipe.

Bending stress is given by $\sigma_b = D_o(M)/2I$,

where

M = bending moment

I = moment of inertia

$= (\pi/64)*(D_o^4-D_i^4)$

For thermal expansion moments, the maximum operating thermal moments ($M_{max\ oper}$), from Section 4, are scaled by the ratio of the transient temperature ranged ($\Delta T$) to the operating temperature range ($\Delta T_{oper}$):

$$M_t = M_{max\ oper}\ (\Delta T/\Delta T_{oper}),$$

where $\Delta T_{oper}$ is based on the temperatures at which the thermal expansion moments were calculated. $\Delta T_{oper}$ = 607.4 – 70 = 537.4°F for the hot leg and 552 – 70 = 482°F for the cold leg.

Table 6-5 gives the bounding non-scaled moments, based on the Section 4 tables. The operating conditions used for this evaluation have been provided in Section 4.1.

Non-cyclic stresses were also considered as they affect crack growth rate. The dead weight stresses are computed from the dead weight moments presented in Table 6-5. In addition, weld residual stresses are considered in the evaluation. The weld residual stress is conservatively represented by a pure through-wall bending stress approximately equal to the base metal material yield stress at the operating temperature. Thus, for the cold leg, $S_y$ = 19.3 ksi at 550°F was used, while for the hot leg, $S_y$ = 18.8 ksi at 607.4°F was used.

Thermal transient stresses ($\sigma_{TT}$) and thermal stresses associated with material discontinuities ($\sigma_{TD}$) are also included in this evaluation and are presented in Tables 6-6 and 6-7. The computer program PIPETRAN [31] was used to derive the through-wall thermal transient and discontinuity stresses for the given transients. This program performs two-dimensional axisymmetric transient thermal stress analysis for cylindrical components. This program is maintained under SI's software quality assurance program.

The axial pressure, thermal, dead weight and residual stresses were combined to obtain the stress ranges corresponding to each load group. Within a load group, the maximum stresses were used. The resulting stress ranges are shown in Tables 6-8 through 6-11 where the pressure and bending moment stresses are taken as uniform tension across the pipe thickness and the other stresses are considered to have a linear through-wall distribution.

## 6.3 Model for Stress Intensity Factor

The stress intensity factors, K, corresponding to the point of the maximum depth of a semi-elliptical crack are calculated using fracture mechanics solutions presented in Reference 15. The stress intensity factors are determined for a conservative aspect ratio ($a/\ell$) of 0.1.

The stress intensity factor for the deepest point on the semi-elliptical flaw from Reference 15 is given as:

$$K_I = (\pi t)^{0.5} \bullet \left[ \sum_{i=0}^{3} \sigma_i (a/t)^i G_i \right]$$

where $\sigma_i$ are the coefficients of the stress polynomial describing the axial stress ($\sigma$) variation through the cylinder wall and are defined below.

$$\sigma = \sigma_o + \sigma_1 (z/t) + \sigma_2 (z/t)^2 + \sigma_3 (z/t)^3,$$

z is the distance measured from the inner surface of the cylinder wall and t is the cylinder wall thickness. The $G_i$ are the influence coefficients associated with the coefficients of the stress polynomial $\sigma_i$ and are expressed by the following general form:

$$G_i = A_1\alpha_i + A_2\alpha_i^2 + A_3\alpha_i^3 + A_4\alpha_i^4 + A_5\alpha_i^5 + A_6\alpha_i(R/t - 5)$$

$$\alpha_i = (a/t)/(a/c)^m$$

The values of $A_1$ through $A_6$ and m are provided in Reference 15 for each $G_i$. The constant R is the mean radius of the cylinder. The parameters 2c and *a* are the flaw length measured at the cylinder inner surface and flaw depth at the deepest point of the flaw, respectively.

## 6.4 Fatigue Crack Growth Analysis and Results

Fatigue crack growth analysis requires the use of appropriate fatigue crack growth law for the stainless steel piping. Per the recommendation of ASME Code, Section XI Task Group for Piping Flaw Evaluation [32], the fatigue crack growth law for stainless steel is given as:

$$\frac{da}{dN} = CES\,(\Delta K_I)^n$$

where n equals 3.3, $C = 2 \times 10^{-19}$ (in/cycle) (psi/$\sqrt{in}$), and E is the environmental factor, equal to 2 for the PWR water environment. S is a scaling parameter to account for the R ratio ($K_{min}/K_{max}$), and is given by:

$$S = (1.0 - 0.5\ R^2)^{-4}$$

The R ratio was calculated for each $K_{max}$ and $K_{min}$ for each location.

The stresses are cycled between maximum and the minimum stress conditions shown in Tables 6-2 through 6-4. For each location, the actual K values for the fatigue crack growth are calculated based on the stresses.

The initial flaw size is linearly interpolated based on the allowable flaw sizes for various thicknesses from Table IWB-3514-2, Inservice Examination, surface crack, for a crack with aspect ratio $a/\ell$ = 0.15. However, for the crack growth analysis, an aspect ratio of 0.1 has been conservatively used. The crack depths used as input are presented in Table 6-12.

The results of the fatigue crack growth analysis are presented in Table 6-13. The results show that for the 6-inch cold leg safety injection and draindown piping, crack growth is very minimal. After 250 heatup/cooldown cycles, the crack depth is significantly below the ASME Section XI Code allowables. It should be noted that the results for the 6-inch cold leg safety injection piping can be conservatively applied to the 6-inch capped nozzle on the hot leg since only pressure stresses exist at the capped nozzle.

However, for the 12" Sch 160 SI Accumulator line, it takes 38 heatup/cooldowns at the worst location to reach the allowable flaw size, and for the 8" Sch 140 RHR Suction line, it takes 123 heatup/cooldowns at the most critical location to reach the allowable flaw size. The relatively few number of cycles for the 8-inch RHR and 12" safety injection accumulator piping can be attributed to the RHR transients listed in Table 6-2. For the last ten years, Prairie Island has experienced 13 heatup/cooldown cycles which are significantly less than the minimum allowable number of 38 calculated at the most critical location. Given that the piping is inspected in

accordance with ASME Section XI requirements in each 10-year interval, it is believed that the potential for crack growth can be managed by the current in-service inspection program at Prairie Island.

Table 6-1. Plant Design Transients Used for LBB Evaluations

| Event | Cycles | [redacted] |
|---|---|---|
| Plant Heatup/Cooldown (HU/CD) | 250 | |
| Plant Loading/Unloading | 18,300 | |
| 10% Step Load Decrease | 2,000 | |
| 10% Step Load Increase | 2,000 | |
| Large Step Decrease | 200 | |
| Loss of Load | 80 | |
| Loss of Power | 40 | |
| Loss of Flow | 80 | |
| Reactor Trip from Full Power | 400 | |
| Turbine Roll Test | 10 | |
| Primary Side Hydro Test | 5 | |
| Primary Side Leak Test | 50 | |
| Operating Basis Earthquake (±) | 200 | |

Table 6-2. Additional System Transients Used Specifically for LBB Evaluations

| Piping | Transient | Cycles | $T_{min}$, °F | $T_{max}$, °F | ΔT, °F |
|---|---|---|---|---|---|
| 6" Cold Leg SI | High Head Safety Injection | 10 | 32 | 560 | 528 |
| 12" SI Accumulator | RHR Operation at Cooldown | 250 | 100 | 400 | 300 |
| 12" SI Accumulator | Refueling Floodup | 120 | 50 | 150 | 100 |
| 8" RHR Suction | RHR Initiation (away from RC nozzle) | 250 | 100 | 400 | 300 |

Table 6-3. Combined Transients for Crack Growth, Hot Leg

| No. | Load Set Pair | Cycles | $T_{min}$, °F | $T_{max}$, °F | ΔT, °F | $P_{min}$, psig | $P_{max}$, psig | ΔP, psi |
|---|---|---|---|---|---|---|---|---|
| 1 | CD & HU/Loss of Load/OBE | 20 | 70 | 624 | 554 | 0 | 2335 | 2335 |
| 2 | CD & HU/Loss of Load | 60 | 70 | 624 | 554 | 0 | 2335 | 2335 |
| 3 | CD & HU/Loss of Power | 40 | 70 | 616 | 546 | 0 | 2335 | 2335 |
| 4 | CD & HU/10% Load Increase | 130 | 70 | 606 | 536 | 0 | 2335 | 2335 |
| 5 | TR Test & 10% Load Increase | 10 | 480 | 606 | 126 | 1935 | 2335 | 400 |
| 6 | Loss of Flow & 10% Load Increase | 80 | 486 | 606 | 120 | 1855 | 2235 | 380 |
| 7 | Step Decr. & 10% Load Increase | 200 | 516 | 606 | 90 | 2135 | 2335 | 200 |
| 8 | Rx Trip & 10% Load Increase | 400 | 520 | 606 | 86 | 2135 | 2335 | 200 |
| 9 | Unload & Load/10% Load Increase | 1180 | 547 | 606 | 59 | 2135 | 2335 | 200 |
| 10 | Unload & Load/10% Load Decrease | 2000 | 547 | 601 | 54 | 2135 | 2335 | 200 |
| 11 | Loading/Unloading | 15120 | 547 | 596 | 49 | 2135 | 2335 | 200 |
| 12 | Primary Side Hydro Test | 5 | 120 | 120 | 0 | 0 | 3105 | 3105 |
| 13 | Primary Side Leak Test | 50 | 120 | 547 | 427 | 0 | 2485 | 2485 |

Table 6-4. Combined Transients for Crack Growth, Cold Leg

| No. | Load Set Pair | Cycles | $T_{min}$, °F | $T_{max}$, °F | ΔT, °F | $P_{min}$, psig | $P_{max}$, psig | ΔP, psi |
|---|---|---|---|---|---|---|---|---|
| 1 | CD & HU/Loss of Load/OBE | 20 | 70 | 572.2 | 502.2 | 0 | 2335 | 2335 |
| 2 | CD & HU/Loss of Load | 60 | 70 | 572.2 | 502.2 | 0 | 2335 | 2335 |
| 3 | CD & HU | 170 | 70 | 547 | 477 | 0 | 2235 | 2235 |
| 4 | Turbine Roll Test Range | 10 | 480 | 547 | 67 | 1935 | 2335 | 400 |
| 5 | Flow Loss & 10% Load Decrease | 80 | 489.2 | 547.2 | 58 | 1855 | 2335 | 480 |
| 6 | 10% Load Incr. & 10% Load Decr. | 1920 | 517.2 | 547.2 | 30 | 2135 | 2335 | 200 |
| 7 | 10% Load Incr & Load/Unload | 80 | 517.2 | 547 | 29.8 | 2135 | 2335 | 200 |
| 8 | Reactor Trip & Load/Unload | 400 | 522.2 | 547 | 24.8 | 2135 | 2335 | 200 |
| 9 | Large Step Decrease & Load/Unload | 200 | 522.2 | 547 | 24.8 | 2135 | 2335 | 200 |
| 10 | Loading/Unloading Range | 17620 | 532.2 | 547 | 14.8 | 2135 | 2335 | 200 |
| 11 | Loss of Power Range | 40 | 530.2 | 542.2 | 12 | 2135 | 2335 | 200 |
| 12 | Primary Side Hydro Test | 5 | 120 | 120 | 0 | 0 | 3105 | 3105 |
| 13 | Primary Side Leak Test | 50 | 120 | 547 | 427 | 0 | 2485 | 2485 |

Table 6-5. Bounding Moments

| Line | Plant | Node | TE Moment, ft-lb | | | DW Moment, ft-lb | | | OBE Moment, ft-lb | | |
|---|---|---|---|---|---|---|---|---|---|---|---|
| | | | $M_x$ | $M_y$ | $M_z$ | $M_x$ | $M_y$ | $M_z$ | $M_x$ | $M_y$ | $M_z$ |
| 6" Sch 160 Cold Leg SI | Kewaunee | 280 | 750 | 254 | 941 | -518 | -2 | 395 | 102 | 65 | 211 |
| | PI Unit 2 | 826 | -846 | 49 | -252 | -4 | -2 | 1 | 76 | 11 | 54 |
| 12" Sch 160 SI Accumulator | Kewaunee | 125 | -6207 | 37869 | -76432 | 706 | -946 | -1151 | 708 | 1744 | 109 |
| | Kewaunee | 310 | 53964 | -28733 | 32398 | -1752 | 254 | -474 | 331 | 520 | 356 |
| | PI Unit 1 | 855 | 46008 | -11027 | -18203 | 2559 | -476 | -2946 | 4894 | 809 | 5269 |
| | PI Unit 1 | 910 | -34147 | -27905 | -1668 | -1102 | -400 | -3334 | 3322 | 1620 | 6171 |
| 8" Sch 140 RHR Suction | PI Unit 1 | 2000 | 2967 | -4507 | 16159 | -142 | -216 | -1161 | 667 | 1892 | 396 |
| | PI Unit 1 | 2324 | 7449 | -2958 | -4764 | -763 | 278 | -2078 | 2551 | 425 | 4261 |
| | PI Unit 2 | 246 | -1295 | -6489 | -1932 | -825 | 10 | 1622 | 4857 | 1661 | 15274 |
| | PI Unit 2 | 255A | 7466 | -8370 | 32915 | 51 | -6 | 367 | 733 | 1390 | 1588 |
| | PI Unit 2 | 270 | 7719 | 3075 | 5261 | 1775 | -53 | -868 | 445 | 3167 | 12240 |
| 6" Sch 160 Draindown | PI Unit 1 | 730 | -355 | 81 | 184 | -528 | -2 | 410 | 117 | 276 | 275 |

Table 6-6. Maximum and Minimum Transient and Discontinuity Stress

| Transition | Transient | Stress, ksi |
|---|---|---|
| 6" SI Line to CL Nozzle | High Head Safety Injection | 100.23 |
| 6" SI Line to CL Nozzle | High Head Safety Injection | -67.87 |
| 12" SI Line to CL Nozzle | RHR Operation at Cooldown | 65.09 |
| 12" SI Line to CL Nozzle | RHR Operation at Cooldown | -1.96 |
| 12" SI Line to CL Nozzle | Inadvertent Accumulator Blowdown | 53.45 |
| 12" SI Line to CL Nozzle | Inadvertent Accumulator Blowdown | -59.08 |
| 12" SI Line to CL Nozzle | Refueling Floodup | 20.93 |
| 6" SI Line to Valve | High Head Safety Injection | 124.05 |
| 6" SI Line to Valve | High Head Safety Injection | -99.03 |
| 12" SI Line to Valve | RHR Operation at Cooldown | 69.56 |
| 12" SI Line to Valve | RHR Operation at Cooldown | -0.50 |
| 12" SI Line to Valve | Inadvertent Accumulator Blowdown | 78.20 |
| 12" SI Line to Valve | Inadvertent Accumulator Blowdown | -82.54 |
| 12" SI Line to Valve | Refueling Floodup | 24.84 |
| 8" RHR Line to Valve | RHR Initiation | -57.24 |

Table 6-7. Maximum and Minimum Transient Stress

| Transition | Transient | Stress, ksi |
|---|---|---|
| 6" SI Line to CL Nozzle | High Head Safety Injection | 96.60 |
| 6" SI Line to CL Nozzle | High Head Safety Injection | -64.80 |
| 12" SI Line to CL Nozzle | RHR Operation at Cooldown | 65.09 |
| 12" SI Line to CL Nozzle | RHR Operation at Cooldown | -2.08 |
| 12" SI Line to CL Nozzle | Inadvertent Accumulator Blowdown | 52.72 |
| 12" SI Line to CL Nozzle | Inadvertent Accumulator Blowdown | -58.36 |
| 12" SI Line to CL Nozzle | Refueling Floodup | 20.82 |
| 6" SI Line to Valve | High Head Safety Injection | 96.28 |
| 6" SI Line to Valve | High Head Safety Injection | -64.66 |
| 12" SI Line to Valve | RHR Operation at Cooldown | 64.85 |
| 12" SI Line to Valve | RHR Operation at Cooldown | -2.05 |
| 12" SI Line to Valve | Inadvertent Accumulator Blowdown | 52.64 |
| 12" SI Line to Valve | Inadvertent Accumulator Blowdown | -58.28 |
| 12" SI Line to Valve | Refueling Floodup | 20.84 |
| 8" RHR Line to Valve | RHR Initiation | -36.13 |

Table 6-8. Total Constant ($\sigma_0$) and Linear (($\sigma_1$) Through-Wall Stresses, 6" Sch 160 Cold Leg SI

| Load Set Pair | Cycles | Stresses (psi) | | | |
|---|---|---|---|---|---|
| | | Minimum | | Maximum | |
| | | $\sigma_0$ | $\sigma_1$ | $\sigma_0$ | $\sigma_1$ |
| CD & HU/Loss of Load/OBE | 20 | 19395 | -53760 | 24268 | -53760 |
| CD & HU/Loss of Load | 60 | 19397 | -53760 | 24109 | -53760 |
| CD & HU | 170 | 19402 | -53760 | 23912 | -53760 |
| Turbine Roll Test Range | 10 | 23178 | -53760 | 23928 | -53760 |
| Flow Loss & 10% Load Decrease | 80 | 23067 | -53760 | 23928 | -53760 |
| 10% Load Incr. & 10% Load Decr. | 1920 | 23559 | -53760 | 23928 | -53760 |
| 10% Load Incr & Load/Unload | 80 | 23559 | -53760 | 23928 | -53760 |
| Reactor Trip & Load/Unload | 400 | 23568 | -53760 | 23928 | -53760 |
| Large Step Decrease & Load/Unload | 200 | 23568 | -53760 | 23928 | -53760 |
| Loading/Unloading Range | 17620 | 23585 | -53760 | 23928 | -53760 |
| Loss of Power Range | 40 | 23583 | -53760 | 23921 | -53760 |
| Primary Side Hydro Test | 5 | 19746 | -53760 | 24674 | -53760 |
| Primary Side Leak Test | 50 | 19488 | -53760 | 24166 | -53760 |

Table 6-9. Total Constant ($\sigma_0$) and Linear (($\sigma_1$) Through-Wall Stresses, 12" Sch 160 SI Accumulator

| Load Set Pair | Cycles | Stresses (psi) | | | |
|---|---|---|---|---|---|
| | | Minimum | | Maximum | |
| | | $\sigma_0$ | $\sigma_1$ | $\sigma_0$ | $\sigma_1$ |
| CD & HU/Loss of Load/OBE | 20 | 19134 | -29421 | 30357 | -29421 |
| CD & HU/Loss of Load | 60 | 19134 | -29421 | 30337 | -29421 |
| CD & HU | 170 | 19134 | -29421 | 29812 | -29421 |
| Turbine Roll Test Range | 10 | 28204 | -29421 | 29829 | -29421 |
| Flow Loss & 10% Load Decrease | 80 | 28196 | -29421 | 29832 | -29421 |
| 10% Load Incr. & 10% Load Decr. | 1920 | 29068 | -29421 | 29832 | -29421 |
| 10% Load Incr & Load/Unload | 80 | 29068 | -29421 | 29829 | -29421 |
| Reactor Trip & Load/Unload | 400 | 29139 | -29421 | 29829 | -29421 |
| Large Step Decrease & Load/Unload | 200 | 29139 | -29421 | 29829 | -29421 |
| Loading/Unloading Range | 17620 | 29279 | -29421 | 29829 | -29421 |
| Loss of Power Range | 40 | 29251 | -29421 | 29761 | -29421 |
| Primary Side Hydro Test | 5 | 19841 | -29421 | 25145 | -29421 |
| Primary Side Leak Test | 50 | 19837 | -29421 | 30085 | -29421 |
| Refueling Floodup | 80 | 18855 | -29421 | 49346 | -79101 |
| RHR Operation at Cooldown | 250 | 19056 | -28421 | 94359 | -168541 |

Table 6-10. Total Constant ($\sigma_0$) and Linear ($\sigma_1$) Through-Wall Stresses, 8" Sch 140 RHR Suction

| Load Set Pair | Cycles | Stresses (psi) | | | |
|---|---|---|---|---|---|
| | | Minimum | | Maximum | |
| | | $\sigma_0$ | $\sigma_1$ | $\sigma_0$ | $\sigma_1$ |
| CD & HU/Loss of Load/OBE | 20 | 19147 | -47537 | 27393 | -47537 |
| CD & HU/Loss of Load | 60 | 19504 | -47537 | 27377 | -47537 |
| CD & HU/Loss of Power | 40 | 19504 | -47537 | 27184 | -47537 |
| CD & HU/10% Load Increase | 130 | 23243 | -47537 | 27146 | -47537 |
| TR Test & 10% Load Increase | 10 | 25483 | -47537 | 27146 | -47537 |
| Loss of Flow & 10% Load Increase | 80 | 26059 | -47537 | 27146 | -47537 |
| Step Decr. & 10% Load Increase | 200 | 26235 | -47537 | 27146 | -47537 |
| Rx Trip & 10% Load Increase | 400 | 26258 | -47537 | 27146 | -47537 |
| Unload & Load/10% Load Increase | 1180 | 26416 | -47537 | 27146 | -47537 |
| Unload & Load/10% Load Decrease | 2000 | 26416 | -47537 | 27118 | -47537 |
| Loading/Unloading | 15120 | 26417 | -47537 | 27090 | -47537 |
| Primary Side Hydro Test | 5 | 20149 | -47537 | 26146 | -47537 |
| Primary Side Leak Test | 50 | 19807 | -47537 | 28299 | -47537 |
| RHR Operation at Cooldown | 250 | -37688 | 66943.1 | 22639 | -47537 |

Table 6-11. Total Constant ($\sigma_0$) and Linear ($\sigma_1$) Through-Wall Stresses, 6" Sch 160 Draindown

| Load Set Pair | Cycles | Stresses (psi) | | | |
|---|---|---|---|---|---|
| | | Minimum | | Maximum | |
| | | $\sigma_0$ | $\sigma_1$ | $\sigma_0$ | $\sigma_1$ |
| CD & HU/Loss of Load/OBE | 20 | 19694 | -53760 | 23973 | -53760 |
| CD & HU/Loss of Load | 60 | 19744 | -53760 | 23872 | -53760 |
| CD & HU/Loss of Power | 40 | 19744 | -53760 | 23714 | -53760 |
| CD & HU/10% Load Increase | 130 | 22815 | -53760 | 23725 | -53760 |
| TR Test & 10% Load Increase | 10 | 22898 | -53760 | 23725 | -53760 |
| Loss of Flow & 10% Load Increase | 80 | 23346 | -53760 | 23725 | -53760 |
| Step Decr. & 10% Load Increase | 200 | 23361 | -53760 | 23725 | -53760 |
| Rx Trip & 10% Load Increase | 400 | 23363 | -53760 | 23725 | -53760 |
| Unload & Load/10% Load Increase | 1180 | 23377 | -53760 | 23725 | -53760 |
| Unload & Load/10% Load Decrease | 2000 | 23377 | -53760 | 23722 | -53760 |
| Loading/Unloading | 15120 | 23377 | -53760 | 23720 | -53760 |
| Primary Side Hydro Test | 5 | 19775 | -53760 | 24703 | -53760 |
| Primary Side Leak Test | 50 | 19770 | -53760 | 23933 | -53760 |

Table 6-12. Initial Crack Depths for Various Locations

| | t (in.) | a/t | a (in.) |
|---|---|---|---|
| 6" Sch 160 Cold Leg SI | 0.718 | 0.1163 | 0.0835 |
| 12" Sch 160 SI Accumulator | 1.312 | 0.1091 | 0.1432 |
| 8" Sch 140 RHR Suction | 0.812 | 0.1146 | 0.0930 |
| 6" Sch 160 Draindown | 0.718 | 0.1163 | 0.0835 |

Table 6-13. Results of Fatigue Crack Growth Analysis

| | Assumed Initial Depth (in.) | Final Depth (in.) | Code Allowable Depth (in.) | Calculated Heatup/Cooldown Cycles to Reach Allowable Depth |
|---|---|---|---|---|
| 6" Sch 160 Cold Leg SI | 0.0835 | 0.0839 | 0.5385 | > 250 |
| 12" Sch 160 SI | 0.1432 | 0.984 | 0.984 | 38 |
| 8" Sch 160 RHR | 0.0930 | 0.609 | 0.609 | 123 |
| 6" Sch 160 Draindown | 0.0835 | 0.0837 | 0.5385 | > 250 |

## 7.0 SUMMARY AND CONCLUSIONS

Leak-before-break (LBB) evaluations are performed for the RCS attached piping at Prairie Island Units 1 and 2 in accordance with the requirements of NUREG-1061. The evaluation included portions of the safety injection and the residual heat removal systems. The nominal pipe sizes range from 6 inches to 12 inches. The analysis has been performed using conservative generic material properties for the base metals and weldments and location specific stresses consisting of pressure deadweight, thermal and seismic loads from both Originally Licensed Thermal Power (OLTP) considering only RHR Normal Thermal & Uprate Conditions considering RHR Thermal Stratification. In the evaluations, circumferential flaws have been considered since they are more limiting than axial flaws. Critical flaw sizes and leakage flaw sizes were calculated on a location specific basis using both elastic-plastic J-Integral/Tearing modulus and limit load analyses. The most limiting critical flaw size at each location from these two analyses methods has been used in the LBB evaluation. The leakage flaw size is defined as the minimum of one half the critical flaw size with a factor of one on the stresses or the full critical flaw size with a factor of $\sqrt{2}$ on the stresses. Leakage was then calculated through the leakage flaw size. Because all the piping is of relatively small diameter, the effect of piping restraint was considered in the LBB evaluation. Fatigue crack growth analysis was also performed to determine the extent of growth of any pre-existing flaws.

For Originally Licensed Thermal Power (OLTP) conditions, considering only RHR Normal Thermal, the following conclusions can be made:

- Without the consideration of piping restraint effect, the predicted leakage range for all the lines considered in this evaluation are summarized below:

| | | |
|---|---|---|
| 6-inch Safety Injection Attached to RPV and Cold Leg | Unit 1 | 4.60 – 5.27 gpm |
| | Unit 2 | 4.91 – 5.71 gpm |
| 6-inch Draindown Line Attached to Hot Leg | Unit 1 | 3.94 – 3.97 gpm |
| | Unit 2 | 3.88 – 3.90 gpm |
| 8-inch RHR Line Attached to Hot Leg | Unit 1 | 6.96 – 11.20 gpm |
| | Unit 2 | 3.78 – 11.73 gpm |

| | | |
|---|---|---|
| 12-inch Safety Injection Line Attached to Cold Leg - | Unit 1 | 22.42 – 26.98 gpm |
| | Unit 2 | 22.63 – 26.67 gpm |
| 6-inch Hot Leg Capped Nozzles | Units 1/2 | 3.74 gpm |

- The piping restraint effects have no significant impact on the predicted leakages for the 6-inch safety injection and draindown lines. At the worst location, piping restraint produces about 13% reduction of the leak rate on the 8-inch RHR line.

- The lowest predicted leakage for the safety injection and RHR lines considered in this evaluation is 3.78 gpm without consideration of the piping restraint effect. When the restraint effect is considered, the minimum leakage for all the piping systems considered is 3.4 gpm.

- Based on the capability of all the available leak detection systems, Prairie Island is capable of detecting leak rates as low as 0.1 gpm. However, for this evaluation a detectable leak rate of 0.2 gpm is assumed based on previous NRC approval for a sister plant. When the NUREG-1061 margin of 10 is applied to this rate, Prairie Island leak detection capability is 2.0 gpm. The minimum predicted leakage under Originally Licensed Thermal Power (OLTP) considering only RHR Normal Thermal, 3.4 gpm is greater than the leak detection at Prairie Island hence justifying leak-before-break for all the systems considered.

- Fatigue crack growth of an assumed subsurface flaw of 11% of pipe wall shows that fatigue crack growth can be managed by the current Section XI inservice inspection program at Prairie Island and therefore does not invalidate the application of leak-before-break evaluation of the safety injection and RHR lines under consideration.

- The effect of degradation mechanisms which could invalidate the LBB evaluations were considered in the evaluation. It was determined that there is no potential for water hammer, intergranular stress corrosion cracking (IGSCC) and erosion-corrosion for portions of the safety injection and RHR systems considered in the LBB evaluations.

For Uprate Conditions considering RHR Thermal Stratification, the following conclusion can be made:

- The LBB evaluation due under Uprate conditions considering RHR Thermal Stratification demonstrates that LBB is still applicable for all the piping considered if fatigue crack morphology is used. The minimum leakage under uprate conditions considering RHR Thermal Stratification is 2.12 gpm associated with the 8-inch RHR piping in Unit 2 considering the maximum 13% reduction of the leak rate due to piping restraint. This is above the required leak detection of capability of 2.0 gpm for Prairie Island.

## 8.0 REFERENCES


1. Structural Integrity Associates Report No. SIR-00-045, Rev. 0, "Leak-Before-Break Evaluation, 6-inch to 12-inch Safety Injection and Residual Heat Removal Piping Attached to the RCS, Kewaunee Nuclear Power Plant."

2. Stello, Jr., V., "Final Broad Scope Rule to Modify General Design Criterion 4 of Appendix A, 10 CFR Part 50," NRC SECY-87-213, Rulemaking Issue (Affirmation), August 21, 1987.

3. NUREG-1061, Volumes 1-5, "Report of the U. S. Nuclear Regulatory Commission Piping Review Committee," prepared by the Piping Review Committee, NRC, April 1985.

4. NUREG-0800, "U.S. Nuclear Regulatory Commission Standard Review Plan, Office of Nuclear Reactor Regulation, Section 3.6.3, Leak-Before-Break Evaluation Procedure," Revision 1, March 2007.

5. Northern States Power, Prairie Island Nuclear Generating Plant, "Coolant Leakage Detection System Performance at the Prairie Island Nuclear Generating Plant," Report to the United States Nuclear Regulatory Commission, Division of Operating Reactors, Docket Nos. 50-282, 50-306, License No. DRP-42, DRP-60, March 31, 1976.

6. Letter from G. S. Vissing (USNRC) to R. C. Mecredy (RG&E) including Safety Evaluation Report, "Staff Review of the Submittal by Rochester Gas and Electric Company to Apply Leak-Before-Break Status to Portions of the R. E. Ginna Nuclear Power Plant Residual Heat Removal System Piping (TAC No. MA039)," dated February 25, 1999, Docket No. 50-244.

7. NUREG-0927, "Evaluation of Water Hammer Occurrence in Nuclear Power Plants," Revision 1.

8. W. S. Hazelton and W. H. Koo, "Technical Report on Material Selection and Processing Guidelines for BWR Coolant Pressure Boundary Piping," NUREG-0313, Rev. 2, USNRC, January 1988.

9. U. S. Nuclear Regulatory Commission, Bulletin 88-08, "Thermal Stresses in Piping Connected to Reactor Coolant Systems," June 22, 1998 (Plus Supplements 1, 2 and 3).

10. [redacted]

11. [redacted]

12. Excerpts from "Northern States Power Company Prairie Island Nuclear Generating Plant Design Basis Document," Revision 2, Pages 131, 132 and 134 of 308 "Reactor Coolant System."

13. NSP Document SS-M370 9-69, "Standard Specification for Piping Material, Stainless Steel Piping," Rev. 9-11-72.

14. NSP Document SS-M327, Sheet 52A, "Standard Specification – Mechanical, "Piping Design Tables," Rev. 5-22-72.

15. EPRI Report No. NP-6301-D "Ductile Fracture Handbook," June 1989.

16. Chopra, O.K., "Estimation of Fracture Toughness of Cast Stainless Steels during Thermal Aging in LWR Systems," NUREG/CR-4513, ANL-93/22, Rev. 1.

17. "Safety Injection and RHR Piping Stress Reports," Northern States Power Prairie Island Nuclear Generating Plant Units 1 and 2 (Project No. 21-7450-255):

    a) Stress Report No. PI-205-IV for Unit 1, "Piping Stress Analysis for Safety Injection Line 48," August 1979.

    b) Stress Report No. PI-205-III for Unit 1, "Piping Stress Analysis for Safety Injection Line 28B," August 1979.

    c) Stress Report No. PI-1-216-II for Unit 1, "Piping Stress Analysis for Residual Heat Removal Line 10," August 1979.

    d) Stress Report No. PI-1-205-V for Unit 1, "Piping Stress Analysis for Safety Injection Line 101," March 1980.

    e) Stress Report No. PI-216-II for Unit 1, Project No. 832642, "Piping Stress Analysis for Residual Heat Removal Part 9," August 4, 1988.

    f) Stress Report No. PI-205-X for Unit 2, "Piping Stress Analysis for Safety Injection Line 28B & 104," August 1979.

    g) Stress Report No. PI-205-X for Unit 2, "Piping Stress Analysis for Safety Injection Line 28B & 103," August 1979.

    h) Stress Report No. PI-205-IX for Unit 2, "Piping Stress Analysis for Safety Injection Line 48," August 1979.

    i) Unit 2 "Piping Stress Analysis Residual Heat Removal System 216 Lines 9A & 9B," May 1974.

    j) Stress Report No. PI-2-205-XXI for Unit 2, "Piping Stress Analysis for Safety Injection Line 101," August 1979.

18. "RCS Draindown Piping Stress Reports," Northern States Power Prairie Island Nuclear Generating Plant Units 1 and 2 (W. O. No. 12911.76):

a) S&W Calc. No. 3, Rev. 1, "Pipe Stress Analysis Of RCS Draindown Modification, Unit 1," December 1992.

b) S&W Calc. No. 10, Rev. 0, "Pipe Stress Analysis Of RCS Draindown Modification, Unit 2," February 1993.

19. Letter from Dr. A. V. Setlur (Automated Engineering Services Corp.) to Ms. Patrice Braaten (Northern States Power), dated January 6, 1993, including enclosure, "Unit 2 SI Line to Cold Leg "A" (X-HIAW-1106-2705, Rev. A); Evaluation of Piping for Additional Clamp and Furmanite Sealer Loads of 130 Pounds on Check Valve 2-SI-9-2."

20. Letter from Dr. A. V. Setlur (Automated Engineering Services Corp.) to Mr. Gregory M. Thoraldson (Northern States Power Company), dated May 12, 1999 including enclosure, "Evaluation of SI Piping Due to the Addition of Furmanite Clamp on Valve SI-9-2."

21. Kumar, V., et al., "An Engineering Approach for Elastic-Plastic Fracture Analysis," EPRI NP-1931, Electric Power Research Institute, Palo Alto, CA, July 1981.

22. Kumar, V., et al., "Advances in Elastic-Plastic Fracture Analysis," EPRI NP-3607, Electric Power Research Institute, Palo Alto, CA, August 1984.

23. Structural Integrity Associates, Inc., "**pc-CRACK™** Fracture Mechanics Software," Version 3.0 - 3/27/97.

24. EPRI Report NP-3596-SR, "PICEP: Pipe Crack Evaluation Computer Program," Rev. 1, July 1987.

25. P.E. Henry, "The two-Phase Critical Discharge of Initially Saturated or Subcooled Liquid," Nuclear Science and Engineering, Vol. 41, 1970.

26. EPRI Report NP-3395, "Calculation of Leak Rates Through Crack in Pipes and Tubes," December 1983.

27. NUREG/CR-6443, BMI-2191, "Deterministic and Probabilistic Evaluation for Uncertainty in Pipe Fracture Parameters in Leak-Before-Break and in Service Flow Evaluations," June 1996.

28. ANSYS LinearPlus/Thermal, Revision 5.5.1, ANSYS, Inc., October 1998.

29. NUREG/CR-4572, BMI-2134, "NRC Leak-Before-Break (LBB.NRC) Analysis Method for Circumferentially Through-Wall Cracked Pipes Under Axial Plus Bending Loads," May 1986.

30. ASME Boiler and Pressure Vessel Code, Section XI, 1989 Edition.

31. PIPETRAN, Version 2.0, Structural Integrity Associates, Inc., 4/8/99.

32. ASME Section XI Task Group for Piping Flaw Evaluation, "Evaluation of Flaws in Austenitic Steel Piping," Journal of Pressure Vessel Technology, Vol. 108, August 1986, pp. 352-366.

33. E. Smith, "The Effect of System Flexibility on the Formulation of a Leak Before Break Case for Cracked Piping," Proceedings, ASME Pressure Vessel and Piping Conference, PVP - Vol. 313-1, Codes and Standards, Vol. 1, 1995.

34. ENG-CS-378, Rev. 0, "Evaluation of The Effects of $T_{ave}$ Reconciliation, MUR And Transition to 422V+ Fuel On The Unit 1 Branch Lines And Nozzles Connected to The RCS Loop Piping and Components,".

35. ENG-CS-376, Rev. 0, "Evaluation of The Effects of $T_{ave}$ Reconciliation, MUR And Transition to 422V+ Fuel On The Unit 2 Branch Lines And Nozzles Connected to The RCS Loop Piping and Components,".

36. Design Information Transmittal 1006-4, "Unit 2 Pressurizer Surge Nozzle Design Data; Surge Line Data; Engineering Manual Data; Actual Operating Data", October 12, 2009.

37. NUREG/CR-6300, "Refinement and Evaluation of Crack-Opening Analyses for Short Circumferential Through-Wall Cracks in Pipes," U.S. Nuclear Regulation Commission, April 1995.

38. D. Ruland, R. Wolterman, G. Wilkowski, R. Tregoning, "Impact of PWSCC and Current Leak Detection on Leak-Before-Break," Proceedings of Conference on Vessel Head Penetration, Inspection, Cracking, and Repairs, Sponsored by USNRC, Marriot Washingtonian Center, Gaithersburg, MD, September 29 to October 2,2003.

39. D. Abdollahian and B. Chexal, "Calculation of Leak Rates Through Cracks in Pipes and Tubes," EPRI NP-3395, Electric Power Research Institute, Palo Alto, CA, December 1983.

40. [redacted]

# APPENDIX A

## DETERMINATION OF RAMBERG-OSGOOD PARAMETERS AT 650°F

## A.1 INTRODUCTION

The Ramberg-Osgood stress-strain parameters ($\alpha$ and n) are necessary for elastic-plastic fracture mechanics analysis. These parameters may be a function of temperature. This section provides the methodology for making adjustment for the Ramberg-Osgood stress-strain parameters at a different temperature when the parameters for another temperature are known. In this case, the Ramberg-Osgood parameters are derived for at 650°F for given values at 550°F for the Type 316 stainless steel piping SMAW welds at Prairie Island.

## A.2 METHODOLOGY

The Ramberg-Osgood model is in the form:

$$\frac{\varepsilon}{\varepsilon_o} = \frac{\sigma}{\sigma_o} + \alpha\left[\frac{\sigma}{\sigma_o}\right]^n \qquad (1)$$

Where $\sigma$ and $\varepsilon$ are the true stress and true strain, $\sigma_o$ and $\varepsilon_o$ are the reference stress and reference strain (in general yield stress and yield strain) and $\alpha$ and n are the so called Ramberg-Osgood (R-O) parameters.

When the stress-strain curve at the temperature of interest is available, the R-O parameters can be obtained by curve fitting over the strain range of interest. In the absence of the stress-strain curve of the material, a methodology for determining the R-O parameters based on ASME Code-specified mechanical properties is provided in Reference A-1. The suggested method is described by the following equations:

$$\alpha \approx \frac{0.002}{e_y} \qquad (2)$$

$$n = \frac{\ell n\left[\frac{1}{\alpha}\left(\frac{\ell n(1+e_u)}{\ell n(1+e_y)}\right) - \frac{S_u(1+e_u)}{S_y(1+e_y)}\right]}{\ell n\left[\frac{S_u(1+e_u)}{S_y(1+e_y)}\right]} \tag{3}$$

where $S_u$ and $S_y$ represent ultimate stress and yield stress respectively. They can be obtained from the ASME Code [A-2] for a wide range of temperatures. The yield strain ($e_y$) is determined as:

$$e_y = \frac{S_y}{E} \tag{4}$$

where E (modulus of elasticity) can also be obtained from the ASME Code. The ultimate strain ($e_u$) is not specified at all temperatures in the ASME Code, hence the room temperature elongation value specified in the ASME Code, Section II [A-2] is assumed for all temperatures. The methodology in any case is not sensitive to the choice of $e_u$ [A-1] when determining I and n by using equation (2) and (3).

It is obvious that $\alpha$ is a function of $e_y$, n is a function of $\alpha$, $e_u$, $e_y$, $S_u$, and $S_y$, and both are the function of temperature. Therefore, an adjustment scheme can be used as follows where the material properties at 650°F are adjusted based on the ratio of predicted properties from Equations (2) and (3) using Code minimum properties:

$$(\alpha)_{650°F} = (\alpha)_{Base,\,550°F} \times \frac{\text{Equation}(2)_{550°F,\,\text{Code min.property}}}{\text{Equation}(2)_{650°F,\,\text{Code min.property}}} \tag{5}$$

$$(n)_{650°F} = (n)_{Base,\,550°F} \times \frac{\text{Equation}(3)_{550°F,\,\text{Code min.property}}}{\text{Equation}(3)_{650°F,\,\text{Code min.property}}} \tag{6}$$

Hence, Equations (2), (3), (4), (5) and (6) can be used to obtain R-O parameters at 650°F from the given values at 550°F.

## A.3 RESULTS

The inputs into the evaluation consist of the R-O parameters provided in Tables 4-1 in the main body of the report and ASME Code properties at 550°F and 650°F. The input and results of the analysis which determines the R-O parameters at 650°F are provided in Table A-1.

## A.4 REFERENCES


A-1. Cofie, N.G., Miessi, G.A., and Deardorff, A.F., "Stress-Strain Parameters in Elastic-Plastic Fracture Mechanics," Smirt 10 International Conference, August 14-18, 1989.

A-2 ASME Boiler and Pressure Vessel Code, Sections II and III Appendices, 1989 Edition.

Table A-1

Determination of Ramberg-Osgood Parameters for SMAW at 650°F

| | | |
|---|---|---|
| | $\alpha$, 550°F | 9 |
| | n, 550°F | 9.8 |

| | | |
|---|---|---|
| Temperature (°F) | 550 | 650 |
| E (ksi) | 25550 | 25050 |
| $S_y$ (ksi) | 19.35 | 18.5 |
| $S_u$ (ksi) | 67 | 67 |
| $e_u$ (in/in) | 0.3 | 0.3 |
| $e_y$ (in/in) | 0.0007573 | 0.0007385 |
| $\varepsilon_o = \ell n(1+e_y)$ | 0.0007571 | 0.0007383 |
| $\varepsilon_u = \ell n(1+e_u)$ | 0.2623643 | 0.2623643 |
| $\alpha'$ | 2.6408269 | 2.7081081 |
| n' | 3.2348215 | 3.1407678 |
| $\alpha$ | 9.0 | 9.227 |
| n | 9.8 | 9.515 |